UNIVERSITY OF SOUTHAMPTON

Faculty of Science

Department of Physics

APPLICATION OF ADVANCED TRANSIENT LASER POLARIMETRY TO STUDY OF NONLINEAR REFLECTIVE POLARISATION PHENOMENA IN SOLIDS

by Andrew Malinowski

A thesis submitted for the degree of Doctor of Philosophy

June 1996

UNIVERSITY OF SOUTHAMPTON

ABSTRACT

FACULTY OF SCIENCE

PHYSICS

Doctor of Philosophy

Application of Advanced Transient Laser Polarimetry To Study of Nonlinear Reflective Polarisation Phenomena in Solids

by Andrew Malinowski

A novel femtosecond time-resolved polarimeter for reflective measurements was developed. The instrument was used with a picosecond Nd:YAG laser and an advanced femtosecond Ti:Sapphire laser. Sensitivity to pump-induced reflected probe polarisation rotation of better than 10^{-6} radians combined with time resolution up to 70 femtoseconds has been achieved. Time resolution of 30 femtoseconds was achievable with loss of sensitivity of approximately an order of magnitude. The polarimeter has been tested in a variety of spectroscopic configurations and with different types of solids (metals, semiconductors and superconductors) and was found to be a useful tool for the investigation of the transient nonlinear optical properties of opaque materials. A new type of optical autocorrelator for measurement of the duration of femtosecond optical pulses utilizing a reflective polarisation effect in metallic nickel was designed.

The recently developed spectroscopic polarimetric technique of the Specular Inverse Faraday effect was for the first time used to study a semimagnetic semiconductor ($Cd_{0.6}Mn_{0.4}Te$), a high T_c superconductor ($YBaCuO_{7-\delta}$) and a ferromagnetic metal (Ni). The cubic optical nonlinearity ($\chi^{(3)}{}_{1122}$-$\chi^{(3)}{}_{1221}$) was measured in these opaque solids for the first time. In particular, in nickel a strong ($\chi^{(3)} \sim 2\ 10^{-9}$esu) and exceptionally fast ($\tau < 30$ fs) nonlinearity, which is promising for reflective nonlinear optical applications, was found. The thermalisation and spin-relaxation dynamics in GaAs were investigated with femtosecond time resolution using Specular Inverse Faraday effect spectroscopy for the first time.

Investigations were undertaken into natural and light induced reflective anisotropy in zincblende structure crystals. Transient measurements of induced anisotropy, its orientation dependence and intensity dependence were made for the first time in GaAs, InSb and $Cd_{0.6}Mn_{0.4}Te$. Analysis of microscopic and macroscopic pictures of the light-matter interaction in zincblende structure materials allowed attribution of the observed anisotropic effects to the phenomenon of natural and induced gyrotropic linear dichroism.

A computer program based on the quaternion description of light polarisation, the constitutive equation and the wave equation and suitable for calculation of evolution of partially polarised light in linear and nonlinear optical media with local and nonlocal optical response has been developed. The evolution of the polarisation state of partially polarised light during propagation in an isotropic medium with cubic nonlinearity has been investigated in detail and compared with published analytical and semi-analytical data.

Contents

Acknowledgements

I would like to thank my supervisor, Dr. Nikolay Zheludev, for his advice and encouragement. I would also like to thank Dr. Yuri Svirko for providing much of the theoretical background to the experimental work presented in this thesis, Dr. Sergei Popov and Dr. Adrian Bungay, with whom I collaborated during my experimental work, and Dr Richard Harley and Ian Shatwell together with Dr. Nikolay Zheludev, whose work on the theory of the dynamics of the Specular Inverse Faraday effect in GaAs is outlined in chapter 3. I acknowledge the Department of Physics, University of Southampton for financial support.

Chapter 1
Introduction

1.1 Optical Polarisation Effects

Optical effects arising from the polarisation properties of light have been known for over three centuries. Bartholinus observed birefringence in calcite in 1669 and Huygens discovered the existence of different polarisation states by showing that the refracted rays from the calcite could be distinguished by passing them through a second calcite crystal which was rotated about the propagation direction of the ray. Optical activity (differential absorption and phase retardation of left and right circularly polarised waves) was first observed by Arago in 1811. Linear dichroism was first observed by Biot in 1815. In 1816 Fresnel demonstrated that orthogonally polarised rays do not interfere, leading Young in 1817 to hypothesise that light is a transverse (rather than longitudinal) wave.

In addition to these natural polarisation effects, the behaviour of light in a medium may be influenced by an applied field. An electric field perpendicular to the propagation direction may induce birefringence, which may be linear (Pockels effect) or quadratic (Kerr effect) in field strength. A magnetic field parallel to the direction of propagation may induce circular birefringence which will cause the plane of polarisation of a linearly polarised wave to rotate (optical Faraday effect). It should be noted that this effect is different from conventional optical activity in that it is nonreciprocal i.e. the rotation is doubled rather than cancelled if the light is reflected back through the medium.

In addition to these effects produced by constant applied fields, polarisation changes can also be induced by excitation of the medium by an oscillating field, such as that associated with a light wave. This may arise from self-action of a propagating light wave or the influence of a pump beam on a separate probe beam. The optical Kerr effect, where a linearly polarised pump induces linear dichroism/birefringence was observed by Mayer in 1964 [Mayer, 64; Buckingham, 65]. Self-rotation of the polarisation ellipse was also observed in the same year [Maker, 64]. The inverse Faraday effect, magnetisation of a medium by a circularly polarised pump [Atkins,68] was first observed by [Van der Zeil, 65]. The circular birefringence/dichroism of a linearly polarised pump arising from the inverse Faraday effect was first observed by [Arutyunyan, 75]. There are also nonlinear effects associated with nonlocality of the optical response. Intensity dependent change in optical activity has been observed due to heating of a sample by a pump beam [Vlasov, 71] or by self-heating in a single beam experiment [Bairamov, 73] and due to electronic nonlinearity [Akhamanov, 79]. Nonlocal terms in the optical response also give rise to intensity dependent linear birefringence/dichroism in noncentrosymmetric cubic crystals [Kovrighin, 80].

In addition to these transmission effects, there exist analogous linear and nonlinear effects on reflection. Reflection and transmission effects are closely related [Bungay,93]. The relationship between observable specular effects and the optical constants of materials will be discussed in detail in later chapters. The specular optical Kerr effect, i.e. change in the polarisation state of a reflected probe wave due to the presence of a linearly polarised pump wave, was observed by [Saiki, 92]. The Specular Inverse Faraday effect was first observed by [Kuwata, 87]. The phenomenon of specular optical activity was recently successfully observed for the first time [Bungay, 93a]. The nonlocal effect of linear birefringence/dichroism has also recently been observed in intensity dependent [Zheludev, 90] and in linear [Bungay, 93b; 94] experiments.

1.2 Aims of Thesis

This thesis covers work with four main aims related to polarisation sensitive linear and nonlinear optics: i) development of a specular pump-probe micropolarimeter with femtosecond time resolution, ii) investigation of the Specular Inverse Faraday effect in various materials, iii) experimental investigation and theoretical consideration of natural and light-induced linear birefringence/dichroism in noncentrosymmetric cubic crystals, particularly with reference to the time-nonreversible mechanism of the effect, iv) simulation of the evolution of the polarisation state of partially polarised light propagating in a nonlinear medium.

1.2.1 Time Resolved Specular Micropolarimetry

A pump-probe specular polarimeter which is sensitive to induced polarisation azimuth rotation of 1 μradian has been developed from a linear specular polarimeter described in [Bungay, 93a; 93b]. It was first used in conjunction with a Nd:YAG laser in experiments described in chapters 3 and 4 of this thesis. The time resolution in these experiments was limited by the pulse length of the Nd:YAG laser (80 picoseconds). Another polarimeter of the same design was constructed at about the same time and used in conjunction with a 2-picosecond pulse length Ti:Sapphire laser in measurements of the dynamics of the Specular Inverse Faraday effect in GaAs [Bungay, 94]. Again, time resolution was limited by the pulse length of the laser. In order to improve the time resolution of the experiments, a femtosecond modelocked Ti:Sapphire laser (based on a design kindly provided by M.M.Murnane and H.C.Kapteyn of Washington State University [Murnane, 94]) was constructed for use with the polarimeter. In experiments using this laser, time resolution was limited by spreading of the laser pulse due to dispersion in the elements of the polarimeter. Modifications were made to the design of the polarimeter in order to reduce group velocity dispersion. With these modifications, the polarimeter achieved a time resolution of $\sim$30 femtoseconds.

1.2.2 The Specular Inverse Faraday Effect

As a means of studying the nonlinear optical properties of materials, specular measurements have the advantage that they can be applied to bulk samples of opaque materials. They have the disadvantage that the small interaction depth means that specular polarisation effects are generally much smaller than their transmission analogues.

The first theoretical work on specular pump-probe polarisation phenomena which addressed the Specular Inverse Faraday Effect (SIFE) was by Golubkov and Makarov [Golubkov, 90]. A detailed phenomenological theory of the SIFE in media with instantaneous response was developed by Svirko and Zheludev [Svirko, 94], which shows how to recover the values of components of the 3rd order degenerate optical susceptibility tensor $\chi^{(3)}$ from the induced change in the polarisation of a reflected probe beam, and a more general approach to specular polarisation phenomena has recently been developed by the same authors [Popov, 96]. The Specular Inverse Faraday effect was first used to observe a resonant nonlinearity by [Kuwata, 87] and was recently used for the first time to observe nonresonant nonlinearities by [Popov,94]. The first measurements of the dynamics of the SIFE were made by [Bungay, 94] with 2 picosecond time resolution.

In this thesis the first measurements of the SIFE in a high T_c superconductor ($YBa_2Cu_3O_{7-\delta}$) and a diluted magnetic semiconductor ($Cd_{0.6}Mn_{0.4}Te$) are presented. The relaxation times of the SIFE in the semiconductor GaAs were observed with time resolution significantly better than in [Bungay, 94] (a microscopic theory of the dynamics of the SIFE in GaAs is discussed), and the SIFE was observed for the first time in a ferromagnetic metal (nickel), and was found to be effectively instantaneous with 32 femtosecond time resolution.

1.2.3 Natural and Pump-Induced Gyrotropic Linear Dichroism

Polarisation changing optical phenomena have been used as diagnostic tools for the detection of a variety of symmetry breaking phenomena. An extensive search was carried out for polarisation azimuth rotation of light interacting with an atomic vapour, which results from parity violation in the weak force interaction of an optical electron with the atomic nucleus [Fortson, 84]. There has been considerable interest in recent years in time-nonreversible optical effects in recent years, particularly with reference to high-T_c superconductors. Several groups have attempted to detect specular circular dichroism/birefringence in these materials [Lawrence,92; Spielman,92; Lyons,93], in a search for an optical manifestation of the hypothetical violation of time-reversality in these materials called for in some theories of the origin of their superconductivity [Wen, 89; March-Russell, 88]. Other examples of time-nonreversible optical effects are depolarisation of light scattered by atoms which are time-non-reversible because they possess electronic angular momentum [Hamaguchi,80] and antisymmetric Raman scattering [Barron, 82].

In optics, the condition that an interaction is time-reversible imposes certain restrictions on the allowed components of the optical susceptibilities. Specifically, the restrictions on the dielectric tensor ϵ and the nonlocality tensor γ are

$$\varepsilon_{ij} = \varepsilon_{ji} \quad , \quad \gamma_{ijk} = -\gamma_{jik} \tag{1.1}$$

These restrictions are additional to any symmetry restrictions imposed by the material point group. This means that certain optical effects will only arise if the light-matter interaction is time-nonreversible.

Recently, Svirko and Zheludev [Svirko, 95] have shown that time-nonreversality is a general feature of nonlocal light-matter interactions in noncentrosymmetric media. The time-nonreversible terms arise in particular from the spin-orbit terms in the crystal Hamiltonian. The Hamiltonian of any unperturbed crystal is symmetrical with respect to time inversion (T) and space inversion (P). However, in the Hamiltonian

representing the interaction between the crystal and a light wave, there are terms arising from the spin orbit interaction and the part of the crystal potential which is an odd function of coordinate, which are T-odd and P-odd (i.e. they change sign under either the T or P operations). A possible manifestation of this nonreversality is gyrotropic linear dichroism/birefringence in cubic crystals. A detailed examination of gyrotropic linear dichroism in the zincblende semiconductor GaAs has been conducted by Bungay et.al.[Bungay, 94a; 94b].

In this thesis, observation of this phenomenon is extended to two new materials, and measurements are described of an intensity dependent effect which is interpreted as a light-induced modification to the linear effect. The nature of the effect is considered in terms of the band structure of the materials examined.

1.2.4 Simulation of Evolution of Partially Polarised Light in Nonlinear Media

This work was motivated principally by papers by Zheludev and Svirko [Svirko,94a;94b], which discussed the use of the evolution of partially polarised light as a diagnostic of time-reversality violation. Svirko and Zheludev dealt theoretically with the case of light which is a mixture of a totally polarised component and a totally unpolarised random component with gaussian statistics. This might represent the output of a single mode laser operating close to threshold, where the polarisation state undergoes random fluctuations due to spontaneous emission. In [Svirko, 94a], the use of partially polarised light in detecting broken time reversibility in linear optical interaction with solids was discussed. In [Svirko, 94b], the interaction of partially polarised light with nonlinear media was discussed.

It was considered that a numerical simulation might prove useful in investigating the behaviour of partially polarised light. A program was written which simulates the evolution of the polarisation state of partially polarised light in a nonlinear medium within the scope of the self-action of a single propagating beam. The simulation was based on the quaternion representation approach [Kubo, 80, 81; Sala, 84;

Zheludev,90a] and treated partially polarised light by averaging the results of the propagation of a large number of randomly generated initial polarisation states.

The simulation was applied initially to the case of partially polarised light propagating in an isotropic nonlinear medium, and results of the numerical simulation were compared with analytical predictions in [Svirko, 94b].

1.3 Thesis Plan

This thesis consists of 6 chapters.

Chapter 1 is an introduction to the topics dealt with in the thesis and an outline of its aims.

Chapter 2 describes the principle of operation of the pump-probe polarimeter used in the experimental work of this thesis, and discusses the modifications made to it in order to minimize dispersion and hence to obtain the best possible time resolution. The construction and operation of a femtosecond Ti:Sapphire laser which was used as the optical source for the polarimeter is also described. Possible sources of noise limiting the sensitivity of the polarimeter are considered, and the magnitudes of the various contributions to the noise are investigated. The possible use of the polarimeter as an autocorrelator, utilizing an ultrafast nonlinear optical response of nickel, is considered.

Chapter 3 describes investigation of the Specular Inverse Faraday effect (SIFE) in a variety of materials. The theory of the SIFE in terms of the material tensors in materials with instantaneous nonlinearity is described. Measurements were made in the high T_c superconductor $YBa_2Cu_3O_{7-\delta}$, the diluted magnetic semiconductor $Cd_{0.6}Mn_{0.4}Te$ with picosecond time resolution and in GaAs and nickel with femtosecond time resolution.

Chapter 4 describes investigation of linear and induced gyrotropic linear dichroism in several zincblende semiconductors. These effects are interpreted as being the result of lack of time-reversal symmetry in the interaction of light with non-centrosymmetric media.

Chapter 5 describes the use of a computer simulation to investigate the evolution of the polarisation state of partially polarised light during propagation in nonlinear media.

Chapter 6 consists of a brief summary of the results described in the previous chapters and a discussion of possible further work.

1.4 References

[Akhamanov, 79] Akhmananov S.A, Zhadanov, B.V, Zheludev N.I, Kovrighin A.I, Kuznetsov V.I, JETP Lett., **29**, (1979), 264.

[Arutyunyan, 75] Arutyunyan V.M, Papazyan T.A, Adonts G.G, Karmenyan A.V, Ishkhanyan S.P. and Khol'ts L, Sov. Phys. JETP, **41**, (1975), 22.

[Atkins, 68] Atkins P.W. and Miller M.H, Mol. Phys., **15**, (1968), 503.

[Bairamov, 73] Bairamov B.H, Zakharchenia B.P, Toporov V.V, Hazhozhev Z.M, Sov. Phys. Solid State, **15**, (1973), 1245.

[Barron, 82] Barron L.D, "Molecular Light Scattering and Optical Activity", Cambridge University Press, Cambridge, 1982.

[Buckingham, 65] Buckingham A.D, Proc. Phys. Soc., **69B**, (1965), 344.

[Bungay, 93] Bungay A.R, Svirko Yu.P, Zheludev N.I, Phys. Rev. B, **47**, (1993), 11730.

[Bungay, 93a] Bungay A.R, Svirko Yu.P, Zheludev N.I, Phys. Rev. Lett., **70**, (1993), 3039.

[Bungay, 93b] Bungay A.R, Kugler N, Zheludev N.I, Physics Letters A, **174**, (1993), 335.

[Bungay, 94] Bungay A.R, Popov S.V, Shatwell I.R, Zheludev N.I, European Quantum Electronics Conference, Amsterdam, Aug 28-Sep 2, 1994.

[Bungay, 94a] Bungay A.R, Pointel Y, Zheludev N.I, Jnl. of Luminescence, **60**, (1994), 36.

[Bungay, 94b] Bungay A.R, Popov S.V, Svirko Yu.P, Zheludev N.I, Chem. Phys. Lett., **217**, (1994), 249.

[Golubkov, 90] Golubkov A.A. and Makarov V.A, Opt. Spectrosc., **69**, (1990) 369.

[Hamaguchi, 80] Hamaguchi H, Buckingham A.D, Kakimoto M, Opt. Lett., **5**, (1980), 114.

[Kubo, 80] Kubo H, Nagata R, Opt. Comm., **34**, (1980), 306.

[Kubo, 81] Kubo H, Nagata R, J. Opt. Soc. Am., **71**, (1981), 327.

[Kuwata, 87] Kuwata M, J. Lum., **38**, (1987), 247.

[Kovrighin, 80] Kovrighin A.I, Yakovlev D.V, Zhdanov B.V, Zheludev N.I, Opt. Comm., **35**, (1980), 92.

[Lawrence, 92] Lawrence T.W, Szöke A, Laughlin R.B, Phys. Rev. Lett., **69**, (1992), 1439.

[Lyons, 93] Lyons K.B, Dillon J.F, Duclos S.J et. al., Phys. Rev. B, **47**, (1993), 8195.

[Maker, 64] Maker P.D, Terhume R.W, Savage C.M, Phys. Rev. Lett., **12**, (1964), 507.

[March-Russell, 88] March-Russell J, Wilczek F, Phys. Rev. Lett., **61**, (1988), 2066.

[Mayer, 64] Mayer G, Gires F, C. R. Acad. Sc. (Paris), **258**, (1964), 2039.

[Murnane, 94] Murnane M.M, Kapteyn H.C, private communication, (1994).

[Popov, 94] Popov S.V, Svirko Yu.P. and Zheludev N.I, Optics Letters, **19**, (1994), 13.

[Popov, 96] Popov S.V, Svirko Yu.P. and Zheludev N.I, submitted to JOSA.

[Saiki, 92] Saiki T, Takeuchi K, Kuwata-Gonokami M, Mitsuyu T. and Ohkawa K, App. Phys. Lett., **60**, (1992), 192.

[Sala, 84] Sala K.L, Phys. Rev. A, **29**, (1984), 1944.

[Spielman, 92] Spielman S, Dodge J.S, Lombardo L.W et. al., Phys. Rev. Lett., **68**, (1992), 3472.

[Svirko, 94] Svirko Yu. P. and Zheludev N.I, JOSA B, **11**, (1994), 1388.

[Svirko, 94a] Svirko Yu.P, Zheludev N.I, Jnl. of Luminescence, **58**, (1994), 399.

[Svirko, 94b] Svirko Yu.P, Zheludev N.I, Phys. Rev. A, **50**, (1994), 709.

[Svirko, 95] Svirko Yu.P, Zheludev N.I, Opt. Lett., **20**, (1995), 1809.

[Tratnik, 87] Tratnik M.V, Sipe J, Phys. Rev. A, **35**, (1987), 2965.

[Van de Zeil, 65] Van der Zeil J.P, Pershan P.S. and Malmstron L.D, Phys.Rev.Lett. **15**, (1965), 190.

[Vlasov, 71] Vlasov D.V, Zaitseva V.P, JETP Lett., **14**, (1971), 171.

[Wen, 89] Wen X.G, Zee A, Phys. Rev. Lett., **62**, (1989), 2873.

[Zheludev, 90] Zheludev N.I, Parashchuk D.Yu, Soviet Physics JETP Lett., **52**, (1990), 35.

[Zheludev, 90a] Zheludev N.I, Svirko Yu.P, in "Nonlinear Optical Diagnostics of Semiconductor Crystals" ed. Akhmanov S.A and Zheludev N.I, VINITI, Moscow, 1990 (in Russian).

Chapter 2
Time Resolved Specular Micropolarimetry

2.1 Synopsis

A pump-probe polarimeter sensitive to polarisation azimuth rotation of 1 μradian and with femtosecond time resolution is described. An introduction to nonlinear polarimetry is given in (2.2). The design of the polarimeter is described in (2.3). A femtosecond modelocked Ti:Sapphire laser constructed for use with the polarimeter is described in (2.4). Improvements to the time resolution of the polarimeter are described in (2.5). The use of the polarimeter in pulse duration measurements is discussed in (2.6). The limits on the polarimeter's angular sensitivity are discussed in (2.7).

2.2 Introduction to Polarimetry

A polarimeter is a device which measures the effect of interaction with a sample on the polarisation state of a light beam [for review see: Hauge, 80]. A polarimeter requires a light source and a polariser to set the initial polarisation state of the light, and a second polarising element (the analyzer) and a photodetector to determine the final polarisation state of the light after interaction with the sample. For a polarimeter which does not rely on modulation, sensitivity will in general be limited by the extinction ratio of the polariser/analyzer pair. Dichroic polarisers (e.g. polaroid) typically have extinction ratios of $\sim 10^{-2}$, and birefringent prism polarisers (e.g. Glan prisms) have typical extinction ratios of 10^{-6}, although better values can be achieved by careful selection of the prisms. The use of harmonic generating crystals as

analyzers can produce extinction ratios of 10^{-9} [Saltiel, 87], but this is not likely to be a generally convenient approach.

The use of modulation techniques allows the sensitivity of polarimeters to be increased without improving the quality of the polarisers. The desired signal is extracted at the modulation frequency, and signals at other frequencies (such as the broad bandwidth noise and the zero frequency signal due to the extinction ratio) are electronically suppressed, except in a narrow frequency band centred on the modulation frequency. This means that the extinction ratio is no longer a limitation on sensitivity, and that detected noise is greatly suppressed. An obvious and widely used method of modulation is the use of a rotating polarising element [see, for example: Aspnes, 75; Azzam, 85; Hauge, 75]. However, modulation of the characteristics of a polarisation element by means of an electrooptical or magnetooptical effect allows a frequency of modulation much higher than any easily achievable frequency of rotation of a mechanical modulator. This is advantageous, since there are some noise sources (e.g. (1/f)-noise, harmonics of mains frequency, mechanical noise) which become less significant at higher frequencies. Examples of electronically driven modulators include piezo-birefringent modulators [Martin, 78; Sato, 81] and modulation of the plane of polarisation of light by means of the optical Faraday effect. Polarimeters based on Faraday modulators have been used in the study of intensity beats in radiation from atoms with a split excited state [Aleksandrov, 65], to study the optical properties of crystals [Becker, 91], and to search for rotation of light polarisation azimuth due to parity non-conservation in atomic vapours [Soreide, 76; Baird, 76; Lewis, 77; Fortson, 80; Hollister, 81; Tregidgo, 86; Macpherson, 87; Taylor, 87; Wolfenden, 90; Edwards, 95]. In the above work, polarimeters with Faraday modulators have been developed with better than 10^{-7} radian angular sensitivity.

Reflective polarisation measurement techniques have been used in the study of surface anisotropy [Aspnes, 85; Habraken, 80; Hanekamp, 82; Kotz, 83]. The surface magneto-optical Kerr effect has been used to measure surface magnetic anisotropy

[Qian, 90; Gudeman, 90; Mulhollan, 91]. Specular (i.e. normal incidence reflection) polarisation measurements have been made by a number of groups in attempts to observe the optical manifestation of the broken time reversal symmetry called for by some theories in the superconducting phase of cuprate materials [Halperin, 89; Weber, 90; Lawrence, 92; Spielman, 92; Lyons, 93].

A number of groups have attempted to observe the controversial effect of specular optical activity [Takizawa, 81; Luk'yanov, 90]. The first successful observation of Specular Optical Activity was made in α-HgS by [Bungay, 93] using a highly sensitive polarimeter based on a Faraday modulator. The same polarimeter was also used to observe Specular Gyrotropic Birefringence in GaAs [Bungay, 93a]. The design of the nonlinear pump-probe polarimeter described below was based on the linear polarimeter used in these experiments.

Pump-probe techniques are used to investigate the effects of excitation of a medium by an intense light beam (the pump) by the use of a separate probe beam. Some pump-probe experiments have been conducted without the use of pulsed lasers [Weiman, 76; Liao, 77]. However, the use of pulsed lasers not only greatly increases the available intensity of the excitation, but allows the temporal behaviour of the material to be monitored, by varying the mutual delay between the pump and probe pulses. In transmission, pump-probe techniques have been widely used in polarimetry [Danishevskii, 81; Afanas'ev, 75; Kuwata, 84; Apanasevich, 87; Takeuchi, 90, Kawazoe, 93]. Pump-probe measurements have also been used to study coherent interactions of the pump and probe [Kuwata, 86].

Transient pump-probe polarimetric measurements in a reflective geometry include observation of electron-hole plasmas in Germanium [Austin, 74] and monitoring of silicon melting by a pulsed excimer laser [Jellison, 85]. Polarisation dependent photo-reflectivity measurements were used in the first observations of the Specular Inverse Faraday effect in CuCl and HgI_2 [Kuwata, 87] and of the specular Kerr effect in ZnSe [Saiki, 92]. Pump-probe polarimetry has been used to investigate dynamics of

the nonlinear nonlocal optical response of dense electron-hole plasmas [Zheludev, 90] in GaAs, coherent phonon oscillations in GaAs [Cho, 90] and carrier spin relaxation in quantum wells [Sham, 93; Bar-Ad, 91; Stark, 92].

2.3 Design of Pump-Probe Specular Micropolarimeter

A pump-probe specular polarimeter has been developed from the linear polarimeter described in [Bungay, 93; 93a]. It was first used in conjunction with a Nd:YAG laser in experiments described in chapters 3 and 4 of this thesis. The time resolution in these experiments was limited by the pulse length of the Nd:YAG laser (80 picoseconds). A polarimeter of the same design was used in conjunction with a 2 picosecond pulse length Ti:Sapphire laser in measurements of the dynamics of the Specular Inverse Faraday effect in GaAs [Bungay, 94]. Again, time resolution was limited by the pulse length of the laser. In order to improve time resolution, a femtosecond modelocked Ti:Sapphire laser was constructed for use with the polarimeter (see section 2.4), and modifications were made to the design of the polarimeter in order to reduce dispersion (see section 2.5). With this arrangement, a time resolution of ~ 30 femtoseconds was achieved in some of the experiments described in chapter 3.

2.3.1 Principle of Operation of Specular Micropolarimeter

The polarimeter is designed to measure changes in the polarisation azimuth of a light wave which occur on reflection from the surface of a sample. In order to understand the operation of the polarimeter, we will start by describing its use to measure linear (i.e.intensity independent) polarisation azimuth rotation. The polarimeter is based on modulation of polarisation azimuth by a Faraday modulator and the use of a birefringent calcite prism which acts as both polariser and analyzer. Measurement of polarisation azimuth rotation is by phase sensitive detection at the frequency of polarisation azimuth modulation of the component of the reflected beam which has orthogonal polarisation to that initially set by the birefringent prism (figure 2.1).

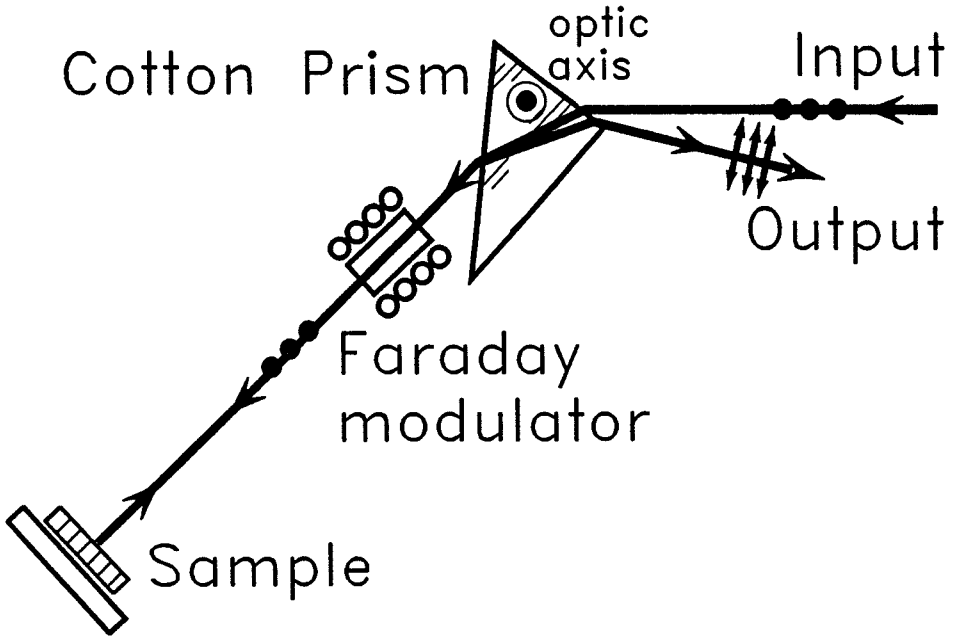

Figure 2.1 Configuration of the polarimeter for single beam experiments

Figure 2.2 illustrates the principle of operation of the polarimeter. It represents the transmitted intensity through the analyzer for a polariser/analyzer pair with their polarisation axes at an angle of $\pi/2$ to one another as a function of the rotation of the polarisation azimuth of the light between the polariser and analyzer. The polarisation azimuth rotation of the light which we wish to measure is represented by α. In addition to the rotation α, the polarization azimuth direction is modulated at frequency Ω_1 by the Faraday cell. In figure 2.2, the magnitude of α is exaggerated with respect to the magnitude of the modulation for the sake of making the origin of the terms in the output intensity at frequencies Ω_1 and $2\Omega_1$ more apparent. If $\alpha=0$, then the polarisation azimuth angle oscillates about the position of minimum transmission at frequency Ω_1. Because transmitted intensity is an even function of azimuth angle, it is modulated at frequency $2\Omega_1$. If $\alpha\neq 0$, then polarisation azimuth angle oscillates about a position other than the position of minimum transmission, and the output intensity contains a component modulated at frequency Ω_1. Since changes in the ellipticity of the light wave between the polariser and analyzer do not move one away from the position of maximum extinction, but merely reduce the extinction ratio, the polarimeter is sensitive only to polarisation azimuth rotation and not to elliptisation

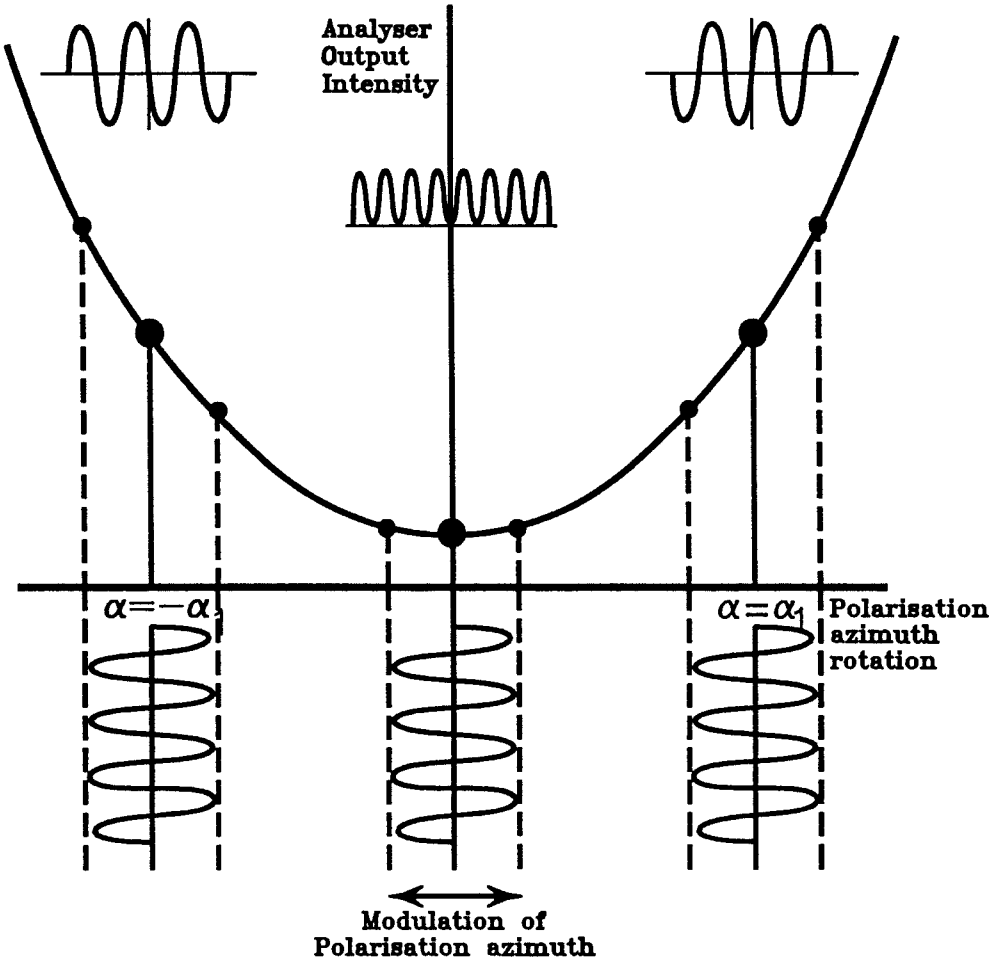

Figure 2.2 Illustration of the principle of operation of the polarimeter

of the light.

For a detailed analysis of the expected output of the polarimeter in terms of the Stokes vector of the light and the Mueller matrices of the optical components, see [Bungay, 95]. If the light wave is reflected from the sample and the Faraday modulator alters the polarisation azimuth of the light by an angle $\phi = 2A\cos\Omega_1 t$ (allowing for the fact that the light wave passes through the modulator twice), then the intensity of the light transmitted by the analyzer will be:

$$I_{out} = \frac{I_r}{2}[1 + h + (h-1)(\cos 2\phi \cos 2\alpha \cos 2\eta + \sin 2\phi \sin 2\alpha \cos 2\eta)] \qquad (2.1)$$

where I_r is the reflected light intensity, α and η are the polarisation azimuth rotation and elliptisation which occur on reflection from the sample and h is the extinction ratio of the polariser/analyzer pair. For A, α, $\eta \ll 1$:

$$I_{out} = I_r[-4A\alpha\cos(\Omega_1 t) + 4A^2(1+\cos(2\Omega_1 t)) + h] \tag{2.2}$$

It can be seen that the transmitted intensity has only one component at the modulation frequency Ω_1, which is linearly dependent on α

$$I_{out}(\Omega_1) = -4A\alpha I_r \tag{2.3}$$

one component at twice the modulation frequency ($2\Omega_1$), which is independent of α

$$I_{out}(2\Omega_1) = 4A^2 I_r \tag{2.4}$$

and terms at zero frequency

$$I_{out}(0) = (4A^2 + h)I_r \tag{2.5}$$

It can be seen that there is no dependence of the output of the polarimeter at frequency Ω_1 on ellipticity η. The output of the polarimeter at frequency Ω_1 is sensitive only to polarisation azimuth rotation.

Most of the experimental work described in this thesis concerns nonlinear pump-probe polarimetry, i.e. changes in the polarisation state of a probe wave induced by a pump wave. A mode-locked laser acts as the optical source, the light is split into separate pump and probe beams, and induced polarisation azimuth rotation is measured as a function of the relative delay between the pump and probe pulses by varying the path length of one of the pulses. The pump-probe polarimeter operates on similar principles to the linear polarimeter, but with an additional high intensity pump beam, coincident on the sample with the probe beam. The pump beam is chopped at a frequency Ω_2 different from the Faraday modulator frequency Ω_1. This makes it possible to extract only the polarisation azimuth rotation which is due to the presence of the pump beam, and neglect any intensity-independent polarisation effects.

In the presence of a pump beam, there are two components to the polarisation azimuth rotation α. If the time dependence of the square wave output of the chopped pump is approximated by $\frac{1}{2}(1+cos\Omega_2)$, then the polarisation azimuth rotation as a function of time is

$$\alpha = \alpha_0 + \frac{1}{2}\alpha_{ind}(1 + \cos\Omega_2 t) \tag{2.6}$$

where α_0 is the component of polarisation azimuth rotation which is independent of the pump intensity and $\alpha_{ind}=\mu I_p$, where μ is a constant and I_p is the intensity of the pump beam. Substituting this equation for α into equation (2.2), we obtain the following formula for the output intensity at frequency $(\Omega_1+\Omega_2)$

$$I_{out}(\Omega_1+\Omega_2) = AI_p\alpha_{ind} \tag{2.7}$$

Detection at the sum-frequency $(\Omega_1+\Omega_2)$ is sensitive solely to pump-induced rotation.

2.3.2 Pump-Probe Specular Micropolarimeter for Picosecond Measurements

The nonlinear polarimeter was constructed for use with a frequency doubled mode-locked CW Nd:YAG laser producing 80 picosecond pulses with 82 MHz repetition rate at wavelength λ = 532 nm as the optical source.

Figure 2.3 is a schematic of the optical components of the polarimeter. All the mirrors used in the polarimeter are first-surface aluminium mirrors. The laser beam is split into pump and probe beams by beamsplitter BS. The pump beam intensity is controlled by variable attenuator VA. The pump arm of the polarimeter consists of a corner cube reflector attached to a translating mount, allowing a variable optical delay. The pump and probe beams both pass through the birefringent prism BP, acquiring identical linear polarisation. The probe beam then passes through the Faraday modulator FM, which modulates the polarisation azimuth of the light with frequency Ω_1. The pump beam is chopped at frequency Ω_2. If the desired polarisation of the pump beam is different from that of the probe, a waveplate may be inserted

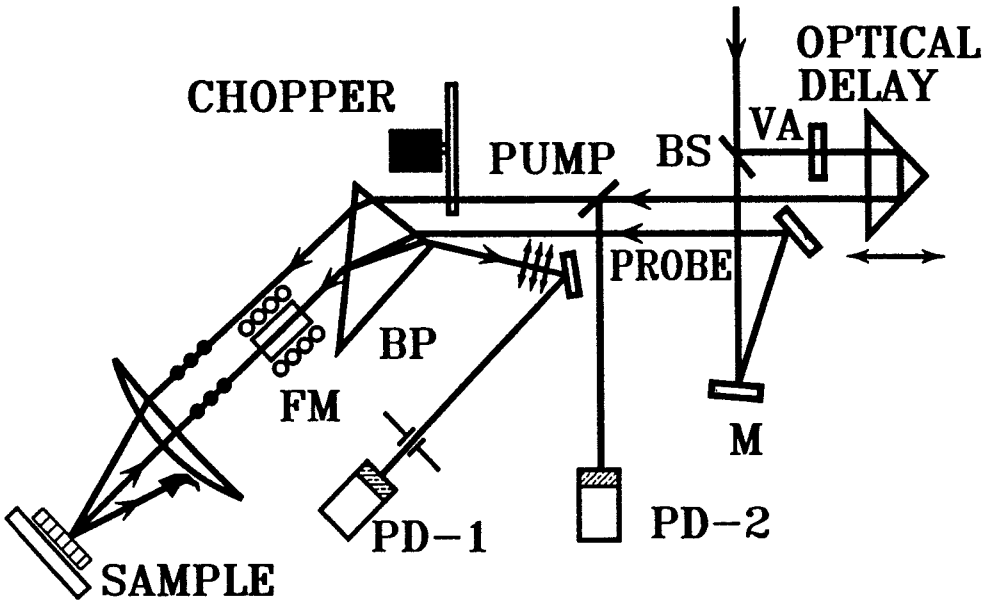

Figure 2.3 Pump-probe specular polarimeter

to modify its polarisation after it has passed through the birefringent prism BP. The pump and probe beams are focused by a lens onto the sample. The probe beam strikes the sample at exactly normal incidence, and the reflected probe retraces its path, passing through the Faraday modulator FM a second time. The component of the reflected probe which has the orthogonal polarisation to that originally set by the prism is isolated by the birefringent prism BP and directed to the photodetector PD-1. The pump beam strikes the sample at a small angle to the normal, and the reflected pump beam is blocked close to the sample surface, in order to minimise the amount of pump light which might leak into PD-1. The intensity of the incident light is monitored by PD-2, which detects light from the pump beam which is reflected from one of the faces of the birefringent prism, and the output of PD-1 is normalised against this.

The pump delay line consists of a glass corner cube retroreflector mounted on a rail with travel of 45 cm, giving a possible range of mutual pump-probe delay of 3 nanoseconds. The delay line is driven by a stepper motor controlled by a personal computer. The minimum step length is equivalent to a change of delay of 0.08 picoseconds.

The birefringent (Cotton) prism BP acts as both polariser and analyzer. This has the advantage of very good mechanical stability; any movement of the polarisation axis of the polariser is matched by movement of the analyzer. Another advantage is that it allows the probe to be exactly normally incident on the sample. The prism was cut from a calcite crystal with polished faces parallel to the optic axis and internal angle 62°. Ideally, the laser light, which should already have fairly good linear polarisation, should enter the prism at Brewsters angle (57° for $\lambda=532$ nm) to minimise reflection losses. Due to the birefringence of calcite ($\Delta n=0.14$) the o- and e- polarised rays emerge from the prism at a mutual angle of $\sim 16°$, making it possible to select one polarisation component. Using a metallic mirror to retroreflect light through the prism, the extinction ratio of the prism was found to be $\sim 10^{-6}$. In practice, imperfections in the samples and the other components of the polarimeter limit the effective extinction ratio to $\sim 5\ 10^{-6}$.

The Faraday effect is rotation of the polarization azimuth of a light wave passing through a medium due to a magnetic field applied along the propagation direction of the light wave. The Faraday modulator FM utilises a ytterbium gallium garnet (TGG) rod of length 5 mm. TGG has a Verdet constant of 170 $\text{radT}^{-1}\text{m}^{-1}$ at $\lambda=532$ nm and 80 $\text{radT}^{-1}\text{m}^{-1}$ at $\lambda=810$ nm. The faces of the TGG rod are slightly non-parallel in order to avoid multiple reflections inside the rod. A sinusoidally time-dependent magnetic field is generated by a coil supplied with an oscillating current, causing the polarisation azimuth of the light passing through the crystal to be modulated at the driving frequency Ω_1. The rotation constant of the coil is $5.7\ 10^{-5}$ rad mA^{-1} at $\lambda=532$ nm and $2.7\ 10^{-5}$ rad mA^{-1} at $\lambda=810$ nm . The resistance of the coil is small (27 Ω), but the inductance of the coil (0.20 L) contributes significantly to the impedance at the driving frequency of 1.44 KHz ($Z=1.8$ kΩ). In order to be able to deliver a sufficiently large driving current, a capacitance is placed in series with the coil, creating a circuit which is resonant at the driving frequency. The FM modulates the polarisation azimuth of a beam which passes through it with amplitude $A=5.10^{-3}$rad. Because the probe beam passes through the FM twice, the polarisation azimuth is in fact modulated with amplitude $2A=10^{-2}$rad.

The pump and probe beams are focused by a lens to a spot size of ~ 20 μm. The pump and probe beam are incident on the sample at a mutual angle of $\sim 5°$. A 10 μm pinhole on a mount with precise 3-axis translation is used to ensure overlap of the spots. Using the pinhole and a power meter the focal plane (where the spot size is smallest) is accurately located. The probe beam is then focused into the pinhole whilst the pump is blocked, and the pinhole position fixed. The pump beam is then aligned to the same position with an accuracy of better than 2 μm.

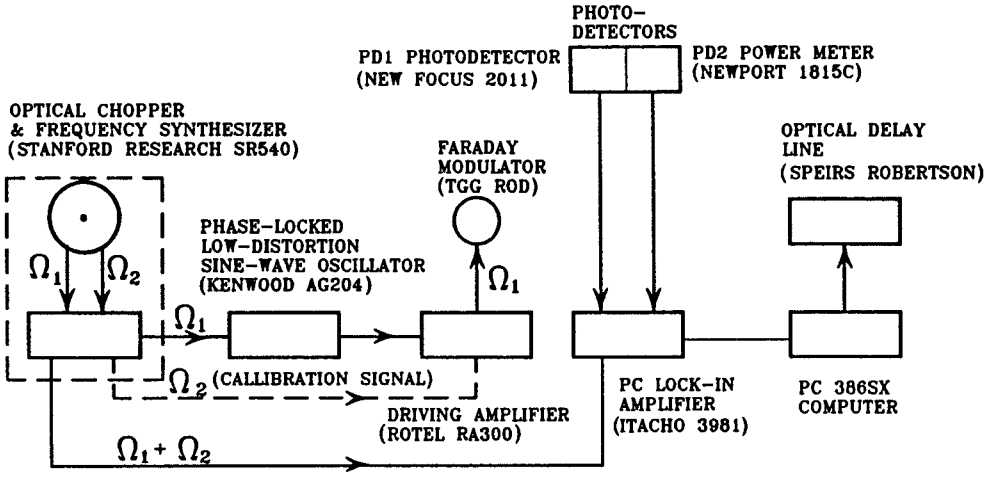

Figure 2.4 Electronic components of pump-probe polarimeter

Figure 2.4 shows a block diagram of the electronic components of the polarimeter. The modulation frequencies Ω_1, Ω_2 are set by the Stanford Research chopper, SR590, which was used to modulate the pump intensity. The chopper disk has two sets of slots; an inner and an outer ring. The inner ring has 25 slots, while the outer has 30. Therefore the ratio of chopping speed of the two rings is 5/6. The pump beam passed through the inner ring, and was chopped at frequency Ω_2=1200 Hz. The chopper is designed to output reference signals at the frequency of the inner and outer rings, or at their sum or difference frequencies. The signal at frequency Ω_1=1440 Hz from the chopper was used as a locking frequency for a Kenwood signal generator, which output a sinusoidal signal to a Rotel RA300 amplifier. The output of the amplifier was used to drive the Faraday modulator. The output from the chopper at frequency $\Omega_1+\Omega_2$ is sent to the ITHACO 3981 lock-in amplifier as a reference frequency. The

output of photodetector PD-1 is monitored by phase sensitive detection using to the ITHACO 3981 lock-in amplifier, which recovers the component of the signal at the sum frequency $\Omega_1+\Omega_2$.

The signal from PD-2 is input to the Analogue to Digital Converter which is incorporated into the lock-in amplifier, and is recorded by the computer and used to normalise the output of PD-1 against laser power fluctuations. The lock-in signal is read directly by the personal computer.

To obtain the value of polarisation azimuth rotation, the output of PD-1 is calibrated against a known rotation. For linear experiments (i.e. with the pump blocked, measuring at frequency Ω_1), this requires that a known d.c. current is applied to the Faraday modulator FM. This is achieved by applying a high resistance source of known voltage in parallel with the sinusoidal driving current. For nonlinear experiments, a signal from the Stanford chopper at the chopping frequency Ω_2 is fed to the Rotel amplifier in parallel with the signal at Ω_1 providing a calibration rotation of 10^{-3}rad at frequency Ω_2.

2.4 Construction of Femtosecond Modelocked Ti:Sapphire Laser

In order to allow femtosecond time resolution experiments to be performed with the polarimeter, a Kerr lens modelocked Ti:Sapphire laser was constructed according to a design kindly provided by M.M.Murnane and H.C.Kapteyn of Washington State University [Murnane, 94]. The Ti:Sapphire was pumped using an Argon ion laser.

2.4.1 Principles of Operation of Ti:Sapphire Laser

If a laser has a number of lasing modes which maintain a fixed phase relationship to each other it is said to be modelocked. If modelocking is complete and all the laser modes are in phase, then the temporal profile of the laser will be the Fourier transform of its spectral profile, and the laser will produce pulses with a duration τ_p

which is related to the FWHM of the laser spectrum $\Delta\nu$ by a factor k which depends only on the pulse shape (e.g. k=0.315 for sech^2 pulses). If modelocking is incomplete or there is phase structure across the spectral profile, then the pulses will be longer.

$$\Delta\nu\tau_p \geq k \tag{2.8}$$

Clearly, a requirement for an ultrafast pulsed laser is that it have a very broad gain bandwidth. Ti:Sapphire is the most commonly used medium for ultrashort pulsed lasers. The first Ti:Sapphire laser was built by Moulton in 1982. Not only does Ti:Sapphire have the broadest bandwidth of any known laser medium, it also has a very high gain cross-section [Moulton, 86]. The Ti:Sapphire laser is a vibronic solid-state laser: strong coupling between the vibrational states of the Sapphire host and electronic states of Titanium ions leads to the broad absorption and emission linewidths [Moulton, 92].

In order to obtain pulses from a laser, it is necessary to provide a mechanism that makes the gain of the laser higher for pulsed operation. A review of numerous mode-locking techniques can be found in [French, 95]. Mode-locking can be performed by modulating the loss in the cavity via an external signal (active mode-locking). The most widely used example of this approach is the method which mode-locks the Nd:YAG laser used in some of the experiments described in this thesis: acousto-optic modulation. This was the method used to produce the first mode-locked laser [Hargrove, 64]. Active mode locking methods have the disadvantage that the width of the modulation is constant and as the pulses become much shorter than the width of the modulation, the difference in loss between the edges and centre of the pulse becomes small, and the pulse compressing effect becomes weak. Active mode locking techniques are generally limited to producing picosecond pulses. Alternately, a mode locked laser may utilise some nonlinear mechanism in the cavity so that the light modulates itself (passive mode-locking) with a modulation width which is equal to that of the pulses. An example of this is the saturable absorber which favours the transmission of intense light. The shortest pulse length possible depends on the response time of the absorber; it ceases to be intensity dependent when the pulse

length is similar to the response time (typically on a picosecond timescale) [DeMaria,66; Bradley,69], although it is possible to obtain shorter pulse widths than this by combining a saturable absorber with a saturable amplifier [Ippen, 72]. Alternately, the optical Kerr effect (intensity dependent change in refractive index) can provide an effectively instantaneous response. The first demonstration of the use of the Kerr effect to modulate cavity losses (by intensity dependent rotation of plane of polarisation) was [Dahlstrom, 72]. Cavity losses can also be made dependent on refractive index through self phase modulation [for example: Mark, 89].

Kerr lens modelocking (KLM), where intensity dependent loss arises from self-focusing of light due to the intensity dependent refractive index, was first observed experimentally by [Spence, 91] and used to produce the first Ti:Sapphire laser pulses shorter than 100 femtoseconds. There results were explained by [Piche, 91]. Intense light induces a non-linear or Kerr lens. If the cavity has lower loss for a more tightly focused beam, this favours shorter more intense pulses. This can be arranged by placing an aperture in the cavity, so that there is lower loss for a narrower beam, or, if the pump beam waist size is smaller than the laser radiation waist, then the self focusing improves the overlap between the laser cavity and the pump [Brabec, 92]. This system has been used to produce the shortest pulses ever generated directly in a laser cavity [Asaki, 93]. Kerr lens modelocking requires high intensities to be effective. For this reason, KLM lasers are not generally self-starting; fluctuations in the single wavelength output of the laser are not sufficient to act as seeds to form the basis of pulses. Numerous methods have been implemented to initiate modelocking in KLM lasers [Curley, 91; Keller, 91; Spielmann, 91]. A mechanism as simple as shaking one of the mirrors may be sufficient to start modelocking [Likforman, 91], and once started the modelocking is self-sustaining.

For pulses much less than ~ 100 femtoseconds in duration, group velocity dispersion (GVD) is an important factor which broadens pulses by causing the different frequency components of the pulse to propagate at different speeds. Dispersion is defined as pulse broadening per unit bandwidth:

$$\frac{\Delta t}{\Delta \omega} = L\frac{d^2k}{d\omega^2} = L\frac{\lambda^3}{2\pi c^2}\frac{d^2n}{d\lambda^2} \tag{2.9}$$

The materials which are generally used in lasers show what is called "normal" or positive dispersion in the visible/near-IR. That is, they transmit shorter wavelengths more slowly than longer wavelengths. At 810 nm, the dispersion of a 1 mm thickness of silica glass is ~ 35 fs^{-2}, while the dispersion of a 5 mm Ti:Sapphire crystal is ~ 300 fs^{-2}. In order to bring the total dispersion in the laser cavity as close to zero as possible, some means of introducing "anomalous" dispersion is required.

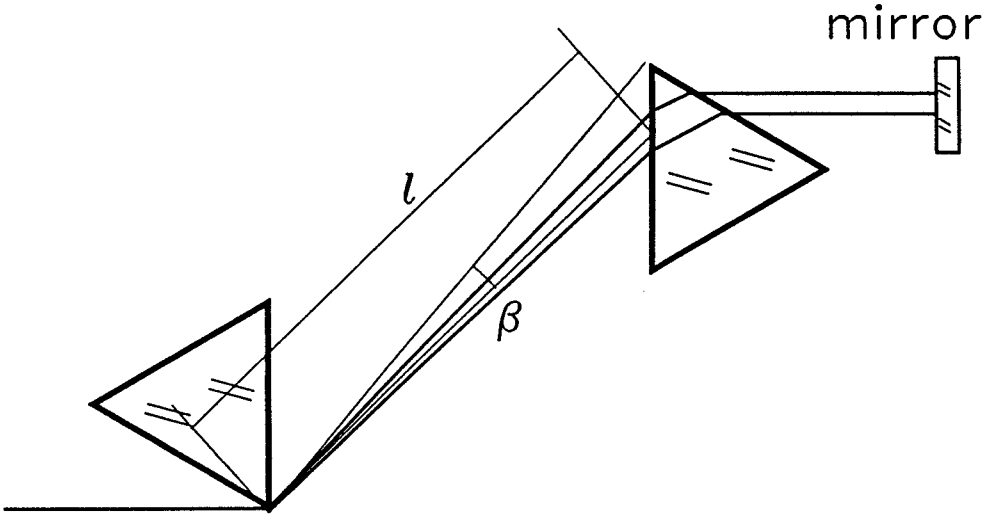

Figure 2.5 Use of prisms to introduce anomalous dispersion

This may be achieved by making use of the dispersive qualities of multilayer dielectric mirrors [DeSilvestri, 84] or using diffraction gratings [Treacy, 69; Kafka,86]. The most common means of introducing anomalous dispersion is by means of a sequence of prisms [Martinez, 84; Fork, 84]. The anomalous dispersion is created by causing the longer wavelengths to travel a greater distance than the shorter wavelengths. A sequence of 4 prisms can be used to produce anomalous dispersion while maintaining the spatial profile of the laser beam. Equivalently, retroreflecting the light after the second prism produces a system of two prisms which has the same value of total dispersion (figure 2.5). The total dispersion of such a system of prisms is [Fork, 84]:

$$\frac{d^2\phi}{d\omega^2} = -\frac{\lambda^2}{2\pi c^2} 4l\{[\frac{d^2n}{d\lambda^2}+(\frac{dn}{d\lambda})^2(2n-\frac{1}{n^3})]\sin\beta - 2(\frac{dn}{d\lambda})^2\cos\beta\} \quad (2.10)$$

where l is prism separation and β is the angle between the laser beam as it propagates between the two prisms and the line joining the vertices of the prisms. The first term is due to material dispersion and the second due to angular dispersion. The path length of the light through the prism material is determined by $l\sin\beta$. In order that the prisms accommodate the beam, $l\sin\beta$ must be greater than or approximately equal to twice the beam diameter, say ~2 mm. This means that the total dispersion of this prism arrangement becomes negative for silica prisms at λ=810 nm for a prism separation greater than 30 cm. The exact amount of anomalous dispersion may be controlled in practical situations by adjusting the prism insertion, hence changing the amount of material dispersion.

Practical limits on laser cavity length place an upper limit on prism separation, and hence on the amount of dispersion that can be compensated in this manner. Therefore the amount of material dispersion in the laser cannot be too great, limiting the length of the lasing medium to a few millimetres.

For very short pulses, even third order dispersion must be considered. A prism material must be selected whose third order dispersion is such as to counter the third order dispersion of the rest of the components of the laser. This makes prism separation a crucial parameter. The amount of third order dispersion will depend on how far the prism is inserted into the beam, meaning that this parameter is no longer freely adjustable. There will be some optimum prism separation l where the correct prism insertion to compensate the second order dispersion of the laser will match the prism insertion required to compensate third order dispersion.

For very short pulses (broad bandwidths) there are other considerations which might limit pulse length, such as nonlinearities in the elements of the laser, but these do not seem to be the significant limiting factors, even for an 11 femtosecond pulse

[Asaki,93].

2.4.2 Design of Femtosecond Ti:Sapphire Laser

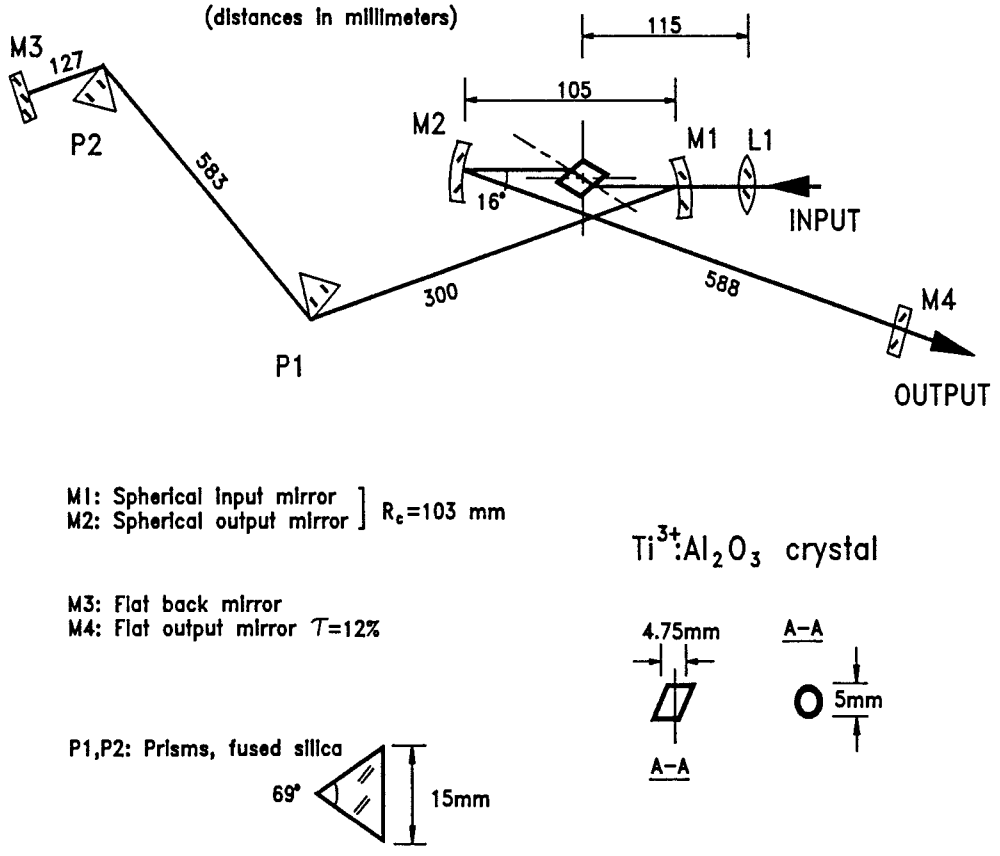

Figure 2.6 Ti:Sapphire laser

The Ti:Sapphire was built according to a design kindly provided by M.M.Murnane and H.C.Kapteyn of Washington State University, U.S.A. [Murnane, 94]. Figure 2.6 is a diagram of the laser, with distances and angles marked.

The laser crystal is a Brewster cut, 5 mm length rod of 0.15% titanium doped sapphire, which absorbs ~90% of the pump light. The crystal is shorter and more heavily doped than is usual for Ti:Sapphire lasers, in order to limit dispersion while allowing high output power. The prisms are made of fused silica, the material being selected so that the third order dispersion of the prism compensates the third order

dispersion in the other elements of the laser [Asaki, 93].

The temperature of the Ti:Sapphire crystal is stabilized at 15°C by cooling water from a reservoir kept at a set temperature. A more precise system of temperature control using a thermocouple and a water-cooled Peltier cooler attached to the crystal mount was considered, but the pump system proved to be adequate to maintain stability of the laser. Since the laboratory is in any case air-conditioned, the cooler does not have to cope with a wide range of temperatures.

The modelocking is not self-starting. A simple shaker is used to initiate modelocking. This consists of a solenoid driven by an a.c. supply at ~ 15 Hz, which is glued to the side of the mount of the mirror M2. The vibrations generated are sufficient to start the laser modelocking. Since the shaker also causes noise on the laser output, it is switched off once the laser is modelocked. The modelocking of the laser is constantly monitored by a fast photodetector, into which a fraction of the output beam of the laser is directed. The output of the detector is fed to a fast oscilloscope, allowing the user of the laser to monitor the modelocking.

The main cause of loss of modelocking is dust falling into the beam. This is particularly important near the laser crystal, where the beam is focused to a small diameter. The optical bench on which the laser (and polarimeter) were constructed is covered by a clean-air cabinet consisting of a solid roof with plastic curtains. A fan with a filter in the roof of the enclosure blows dust free air into the enclosure. In addition, a smaller enclosure with aluminium sides (containing holes for the passage of the laser and pump laser beams) and a perspex lid covers the crystal, focusing mirrors, lens and one of the prisms. The cover must be removed and the curtains rolled back in order to tune the laser, but are put in place when the laser is in use. With the dust protection in place the laser will remain modelocked without interruption for several hours at a time.

2.4.3 Operation of Femtosecond Ti:Sapphire Laser

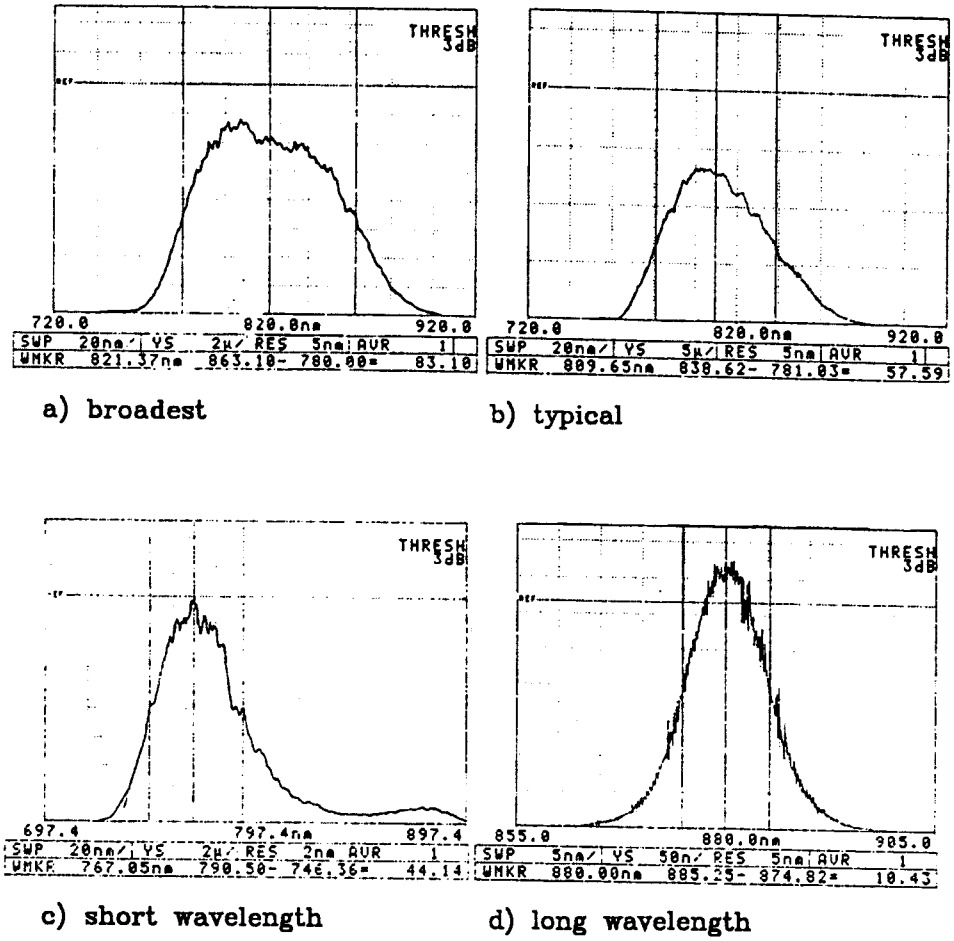

Figure 2.7 Modelocked spectra of Ti:Sapphire laser

Initially, the pump laser used with the Ti:Sapphire was a 21 year old Spectra-Physics Model 171 Argon ion laser. This laser had no feedback system to control beam position and poor pointing stability. It suffered from long-term drift which had the effect of causing the Ti:Sapphire to require retuning every few hours of operation. A custom-made beam-steering system was employed in an attempt to compensate for beam motion. A small fraction of the pump beam was extracted by a beam splitter and was incident on a detector consisting of four photodetectors forming the quadrants of a circle. One of the steering mirrors of the argon ion was mounted on piezoelectric transducers. The voltage to the transducers was controlled by the output of the quadrant photodetector. This system reduced the magnitude of fast fluctuations, but they remained a significant fraction of the beam width. The long term drift was

corrected more precisely by manually adjusting the steering mirrors so that the extracted reflection passed through two pinholes separated by a path length of ~3 m. Another problem with the pump laser was that the mode structure of the beam deteriorated at high output powers, effectively limiting the pump power to less than 4 W. Eventually this laser failed completely, and a new pump laser was purchased.

The new pump laser was a Spectra-Physics Model 2060, with an internal beam pointing stabilising system (Beamlok). This gives the laser a beam pointing stability in beam position of <0.5 μm/°C and in beam direction of <50 μrad/°C, making any deviation of the beam during operation negligible. With this laser the Ti:Sapphire displays stable modelocking and requires only occasional tuning to maintain the modelocking regime.

The Ti:Sapphire can produce about 800 mW in single wavelength operation, and about 600 mW whilst mode-locked, with 4 W pump power. The bandwidth and centre wavelength of the laser can be adjusted by changing the insertion of the prisms and retuning of the laser cavity. Fig.2.7 shows some typical spectral profiles for the laser. With a centre wavelength in the range 800-820 nm, a bandwidth of about 80 nm may be obtained (figure 2.7a), although the laser was generally operated with a somewhat lower bandwidth (figure 2.7b). Centre wavelengths ranging from ~770 nm to ~880 nm (figure 2.7c,d) may be obtained, although the attainable bandwidth becomes narrow and the modelocking becomes less stable at the extremes of this range. Assuming transform limited pulses, a bandwidth of 80 nm should allow pulses as short as 9 femtoseconds to be produced. However, in order to utilise such short pulses, 2nd and 3rd order dispersion compensation would have to be applied to the pulses outside the cavity [Asaki, 93], since the dispersion of elements outside the laser cavity, such as the output coupler and the components of the polarimeter, will significantly increase the pulse length. Measurements of the pulse length for a femtosecond laser by techniques such as second harmonic generation presents a problem for the same reason: dispersion in the frequency doubling crystal and other elements of the autocorrelator. In fact, values of pulse length were obtained by using

the specular polarimeter, which was redesigned to minimise dispersion (see section 2.5 below), and measuring induced polarisation rotation arising from a fast reflective nonlinearity in nickel. The mechanism of this effect will be discussed in section 3.4.4. It returns an intensity autocorrelation of the pulse. Since the principle aim is to optimise the time resolution of the polarimeter, this gives more valuable information than an autocorrelation obtained using a separate device. The shortest obtainable pulses were achieved with a bandwidth rather less than the maximum (figure 2.7b) and were measured to be 32 femtoseconds long. Autocorrelation measurements obtained with two different arrangements of the polarimeter are displayed in the next section.

2.5 Pump-Probe Specular Polarimeter for Femtosecond Measurements

A second polarimeter was constructed for use with the femtosecond Ti:Sapphire laser described in section 2.4. Although the principle of operation of the polarimeter is unchanged, various modifications to the design were made.

Gold mirrors were used for the polarimeter, since aluminium is only ~80% reflective at 810 nm. The pump beam is reflected 4 times in the polarimeter (including the two steering mirrors which are used to direct the laser beam into the polarimeter) which would result in loss of 60% of the light. Gold is 96% reflective at 810 nm, reducing the power loss to 15%.

To make use of the high time resolution potentially available a delay line with a much shorter step length is required. The delay line consists of a translating table with travel of 25 mm, giving a possible range of mutual pump-probe delay of 170 picoseconds. The delay line is driven via a 250:1 gearbox by a stepper motor controlled by the PC. The minimum step length is equivalent to a change of delay of 0.3 femtoseconds.

Figure 2.8 is a block diagram of the electronics of the new version of the polarimeter.

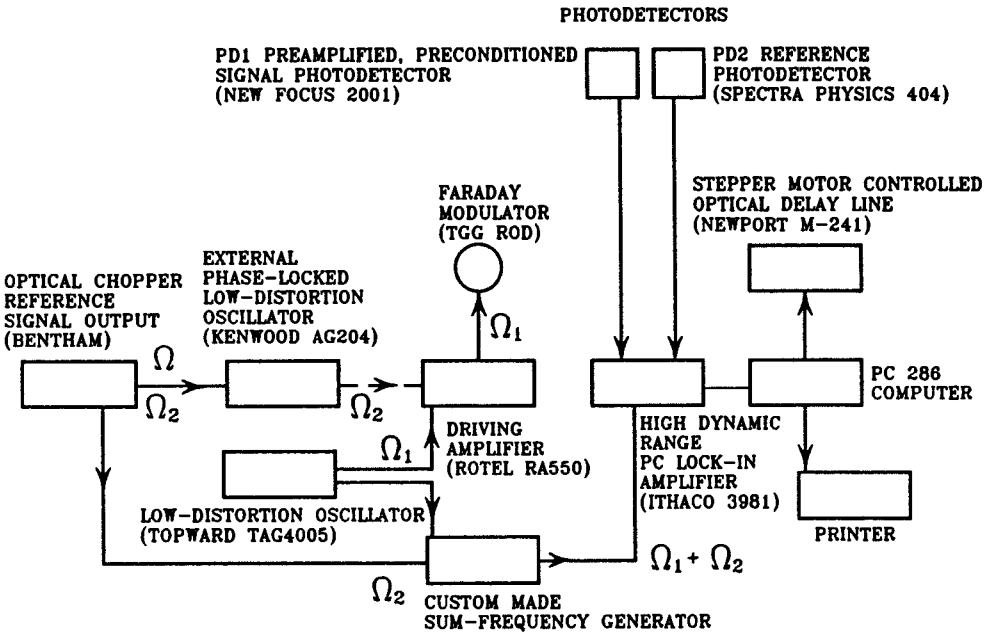

Figure 2.8 Electronic components of modified polarimeter

It was decided that, since laser noise is generally less at higher frequencies, to operate the polarimeter at a higher detection frequency. Since it is practically difficult to chop at high frequencies, it was decided to increase the modulation frequency of the Faraday modulator. The sum frequency $\Omega_1+\Omega_2$ was limited to less than 10 kHz, since this is the highest frequency at which the ITHACO lock-in amplifier is guaranteed accurate. A modulation signal at frequency $\Omega_1 \sim 5.8$ kHz is generated by a Topward TAG4005 low-distortion signal generator and output to the Faraday modulator via a Rotel RA550 amplifier. The amplitude of modulation was $A=4\ 10^{-3}$ rad. A reference signal at Ω_1 from the signal generator is also sent to a custom-built Sum-Frequency Generator. As with the original arrangement, a capacitance is placed in series with the Faraday coil to create a circuit that is resonant at frequency Ω_1. A Bentham optical chopper was used to chop the pump beam at frequency $\Omega_2 \sim 1.8$ kHz. A reference signal from the chopper was also sent to the custom-built Sum-Frequency Generator. There was also provision for a signal from the chopper to the Faraday modulator to act as a calibration signal. Because of the large difference between the frequencies Ω_1 and Ω_2 the fundamental frequency of the chopper reference signal is strongly suppressed in comparison to its harmonics, so sending the square-wave signal

from the chopper directly to the Faraday modulator would produce a heavily distorted signal. The square-wave signal from the chopper was used as a reference for a lockable Kenwood AG204 low-distortion oscillator, which produced a sinusoidal output which could be fed to the low-distortion Rotel amplifier. The calibration signal provided a rotation of peak to peak size 400 μrad. The Sum-Frequency Generator produced an output signal at frequency $\Omega_1+\Omega_2\sim 8$ kHz which was used as the reference frequency for the ITHACO lock-in amplifier.

The most important changes to the polarimeter were concerned with achieving the best possible time resolution. The limit on the time resolution of the polarimeter is given by the duration of the laser pulses when they interact in the sample. Working with ultrashort pulses, it is necessary to minimise the group velocity dispersion of the optical elements of the polarimeter.

The glass corner cube retroreflector was replaced by an open corner-cube reflector with gold surfaces, eliminating this source of dispersion. The Cotton prism was reoriented so that the beams passed through the narrow (28°) corner of the prism, and the beams were aligned vertically with each other. This meant that both beams could pass through the prism as close to the edge as possible, minimising the length of material through which they had to travel. In this way the thickness of calcite through which the beams had to propagate was reduced to ~ 2 mm. Some loss of transmitted power resulted from this, due to the fact that the beams were no longer incident on the prism near brewsters angle, but this was considered acceptable, since the pump intensity potentially available was very high. The silvered glass beam-splitter used in the original polarimeter was replaced by a pellicle beamsplitter, which has negligible dispersion due to its very small thickness. For experiments where a circularly polarised pump was required, a first order waveplate consisting of a ~ 40 μm thick mica sheet was used. Again, the dispersion of this element is negligible due to its small thickness. If we are not concerned with making measurements of the intensity dependence of the effect studied, then clearly the variable attenuator may be removed from the pump arm of the polarimeter.

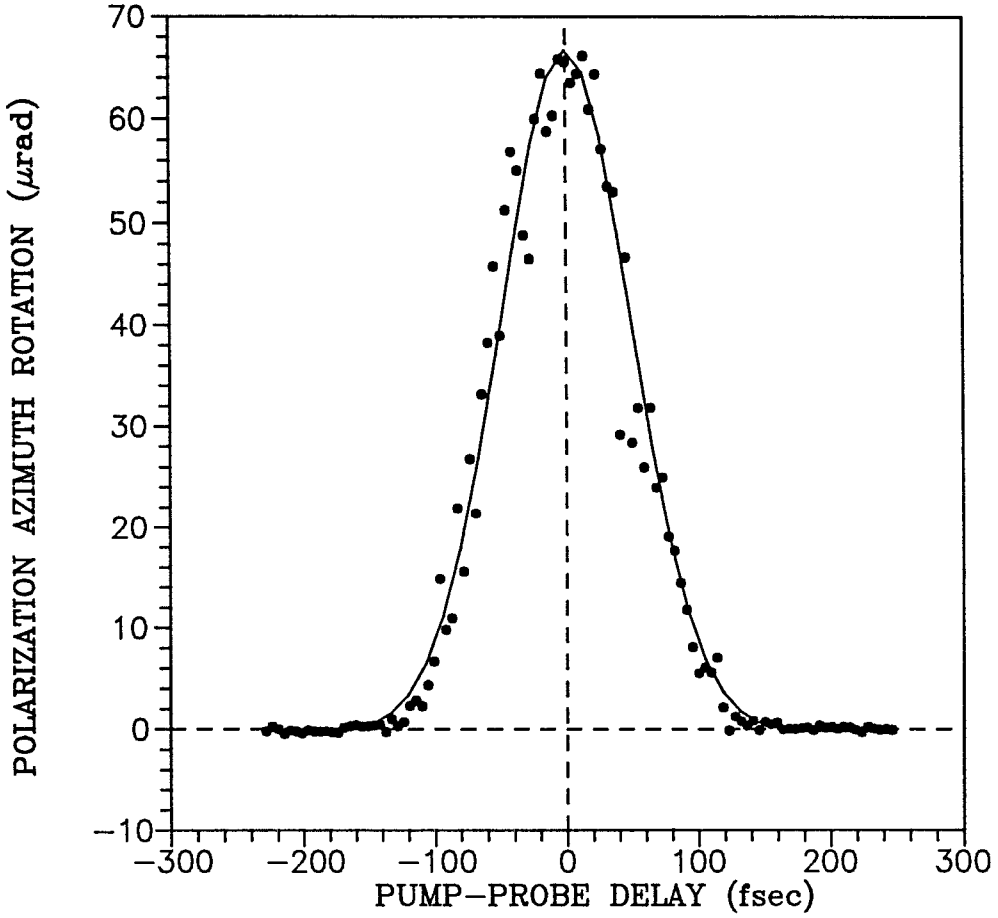

Figure 2.9 Autocorrelation in nickel showing time resolution of polarimeter in standard configuration

The above modifications involved no essential design changes and were made without any sacrifice of sensitivity of the polarimeter. Figure 2.9 shows a pump-probe delay dependence of the Specular Inverse Faraday effect (SIFE) in nickel obtained using the polarimeter in this configuration. The response time of nickel is fast on this timescale (see section 3.4.4), so the time dependence is an intensity autocorrelation of the pulse, from which the pulse length at the sample may be obtained. From this data a pulse length at the sample of 75 femtoseconds is obtained.

This is the configuration in which the time resolved experiments on GaAs described in section 3.4.3 were performed. Since the response time of GaAs in these experiments was on a subpicosecond timescale, the time resolution obtained was considered sufficient. However, in order to fully utilise the potential of the

Ti:Sapphire laser, and in particular with the aim of investigating very fast optical nonlinearities in metals, it was attempted to reduce dispersion in the polarimeter even further.

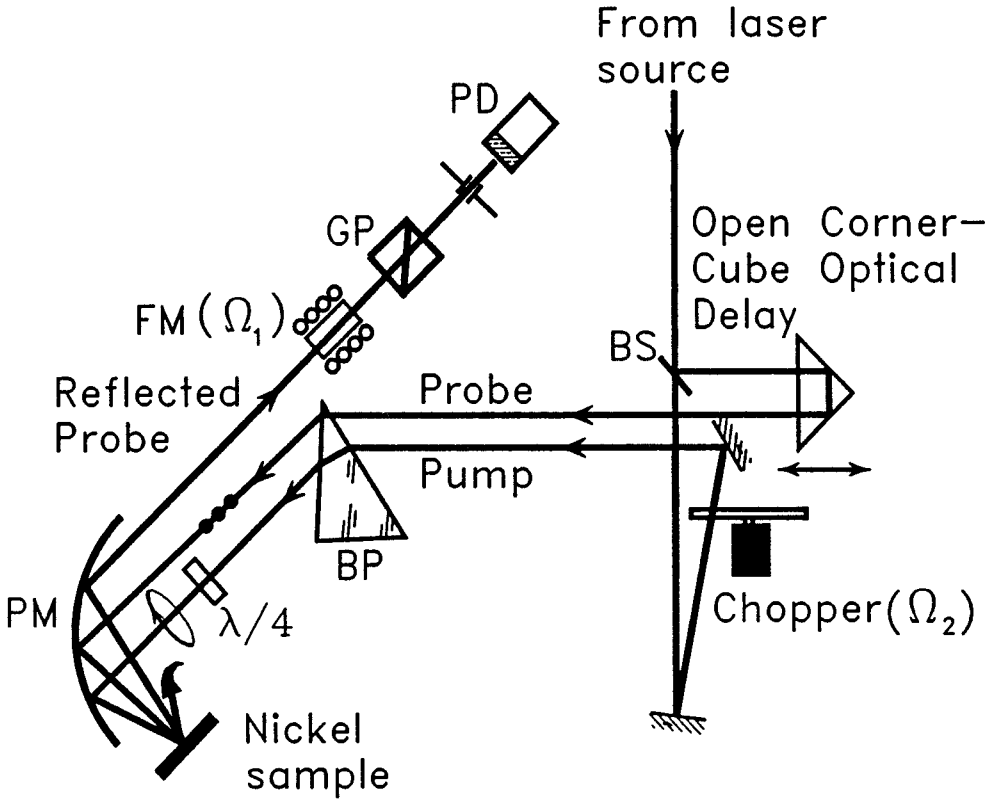

Figure 2.10 Pump-probe specular polarimeter with reduced dispersion, for use with femtosecond Ti:Sapphire laser

The most significant remaining dispersive element was the TGG crystal in the Faraday modulator. However, there is no requirement that the polarisation of the probe beam be modulated before it reaches the sample. If the polarimeter is arranged so that only the reflected probe beam passes through the Faraday modulator, then the effect of the dispersion due to the TGG crystal is eliminated, since the probe does not pass through it until after it has interacted with the pump. This modification has a number of effects on the sensitivity of the polarimeter. The most obvious difference resulting from the probe making only a single pass through the Faraday modulator is that the amplitude of modulation of the probe polarisation azimuth is reduced to half its previous value. The fact that the reflected probe must follow a different path to

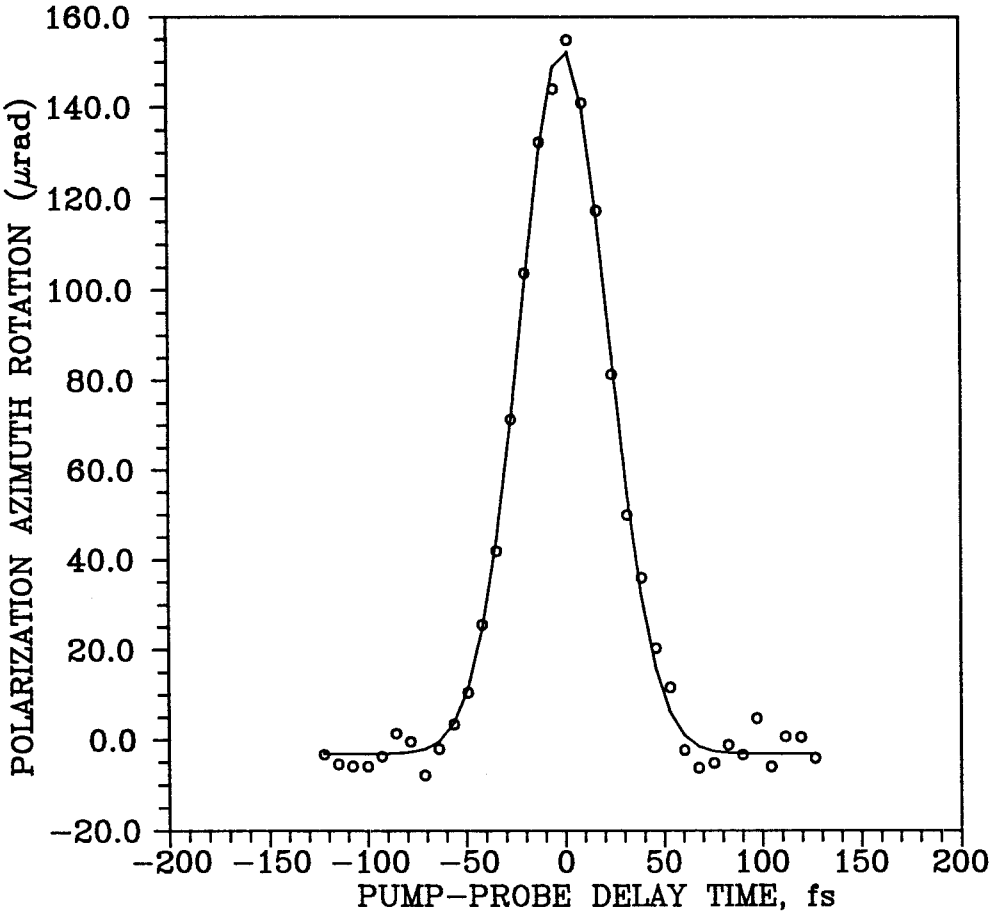

Figure 2.11 Autocorrelation in nickel showing time resolution of polarimeter in reduced dispersion configuration

the incident probe means that the probe cannot be exactly normally incident on the sample, but the angle of incidence can be kept very small ($\sim 1°$) and this should make no significant difference to the optical effects measured. More significantly, the dimensions of the Faraday modulator do not allow it to be inserted between the Cotton prism and the sample if the incident probe is not to pass through the TGG crystal. Also, since the probe is no longer exactly normally incident on the sample, and will undergo some change in polarisation state on reflection as a consequence of this, it becomes desirable to be able to adjust the analyzer independently of the polariser, in order to find the position of maximum extinction. Therefore, the polarimeter must be arranged so that the reflected probe just misses the Cotton prism, and is directed through the Faraday modulator before reaching a Glan prism which acts as analyzer. This arrangement sacrifices the mechanical stability achieved by

using the same prism as both polariser and analyzer.

The focusing lens also contributes to the dispersion of the polarimeter as well as introducing further pulse broadening effects due to chromatic aberration and spherical aberration [Bor, 88; Kempe, 92; 93]. The lens was replaced by a gold parabolic mirror, which eliminated all these problems.

Figure 2.10 shows the reduced dispersion arrangement of the optical components of the polarimeter. The only remaining element in the polarimeter which introduces significant dispersion is the calcite prism. In this (reduced dispersion) configuration, the polarimeter had a time resolution of 32 femtoseconds, as shown in figure 2.11.

The ultimate limit to time resolution of the polarimeter is the transform-limited pulse length of the laser, and should therefore be on the ~ 10 femtosecond timescale. To achieve this time resolution, second and third order dispersion compensation would need to be applied to the laser beam before it entered the polarimeter, to compensate for dispersion outside the laser cavity.

2.6 Use of Polarimeter for Autocorrelation Measurements

As described in section 3.4.4, the polarimeter was used in the reduced dispersion configuration described above in an attempt to resolve the dynamics of the Specular Inverse Faraday effect in nickel. In fact, the pump-probe delay dependence of the SIFE in nickel showed a symmetrical bell-shaped curve even with this time resolution, i.e. the response time of nickel was shorter than the pulse length. As explained in section 3.3 below, the SIFE in a material with fast response will produce an intensity autocorrelation between pump and probe pulses. In effect the polarimeter was used to measure the pulse duration of the Ti:Sapphire laser. This raises the possibility that the polarimeter might form the basis of a new type of femtosecond autocorrelator.

Optical autocorrelation techniques are commonly used for measurement of the duration of femtosecond laser pulses. A variety of nonlinear interactions have been exploited in autocorrelators. These include Second Harmonic Generation [Koldmeder,66], two photon fluorescence [Giodmaine, 67], multiple order fluorescence [Sarukura, 88], the optical Kerr effect [Kane, 93], harmonic generation on reflection [Gierulski, 85] and many others. Clearly, autocorrelation measurements require fast nonlinearities with broad spectral ranges. A technique based on detection of induced polarisation rotation due to the Specular Inverse Faraday effect in nickel has several advantages for autocorrelation. The nonlinear effect used in the correlation is nonresonant and incoherent; it is not strongly sensitive to wavelength, and does not require any phase matching conditions to be met.

Figure 2.12 shows SIFE autocorrelation traces in nickel of a) a Cr:Forsterite laser (λ=1260 nm) with pulse length 76 femtoseconds, measured by Popov.et.al [Popov, 95] using a polarimeter of the same design as that described above, b) the Ti:Sapphire (λ=810 nm) with pulse length 32 femtoseconds.

There is no obvious reason why the technique could not be applied up to wavelengths of several μm, provided a material with fast and strong enough nonlinearity at these wavelengths is available. The only adjustment necessary would be to allow for the different angle at which light of different wavelengths would emerge from the prism. With appropriate dispersion compensation this autocorrelation technique has the potential to measure autocorrelations of pulses as short as $\sim$10 femtoseconds and to be used over a very wide wavelength range in the visible and infrared.

2.7 Sensitivity of Specular Polarimeter

In this section, the limits on the sensitivity of the polarimeter to induced probe polarisation azimuth rotation will be examined. The sensitivity of the polarimeter may be limited by a number of factors. These are discussed below, and table 2.1 provides numerical values for the limits imposed by the various mechanisms described.

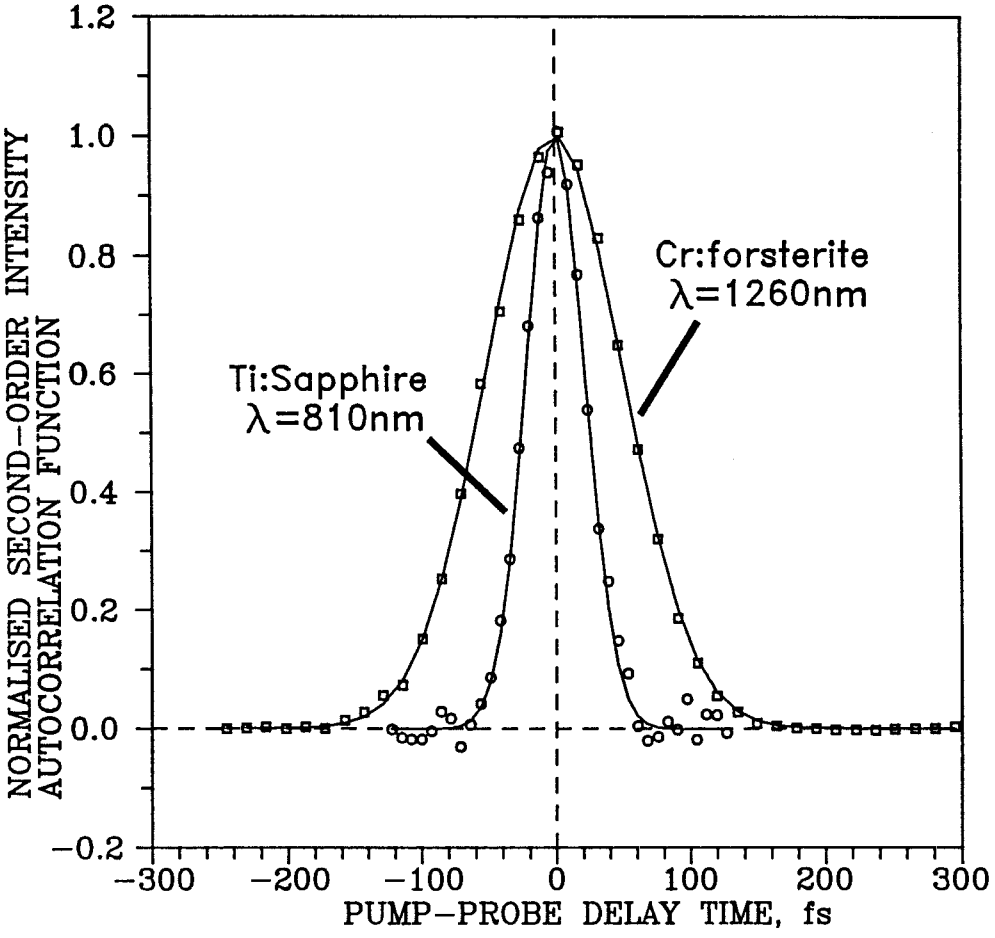

Figure 2.12 Intensity autocorrelation traces in nickel for Ti:Sapphire and Cr:Forsterite lasers

2.7.1 Fundamental Limit to Sensitivity of Polarimeter

The ultimate limit on the angular sensitivity of a polarimeter is given by the uncertainty of the polarisation state of the light, which arises from shot noise in the laser beam [Loudon, 83]. The uncertainty in polarisation azimuth angle due to shot noise is given by $\Delta\alpha_{lim} \sim (2NT)^{-½}$, where N is the number of photons per second emitted by the laser and T is the measurement time. This formula is arrived at for a single mode laser, while modelocked lasers such as the Nd:YAG or Ti:Sapphire have a large number of modes, but for $N \gg 1$ the above formula may be considered reasonably accurate. N may be calculated from the following expression: $N=P_L R\mu_{eff}/\hbar\omega$ where P_L is the power of the probe beam, R accounts for the reflectivity of the sample and other losses and is in the range of 0.1-0.4, μ_{eff} is the

quantum efficiency of the photodiode and $\hbar\omega$ is the energy of a photon. The quantum efficiency of silicon photodetectors depends on wavelength and for the purpose of estimation, the following optimistic values are used: μ_{eff}=0.3 at λ=532 nm, μ_{eff}=0.4 at λ=810 nm. For integration time T=1 sec, we obtain values of $\Delta\alpha_{lim}$= 6 10^{-8} - 1 10^{-7} rad for the Nd:YAG laser and $\Delta\alpha_{lim}$= 1 10^{-8} - 3 10^{-8} rad for the Ti:Sapphire laser.

In practice the sensitivity of the polarimeter is worse than the quantum limit, due to a variety of factors which are considered below.

2.7.2 Laser Noise

Since the signal at the photodetector is proportional to the intensity of the probe beam, variations in laser output will affect the output of the polarimeter. Slow variations in laser output intensity are compensated for by normalisation against a signal which is dependent only on the input laser intensity, as described above. The main contribution to noise on the measurements comes from laser noise at the frequency of detection $\Omega_1+\Omega_2$.

The noise of a laser at the detection frequency may be measured in the following manner. The laser is incident on the a photodetector whose output is read by a lock-in. If the laser beam is chopped at the lockin reference frequency, then the output of the lockin is proportional to the laser power P_L. If the laser beam is not chopped then the output of the lockin will be due to laser noise at the reference frequency. The magnitude of this signal is the noise equivalent power (*NEP*). The value of NEP/P_L was approximately 4 10^{-5} for the Nd:YAG and 3 10^{-5} for the Ti:Sapphire at the appropriate frequencies. A full noise spectrum may be obtained by rapidly sampling the output of the laser via an A/D card and fourier transforming the collected data. Noise spectra of the two lasers are displayed in figure 2.13.

The limit on polarimeter sensitivity imposed by laser noise may be estimated using

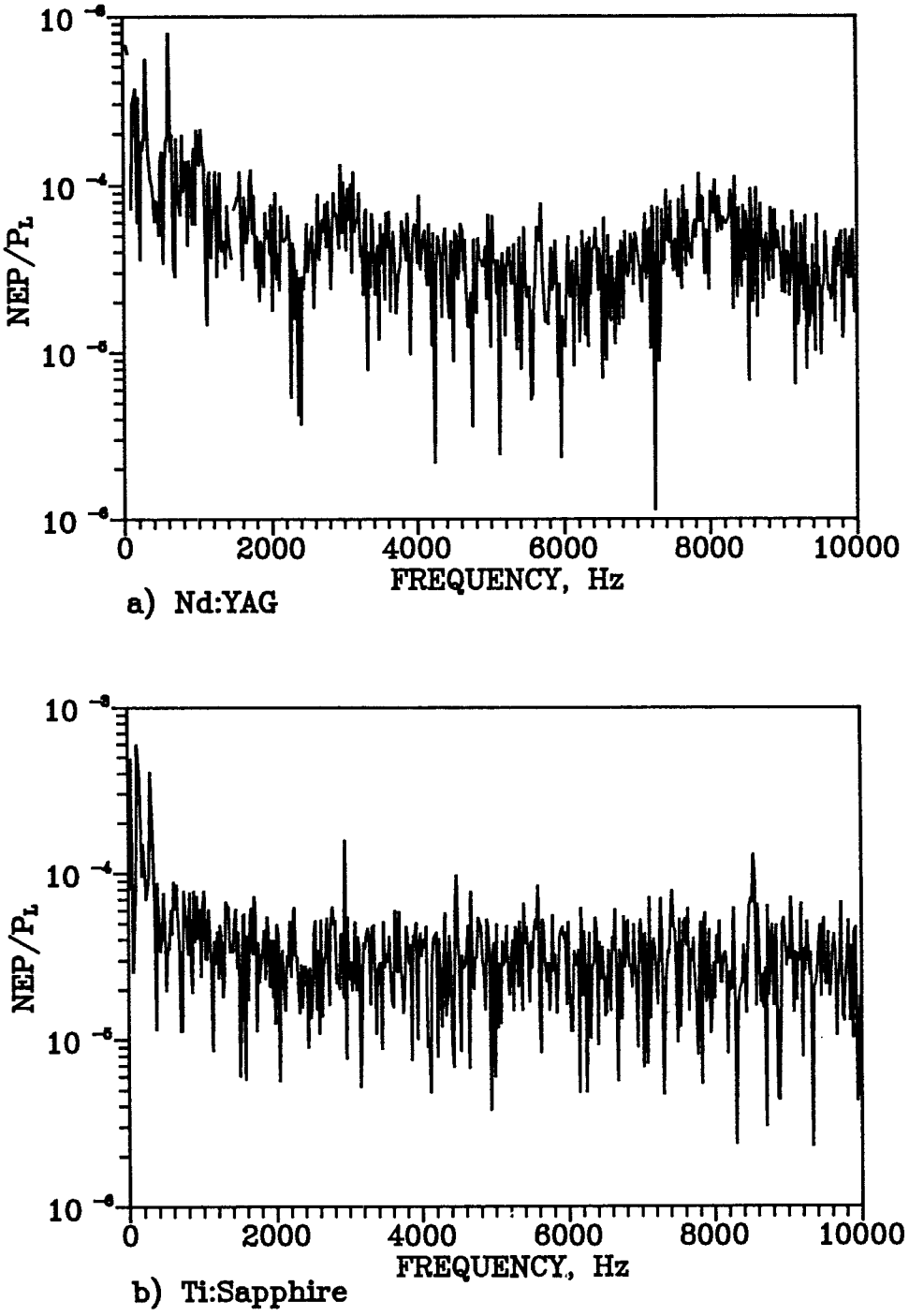

Figure 2.13 Noise spectra of the lasers used with the polarimeter a)Nd:YAG, b)Ti:Sapphire

equations (2.5) and (2.7). The noise at the photodetector will be proportional to the size of the d.c. component of intensity which is transmitted by the analyzer. The minimum angle of polarisation azimuth rotation detectable with a signal to noise ratio of unity is given by:

$$\alpha_{\min}^{LASER} = \frac{NEP(4A^2+h)}{4P_L\sqrt{T}A} \tag{2.11}$$

where T is lockin integration time. For $T\sim$ 1 sec, this gives values of $\alpha_{min}^{LASER}=8$ 10^{-7}rad for the Nd:YAG and $\alpha_{min}^{LASER}=5$ 10^{-7}rad for the Ti:Sapphire.

2.7.3 Photodetector Noise

The average magnitude of fluctuation of the output of the photodetector at the detection frequency $\Delta V(\Omega_1+\Omega_2)$ was measured using the lock-in while the input to the photodetector was blocked. The standard deviation of measurements taken at a rate of 1 per second was found to be $\Delta V \sim 1\ \mu V$ at the appropriate frequencies for the photodetectors used in the experiments with both lasers. This gives a measure of the noise in the photodetector due to noise sources which are not dependent on illumination, such as the dark-current shot noise, Johnson (thermal) noise and (1/f)-noise, and would lead to a limit on sensitivity of about $\alpha_{lim}\sim 10^{-9}$-10^{-8}rad. However, the main contribution to photodetector noise for the polarimetric arrangement described in this chapter can be calculated to come from photocurrent shot noise. Shot noise is given by

$$\Delta I_{shot} = \sqrt{2q(I_{photo}+I_{dark})} \tag{2.12}$$

where ΔI_{shot} is the noise current in A/$\sqrt{}$Hz, I_{photo} is the photocurrent, I_{dark} is the photodetector dark current and q is the charge of an electron. The main contribution to the photocurrent is due to the zero frequency component of the transmitted light: $I_{photo}=(q\mu_{eff}I_r/\hbar\omega)(4A^2+h)$, while the signal current at frequency $\Omega_1+\Omega_2$ is given by: $I_{signal}=(q\mu_{eff}I_r/\hbar\omega)A\alpha$. Therefore, for a signal to noise ratio of unity we have:

$$\alpha_{\min}^{PD} = \sqrt{\frac{2\hbar\omega}{\mu_{eff}I_rT}}\frac{\sqrt{4A^2+h}}{A} \tag{2.13}$$

For $T\sim$1 sec, this gives $\alpha_{min}^{PD}=$1-2 10^{-7}rad for the Nd:YAG and $\alpha_{min}^{PD}=$2-4 10^{-8}rad

for the Ti:Sapphire.

Laser	λ (nm)	α_{lim} (rad)	$\alpha_{min,laser}$ (rad)	$\alpha_{min,PD}$ (rad)
Nd:YAG	532 nm	4-10 10^{-8}	8 10^{-7}	1-2 10^{-7}
Ti:Sapphire	810 nm	1-3 10^{-8}	5 10^{-7}	2-4 10^{-8}

Table 2.1 Limits on polarimeter sensitivity

2.7.4 Dynamic Range of Lock-In Amplifier

The signal due to pump-induced polarisation azimuth rotation at the detection frequency $\Omega_1+\Omega_2$ needs to be recovered from a background of strong signals at various other frequencies. In particular, there is a strong signal at $2\Omega_1$. The dynamic range of the lock in needs to be large enough so that it can accurately measure the small signal at $\Omega_1+\Omega_2$, while not being overloaded by the large signal at $2\Omega_1$. The ratio of detected signal at the detection frequency and at the twice the modulation frequency can be found from equations (2.4) and (2.7):

$$\frac{I(\Omega_1+\Omega_2)}{I(2\Omega_1)} = \frac{\alpha}{4A} \qquad (2.14)$$

The lockin amplifier has a dynamic range of 10^5. For amplitude of modulation A=5 10^{-3}, this gives a maximum sensitivity of 2 10^{-7}rad. However, pre-filtering by the photodetector means that the true limit to sensitivity should be better than this.

2.7.5 Mechanical Stability

If reflection from the sample is not exactly normal incidence, this may produce a spurious rotation of the plane of polarisation of the light. Hence, mechanical instability which affects the orientation of the components of the polarimeter might be a source of noise in the polarimeter. For linear polarisation experiments, long term

drift due to mechanical distortion arising from thermal expansion has a significant effect. This has been studied in detail in [Bungay, 95]. Bungay observed fluctuations in observed polarisation rotation on the order of $\Delta\alpha \sim 10^{-5}$ rad on a timescale of several minutes, equivalent to a variation in probe incidence angle of about 6 10^{-4} rad. However, the nonlinear polarimeter detects only rotation induced by the pump beam, and is therefore insensitive to slow drift in the background rotation.

The standard configuration of the polarimeter, in which the Cotton prism acts as both polariser and analyzer, is very stable against noise due to mechanical vibration. The detectable noise was accounted for by the laser noise (section 2.7.2). However, the reduced dispersion configuration of the polarimeter, with separate polariser and analyzer, showed a much higher noise level than the standard configuration, and this was attributed to mechanical instability.

2.7.6 Noise Measurements

Figures 2.14 shows noise measurements for a) the polarimeter shown in figure 2.3, used with the Nd:YAG laser, b) the "standard" configuration of the polarimeter (figure 2.3) with the Ti:Sapphire laser and c) the reduced dispersion configuration of the polarimeter (figure 2.10) with the Ti:Sapphire laser. The data comes from experimental graphs like those shown in chapters 3 and 4, from the portion of the data where pump-probe delay is negative (i.e. when the probe pulse arrives at the sample before the pump pulse). With the Nd:YAG laser the noise level $\sim 3\ 10^{-6}$rad, which is slightly worse than the sensitivity calculated from the laser noise. In the conventional configuration with the Ti:Sapphire laser, the polarimeter shows resolution of better than 10^{-6}rad, in line with the laser noise measurements. The reduced dispersion configuration has a sensitivity of $\sim 10^{-5}$rad, indicating that mechanical noise substantially reduces the sensitivity of the polarimeter in this arrangement.

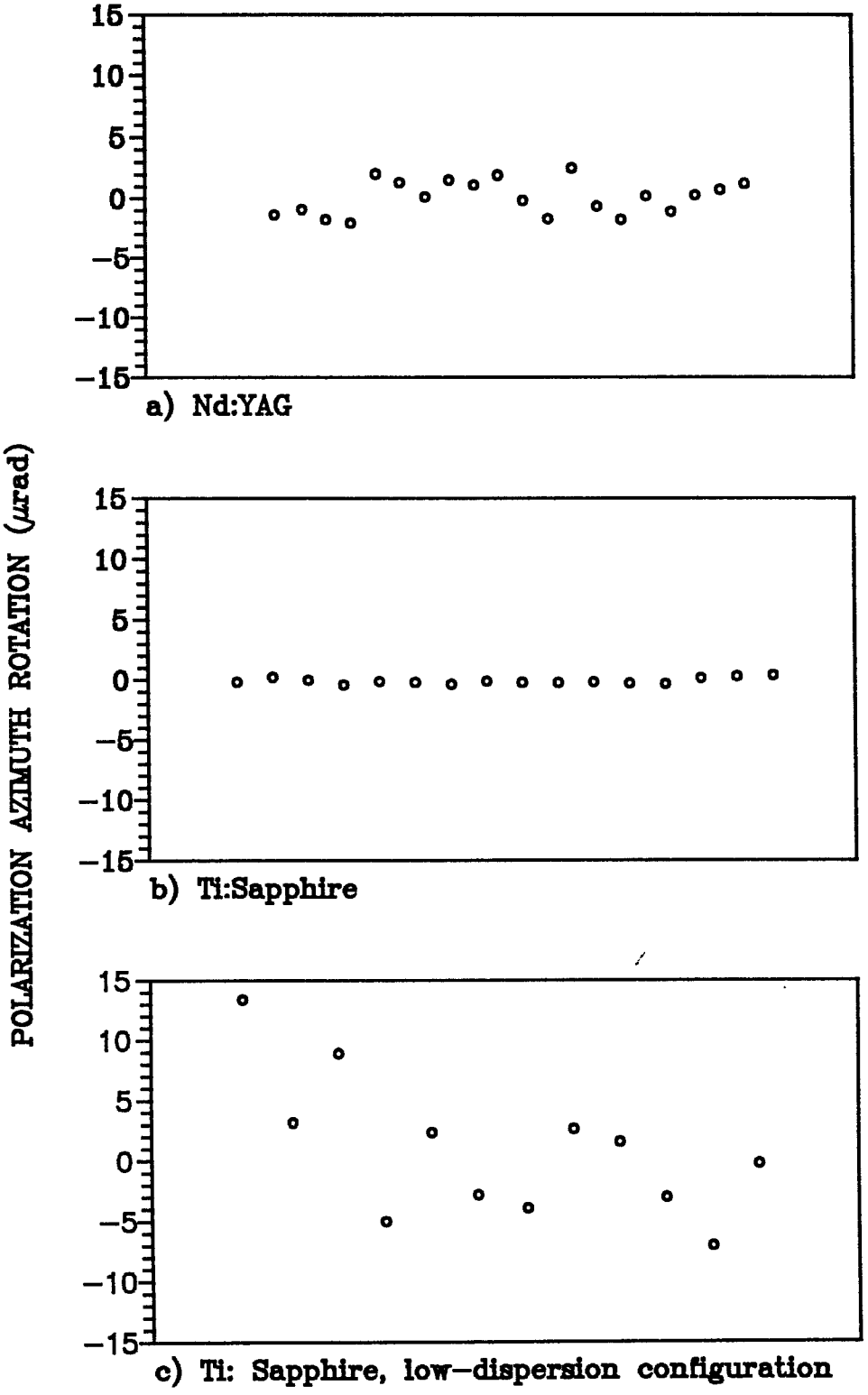

Figure 2.14 Polarimeter noise measurements a) in standard configuration with Nd:YAG laser, b)in standard configuration with Ti:Sapphire laser, c) in reduced dispersion configuration with Ti:Sapphire laser

2.8 Conclusions

A pump-probe polarimeter was constructed, based on a linear polarimeter designed by Bungay et.al. [Bungay, 93; 93a]. A femtosecond Kerr-modelocked Ti:Sapphire was constructed for use with the polarimeter. The polarimeter has angular resolution of better than 10^{-6} rad, and a temporal resolution which is limited by dispersion. The temporal resolution can be made as fast as 30 femtoseconds, although this can only be achieved with some sacrifice of sensitivity. Potentially, the time resolution of the polarimeter could be improved to the limit imposed by the pulse duration of the laser, whilst maintaining the better than 10^{-6} rad sensitivity, if anomalous dispersion were introduced into the polarimeter via a prism pair. The polarimeter provides an excellent tool for probing specular nonlinear optical effects with high time resolution. The measurement of ultrafast reflective nonlinearity in bulk metals also opens the possibility that the polarimeter might form the basis of a femtosecond autocorrelator with a very broad spectral range.

2.9 References

[Afanas'ev, 75] Afanas'ev M.M, Zakharchenia B.P, Kompan M.E, Fleisher V.G. and Shul'man S.G, JETP Lett., **21**, (1975), 224.

[Aleksandrov, 65] Aleksandrov E.B, Opt. Spectrosc., **19**, (1965), 252.

[Apanasevich, 87] Apanasevich S.P, Dovchenko, D.N. and Zheludev N.I, Opt. Spectrosc., **62**, (1987), 287.

[Asaki, 93] Asaki M T, Huang C, Garvey D et al., Opt. Lett., **18**, (1993), 977.

[Aspnes, 75] Aspnes D.E. and Studna A.A, Appl. Opt., **14**, (1975), 220.

[Aspnes, 85] Aspnes D.E. and Studna A.A, Phys. Rev. Lett., **54**, (1985), 1956.

[Austin, 74] Austin D.H. and Shank C.V, Phys. Rev. Lett., **32**, (1974), 1120.

[Azzam, 85] Azzam R.M.A, Optics Lett., **10**, (1985), 427.

[Azzam, 77] Azzam R.M.A. and Bashara N.M, "Ellipsometry and Polarisation", North Holland, (1977).

[Baird, 76] Baird P.E.G, Brimicombe M.W.S.M, Roberts G.J, Sandars P.G.H, Soreide D.C, Fortson E.N, Lewis L.L. and Lindahl E.G, Nature, **264**, (1976), 528.

[Bar-Ad, 91] Bar-Ad S. and Bar-Joseph I, Phys. Rev. Lett., **66**, (1991), 2491.

[Becker, 91] Becker H, Brach D, Otto A. and Weber H, Rev. Sci. Instr., **62**, (1991), 1196.

[Bor, 88] Bor Z, J. Mod. Opt., **35**, (1988), 1907.

[Born, 70] Born M. and Wolf E, "Principles of Optics", Pergamon Press, Oxford, (1970).

[Brabec, 92] Brabec T, Spielmann Ch, Curley P.F, Krausz F, Opt. Lett., **17**, (1992), 1292.

[Bradley, 69] Bradley D.J, Durrant A.J.F, O'Neill F, Sutherland B, Physics Letters, **30A**, (1969), 535.

[Bungay, 93] Bungay A.R, Svirko Yu.P, Zheludev N.I, Phys. Rev. Lett., **70**, (1993), 3039.

[Bungay, 93a] Bungay A.R, Kugler N, Zheludev N.I, Phys. Lett. A, **174**, (1993), 335.

[Bungay, 94] Bungay A.R, Popov S.V, Shatwell I.R, Zheludev N.I, European Quantum Electronics Conference, Amsterdam, Aug 28-Sep 2, 1994.

[Bungay, 95] Bungay A.R, Ph.D. thesis, University of Southampton (1995)

[Cardona, 69] Cardona M, "Modulation Spectroscopy", Academic Press, (1969).

[Chapman, 70] Chapman G.D. and Series G.W, J. Phys. B., At. Molec. Phys., **3**, (1970), 72.

[Cho, 90] Cho G.C, Kutt W. and Kurz H, Phys. Rev. Lett., **65**, (1990), 764.

[Curley, 91] Curley P.F, Ferguson A.I, Opt. Lett., **16**, (1991), 1016.

[Dahlstrom, 72] Dahlstrom L, Opt. Comm., **5**, (1972), 157.

[Danishevskii, 81] Danishevskii A.M, Kochegarov S.F. and Subashiev V.K, JETP Lett., **33**, (1981), 611.

[DeMaria ,66] DeMaria A.J, Stetser D.A, Heynau H, Appl. Pys. Lett., **8**, (1966), 174.

[DeSilvstri, 84] DeSilvestri S, Laporta P, Svelto O, Opt. Lett., **9**, (1984), 335.

[Edwards, 95] Edwards N.H, Phipp S.J, Baird P.E.G, Nakayama S, Phys. Rev. Lett., **74**, (1995), 2654.

[Fork, 84] Fork R.l, Martinez O.E, Gordon J.P, Opt. Lett., **9**, (1984), 150.

[Fortson, 80] Fortson E.N and Wilets L, Adv. At. Mol. Phys., **16**, (1980), 319.

[French, 95] French P.M.W, Rep. Prog. Phys., **58**, (1995), 169.

[Gierulski, 85] Gierulski A, Marowsky G, Nikolaus B, Vorob'ev N, Appl. Phys. B, **36**, 133, (1985)

[Giodmaine, 67] Giodmaine J.A, Rentzepis P.M, Shapiro S.L, Wecht K.W, Appl. Phys. Lett, **11**, 216, (1967).

[Gudeman, 90] Gudeman C.S. and Mauri D, J. Appl. Phys., **67**, (1990), 5938.

[Habraken, 80] Habraken F.H.P.M, Gijzeman O.L.J. and Bootsma G.A, Surf. Sci., (1980),

482.

[Halperin, 89] Halperin B.I, March-Russell J. and Wilczek F, Phys. Rev. B., **40**, (1989), 8726.

[Hanekamp, 82] Hanekamp L.J, Lisowski W. and Bootsma G.A, Surf. Sci, **118**, (1982), 1.

[Hargrove, 64] Hargrove L.E, Fork R.L, Pollack M.A, Appl. Phys. Lett., **5**, (1964), 4.

[Hauge, 80] Hauge P.S, Surf. Sci., **96**, (1980), 108.

[Hauge, 75] Hauge P.S. and Dill F.H, Opt. Comm., **14**, (1975), 431.

[Hollister, 81] Hollister J.H, Asperson G.R, Lewis L.L, Emmons T.P, Vold T.G. and Fortson E.N, Phys. Rev. Lett., **46**, (1981), 643.

[Ippen, 72] Ippen E.P, Shank C.V, Dienes A, App. Phys. Lett., **21**, (1972), 348.

[Jellison, 85] Jellison Jr G.E. and Lowndes D.H, App. Phys. Lett., **47**, (1985), 718.

[Kafka, 86] Kafka J.D, Head D.F, Baer T, Proc. Ultrafast Phenomena V, Springer, Berlin, 1986.

[Kane, 93] Kane D.J, Trebino R, J. Opt. Soc. Am. A, **10**, (1993), 1101.

[Kawazoe, 93] Kawazoe T, Masumoto Y. and Tomobumi M, Phys. Rev. B., **47**, (1993), 10452.

[Keller, 91] Keller U, 'tHooft G.W, Knox W.H, Cunningham J.E, Opt. Lett., **16**, (1991), 1022.

[Kempe, 92] Kempe M, Stamm U, Wilhelmi B, Rudolph W, J. Opt. Soc. Am. B, **9**, (1992), 1158.

[Kempe, 93] Kempe M, Rudolph W, Opt. Lett., **18**, (1993), 137.

[Koldemeder, 66] Koldmeder C, Zinth W, Kaiser W, Phys. Rev. Lett., **17**, (1966), 1275.

[Kotz, 83] Kotz R. and Hayden B.E, Surf. Sci., **135**, (1983), 374.

[Kuwata, 84] Kuwata M, J. Phys. Soc. Japan, **53**, (1984), 4456.

[Kuwata, 86] Kuwata M, Toshikazu I. and Nobukata N, Japanese J. Appl. Optics, (1986), 1382.

[Kuwata, 87] Kuwata M, J. Luminescence, **38**, (1987), 247.

[Lawrence, 92] Lawrence T.W, Szöke A, Laughlin R.B, Phys. Rev. Lett., **69**, (1992), 1439.

[LeBlanc, 91] LeBlanc C.P, Szabo G, Sauerbrey R, Opt. Lett, **16**, 1508, (1991).

[Lewis, 77] Lewis L.L, Hollister J.H, Soreide D.C, Lindahl E.G. and Fortson E.N, Phys. Rev. Lett., **39**, (1977), 795.

[Liao, 77] Liao P.F. and Bjorklund G.C, Phys. Rev. A, **15**, (1977), 2009.

[Likforman, 91] Likforman J.P Grillon G, Joffre M et.al., Appl. Phys. Lett., **58**, (1991), 2061.

[Loudon, 83] Loudon R, "The Quantum Theory of Light", 2nd edn., Clarendon Press, Oxford, (1983).

[Luk'yanov, 90] Luk'yanov A.Yu. and Novikov M.A, Soviet JETP Letters, **51**, (1990), 591.

[Lyons, 93] Lyons K.B, Dillon J.F, Duclos S.J et. al., Phys. Rev. B, **47**, (1993), 8195.

[Macpherson, 87] Macpherson M.J, Stacey D.N, Baird P.E.G, Hoare J.P, Sandars P.G.H, Tregidgo K.M.J and Guowen W, Eur. Phys. Lett., **4**, (1987), 811.

[Mark ,89] Mark J, Lin L.Y, Hall K.l, Haus H.A, Ippen E.P, Opt. Lett., **14**, (1989), 48.

[Martin, 78] Martin, A.J, Lozykowski H.J, Acta Physica Polonica, **A54**, (1978), 867.

[Martinez, 84] Martinez O.E, Gordon J.P, Fork R.L, J. Opt. Soc. Am. A, **1**, (1984), 1003.

[Mollenauer, 84] Mollenauer L.F, Stolen R.H, Opt. Lett., **9**, (1984), 13.

[Moulton, 86] Moulton P.F, J. Opt. Soc. Am. B, **3**, (1986), 125.

[Moulton, 92] Moulton P.F, Proc. IEEE, **80**, (1992), 348.

[Mulhollan, 91] Mulhollan G.A, Fink R.L. and Erskine J.L, Phys. Rev. B., **44**, (1991), 2393.

[Murnane, 94] Murnane M.M, Kapteyn H.C, private communication, (1994).

[Piche, 91] Piche M, Opt. Comm., **86**, (1991), 156.

[Qian, 90] Qian J.P. and Wang G.C, J. Vac. Sci. Tech., **A8**, (1990), 4117.

[Saiki, 92] Saiki T, Takeuchi K, Kuwata-Gonokami M, Mitsuyu T. and Ohkawa K, Appl. Phys. Lett., **60**, (1992), 192.

[Saltiel, 87] Saltiel S.M, Yankov P.D. and Zheludev N.I, Appl. Phys. B, **42**, (1987), 115.

[Sarukura, 88] Sarukura N, Watanabe M, Endoh A, Watanabe S, Opt. Lett., **13**, 996, (1988).

[Sato, 81] Sato K, Jpn. J. Appl. Phys., **20**, (1981), 2403.

[Sham, 93] Sham L.J, J. Phys: Condens. Matter, **5**, (1993), A51.

[Soriede, 76] Soreide D.C, Roberts D.E, Lindahl E.G, Lewis L.L, Apperson G.R. and Fortson E.N, Phys. Rev. Lett., **36**, (1976), 352.

[Spence, 91] Spence D.E, Kean P.N, Sibbett W, Opt. Lett., **16**, (1991), 42.

[Spielmann, 91] Spielmann Ch, Krausz F, Brabec T, et.al., Opt. Lett., **16**, (1991), 1180.

[Spielman, 92] Spielman S, Dodge J.S, Lombardo L.W et. al., Phys. Rev. Lett., **68**, (1992), 3472.

[Stark, 92] Stark J.B, Knox W.H. and Chelma D.S, Phys. Rev. Lett., **68**, (1992), 3080.

[Svirko, 94] Svirko Yu. P. and Zheludev N.I, JOSA B, **11**, (1994), 1388.

[Takeuchi, 90] Takeuchi A, Muto S, Inata T. and Fujii T, App. Phys. Lett., **56**, (1990), 2213.

[Takizawa, 81] Takizawa T, Journal of the Physical Society of Japan, **50**, (1981), 3054.

[Taylor, 87] Taylor J.D, Baird P.E.G, Hunt R.G, Macpherson M.J.D, Nowicki G, Sandars P.G.H and Stacey D.N, J. Phys. B., At. Mol. Phys., **20**, (1987), 5423.

[Treacy, 69] Treacy E.B, IEEE Jnl. Quantum Electronics, **QE-5**, (1969), 454.

[Tregidgo, 86] Tregidgo K.M.J, Baird P.E.G, Macpherson M.J.D, Palmer C.W.P, Sandars P.G.H, Stacey D.N. and Thompson R.C, J. Phys. B., At. Mol. Phys., **19**, (1986), 1143.

[Watanabe, 89] Watanabe C, Saito H, Ishida Y, Yajima T, Optics Communications, **69**, 405, (1989).

[Weber, 90] Weber H.J, Weitbrecht D, Brach D, Shelankov A.L, Keiter H, Weber W, Wolf Th, Geerk J, Linker G, Roth G, Splittgerber-Hunnekes P.C. and Guntherodt G, Sol. Stat. Comm, **76**, (1990), 511.

[Weiman, 76] Weiman C. and Hansch T.W, Phys. Rev. Lett., **36**, (1976), 1170.

[Wolfenden, 90] Wolfenden T.D, Baird P.E.G, Deeny J.A. and Irie M, Meas. Sci. Tech., **1**, (1990), 1060.

[Zheludev, 90] Zheludev N.I. and Paraschuk D.Yu, JETP Lett, **52**, (1990), 32.
(1992), 3472.

Chapter 3
Observation of the Specular Inverse Faraday Effect

3.1 Synopsis

The results of investigations of the Specular Inverse Faraday effect (SIFE) in a variety of materials are presented. The SIFE is introduced in (3.2) and its potential as a spectroscopic tool is discussed. The theory of the SIFE is described in terms of material tensors in media with instantaneous nonlinearity (3.3). Experimental observation of the SIFE in a variety of materials is described in (3.4). The first measurements of the SIFE in the diluted magnetic semiconductor $Cd_{0.6}Mn_{0.4}Te$ (3.4.1) and in the high T_c superconductor $YBa_2Cu_3O_{7-\delta}$ (3.4.2) are presented. The transient SIFE in GaAs was observed with femtosecond time resolution for the first time (a microscopic theory of the dynamics of the SIFE in GaAs is discussed) (3.4.3), and the SIFE in nickel was observed to be effectively instantaneous with 32 femtosecond time resolution (3.4.4).

3.2 The Specular Inverse Faraday Effect

The Inverse Faraday effect is a classical electrodynamic effect consisting of the magnetisation of a medium due to the presence of a rotating electric field such as that of a circularly polarised light beam [Atkins, 68]. This magnetisation may be directly detected by instruments sensitive to magnetic moment [Krenn, 85; Awschalom, 87]. The result of optical stimulation may also be investigated by using a second weak probe beam and measuring pump-induced polarisation azimuth rotation or circular dichroism [Afanas'ev, 75; Wieman, 76; Kuwata, 84; Takeuchi, 90; Bar-Ad, 92;

Kawazoe, 93].

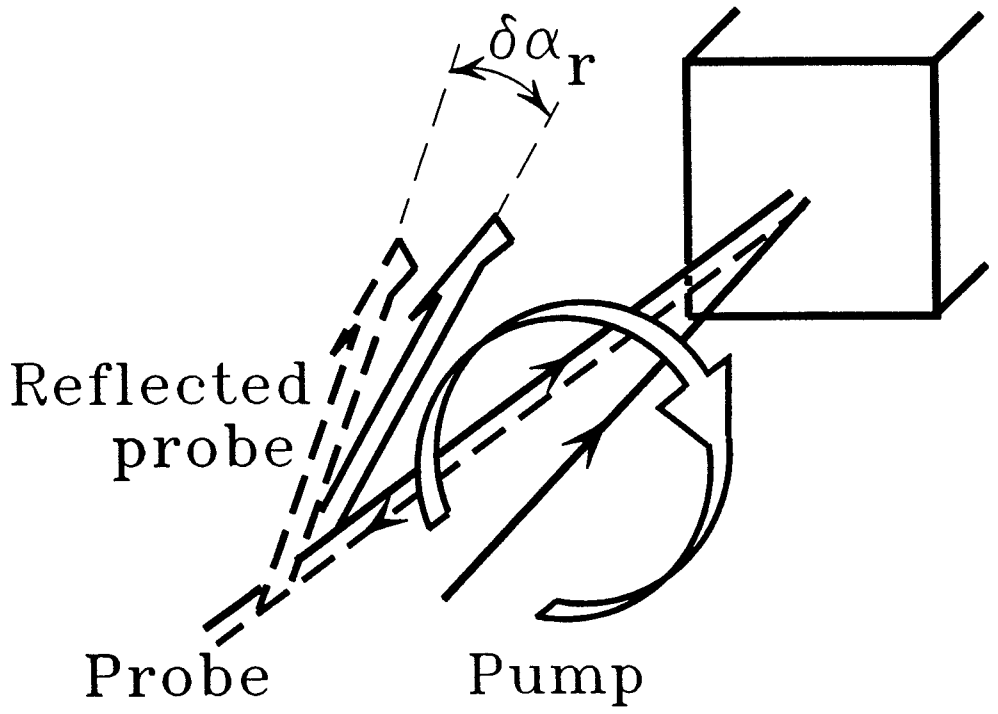

Figure 3.1 Arrangement of pump and probe beams for Specular Inverse Faraday effect measurements

In Specular Inverse Faraday effect (SIFE) measurements, the polarisation of a reflected, rather than transmitted, probe wave is measured. In the scheme used in the experiments described below, a weak linearly polarised probe beam and a circularly polarised pump beam were used (figure 3.1). This arrangement was first utilized by Kuwata for measurement of strong resonant excitonic optical nonlinearity in CuCl and HgI_2 [Kuwata, 87]. However, the measurement of nonresonant nonlinearities using this phenomenon required a highly sensitive polarimeter. The SIFE had not been used to measure a nonresonant nonlinearity until members of our research group did so in the semiconductors GaAs and InSb [Popov, 94]. In this chapter similar experiments are described on the diluted magnetic semiconductor $Cd_{0.6}Mn_{0.4}Te$ and the high-T_c superconductor $YBa_2Cu_3O_{7-\delta}$. The time-resolution in these experiments was not sufficient to observe the transient effect. Dynamics of the SIFE in GaAs were first observed by [Bungay, 94], with 2 picosecond time resolution. The improved time resolution made available by the Ti:Sapphire laser described in chapter 2 allows

observation of fast features of the dynamics of the SIFE in GaAs which were not previously resolved. It also allowed observation of fast nonlinearity in bulk nickel.

The SIFE is a potentially powerful technique for investigating the nonlinear optical properties of opaque materials. The nonlinear optical constants of bulk opaque materials have been relatively little investigated in comparison with transparent materials, since clearly only specular effects are observable, and these are generally much smaller in magnitude than transmission effects. For example, metals are a wide and important class of materials where nonlinear optical data is sparse. Measurements of coherent second and third order nonlinearities of bulk metals have been made by reflective second [Review: Shen, 94] and third [Burns, 71] harmonic generation. However, there is little information available about fast frequency-degenerate nonlinearities, which might be of great interest for device applications. A value of a frequency degenerate nonlinearity of gold has been calculated, rather than directly measured, using data on the nonlinearity of glass doped with gold micro-particles [Hache, 86]. Changes in reflectivity in the presence of a pump beam have been used to gain information about frequency degenerate nonlinearity of metals [Schoenlein,87; Eesley, 86], but this method is limited by its low sensitivity, and has only been used in a narrow spectral range in copper and gold where a strong Fermi-smearing nonlinearity may be observed. As experiments described in this chapter and by other members of our research group [Zheludev, 95; Bennett, 95; 95a] show, the SIFE has considerable potential to be used in this area.

The SIFE also offers the possibility of optically investigating the spin relaxation and thermalisation times of excited carriers in opaque materials [Bungay, 94]. A variety of optical techniques have been used to measure spin relaxation processes in semiconductors and quantum wells. These include measurement of the polarisation of photoluminescence stimulated by CW excitation with circularly polarised light [Meier, 84; Fishman, 77; Zerrouati, 88]. Time resolved measurement of the luminescence using up-conversion or streak camera techniques allows separation of contributions from electron, hole and exciton spin relaxations [Damen, 91;

Awschalom, 91; Roussignol, 92]. This technique, however, clearly requires that the material is strongly luminescent, a limitation that does not affect SIFE measurements. Pump-probe differential transmission measurements have been widely used to study spin dynamics in bulk semiconductors [Hunsche,93] and quantum wells [Knox,86;88]. Polarisation sensitive measurements have also been widely used to investigate sub-picosecond dynamics [Stark, 92; Takeuchi, 90; Bar-Ad, 91; Bar-Ad, 92; Kawazoe,93]. However, all of these have depended on transmission measurements. A reflective technique such as the SIFE, which may be used on opaque bulk samples, has clear advantages.

3.3 Theory of the Specular Inverse Faraday Effect in Materials with Instantaneous Response

The first theoretical paper on specular pump-probe polarisation phenomena which addressed the SIFE was [Golubkov, 90]. A detailed phenomenological theory of the SIFE in media with instantaneous response, which for the first time dealt with the coherent as well as the incoherent component of the SIFE, was developed by Svirko and Zheludev [Svirko, 94]. This treats the SIFE as a degenerate four-wave mixing phenomenon, describing the separate coherent and incoherent contributions to the effect. It deals with the manifestation of the effect as induced probe polarisation azimuth rotation and elliptisation, and shows how to recover the values of components of the degenerate third order susceptibility tensor $\chi^{(3)}$ from the induced change in the polarisation of a reflected probe beam. Presented below is a more straightforward and general approach to specular polarisation effects recently developed by the same authors [Popov, 96].

Consider a material with instantaneous response and pump and probe waves with narrow spectra centred at frequency ω. Considering only third order nonlinearities, the following material equation may be used:

$$D_i = \epsilon_{ij} E_j e^{ik.r} + \chi^{(3)}_{ijlm} E_j E_l E_m^* e^{ik.r} \tag{3.1}$$

where the electric field is $\mathscr{E}(r) = Ee^{ik.r}$, representing a plane wave propagating in the z direction, **D** is the electric displacement vector and the third order susceptibility

$$\chi_{ijkl} = \chi^{(3)}_{ijkl}(\omega, \omega, \omega, -\omega) + \chi^{(3)}_{ijlk}(\omega, \omega, -\omega, \omega) + \chi^{(3)}_{ilkj}(\omega, -\omega, \omega, \omega) \tag{3.2}$$

can describe any degenerate 4-wave mixing phenomena.

In the case of reflection from the surface of a medium at normal incidence, labelling incident, reflected and transmitted waves by the superscripts *i*, *r* and *t* respectively, the total electric field in the vacuum may be given by: $\mathscr{E}^{(1)}(z) = E^i e^{i\omega z/c} + E^r e^{-i\omega z/c}$. The magnetic field in the vacuum may then be found via Maxwell's equations: $B^{(1)}(z) = (i\omega/c)\,[\hat{z} \times E^i] e^{i\omega z/c} + (i\omega/c)\,[\hat{z} \times E^r] e^{-i\omega z/c}$ where $\hat{z}$ is the unit vector in the direction of propagation.

If the linear or nonlinear anisotropy of the medium is small, so that refractive index *n* and wavevector $k = \omega n/c$ may be introduced, then the light wave propagating in the medium in the positive direction is described by $\mathscr{E}^{(2)}(r) = E^t e^{ik.r}$. In the slowly varying envelope approximation, where the phases and amplitudes of the complex vector $E^t(r)$ are slowly varying functions of the coordinate z, substituting $\mathscr{E}^{(2)}(r) = E^t e^{ik.r}$ into Maxwell's equations and neglecting d^2E^t/dz^2 gives

$$2ik\frac{dE_i^t}{dz} + \frac{\omega^2}{c^2}(\varepsilon_{ij} - n^2\delta_{ij})E_j^t = -\frac{\omega^2}{c^2}(\chi_{ijlm})E_j^t E_l^t E_m^{t\,*} \tag{3.3}$$

where the indices *i,j* cover the *x,y* directions. If the incident light consists of separate pump and probe beams, where the intensity of the pump is much greater than that of the probe, the magnitudes of the incident, reflected and transmitted waves may be represented by $E^{i,r,t} = A^{i,r,t} + a^{i,r,t}$ where *A* and *a* represent the pump and probe beams respectively and $|A^{i,r,t}| \gg |a_{i,r,t}|$.

If the probe wave is much weaker than the pump, we may ignore any effect of the probe on the pump or self-action of the probe wave. The magnitude of the pump is given by equation (3.3), with $\boldsymbol{A}$ substituted for $\boldsymbol{E}$. The magnitude of the probe is given by

$$\frac{da_i^t}{dz} = \frac{ik}{2}\left(\alpha_{ij} a_j^t + \beta_{ij} a_j^{t*}\right) \tag{3.4}$$

where

$$\begin{aligned} \alpha_{ij} &= -\delta_{ij} + \frac{1}{n^2}\left[\left(\varepsilon_{ij} + 2\chi_{ijlm} A_l^t A_m^{t*}\right)\right] \\ \beta_{ij} &= \frac{1}{n^2}\chi_{ilmj} A_l^t A_m^t \end{aligned} \tag{3.5}$$

where the amplitudes A^t_l of the pump wave are, in general, functions of the coordinate z and satisfy equation (3.3).

There is an important difference between α_{ij} and β_{ij}. As follows from equation (3.5), α_{ij} may be represented in terms of the Stokes parameters of the transmitted pump wave $S_0 = A_xA_x^* + A_yA_y^*$, $S_1 = A_xA_x^* - A_yA_y^*$, $S_2 = 2Re(A_xA_y^*)$, $S_3 = 2Im(A_xA_y^*)$: $A^t_i\, A^{t*}_j = \frac{1}{2}\sigma_{ij}^{\alpha} S_{t\alpha}$ where σ_{ij}^{α} are the Pauli matrices, $\alpha = 0, 1, 2, 3$. The Stokes parameters represent intensities of specific polarization components of the pump wave, i.e. they are independent of the phase of the wave. On the other hand, β_{ij} cannot be represented solely in terms of the Stokes parameters. From the relation $A^t_i = (A^t_i)^* \exp\{2i\phi_{ti}\}$, where ϕ_{ti} is the phase of the complex amplitude A^t_i, one obtains $A^t_i\, A^t_j = A^t_i\, A^{t*}_j \exp\{2i\phi_{tj}\} = \frac{1}{2}\sigma_{ij}^{\alpha} S_{t\alpha} \exp\{2i\phi_{tj}\}$. Thus the coefficients β_{ij} depend on the both intensities and phases of the polarization components of the pump wave. This manifests itself as the appearance of a coherent (i.e. dependent on the mutual phase difference between pump and probe) component in the reflected and/or transmitted probe wave.

In order to determine what happens to the probe beam on reflection from the surface of the medium we must consider the boundary conditions for the wave. The electric

and magnetic fields must be continuous across the boundary ($z=0$):

$$\begin{aligned} a^t(z=0)-a^i(z=0)-a^r(z=0) &= 0 \\ b^t(z=0)-b^i(z=0)-b^s(z=0) &= 0 \end{aligned} \tag{3.6}$$

From Maxwell's equations the following expression can be obtained for the magnetic field in the medium $b^t = n[z\times a^t] + (c/i\omega)curla^t$. It follows from the fact that we assume the probe has no effect on the pump that the pump and probe must independently satisfy the boundary conditions. Therefore the amplitudes of the incident, reflected and transmitted probe waves at the boundary of the medium are given by:

$$\begin{aligned} a^T - a^R - a &= 0 \\ na^T + a^R - a &= \frac{ic}{\omega}\left(\frac{da^T}{dz}\Big|_{z=0}\right) \end{aligned} \tag{3.7}$$

Solving equations (3.7) gives:

$$\begin{aligned} a^T &= \frac{2}{1+n}a + \frac{ic}{\omega(1+n)}\left(\frac{da^T}{dz}\Big|_{z=0}\right) \\ a^R &= \frac{1-n}{1+n}a + \frac{ic}{\omega(1+n)}\left(\frac{da^T}{dz}\Big|_{z=0}\right) \end{aligned} \tag{3.8}$$

The polarization azimuth and ellipticity of a wave may be described via the Stokes vector parameters of the wave. The polarization azimuth orientation ϕ and the degree of ellipticity η will then be given by $\phi = \frac{1}{2}tan^{-1}(S_2/S_1)$ and $\eta = \frac{1}{2}sin^{-1}(S_3/S_0)$.

The polarization azimuth and ellipticity of the reflected probe beam is given by

$$\begin{aligned} \tan 2\phi^r &= \tan 2\phi^i - \frac{\lambda}{\pi S_{1i}^2} Im\left\{\frac{J^R}{1-n}\right\} \\ \sin 2\eta^r &= \sin 2\eta^i - \frac{\lambda}{\pi S_{0i}^2} Re\left\{\frac{J^R}{1-n}\right\} \end{aligned} \tag{3.9}$$

where

$$J^R = (a_x \frac{da_y^T}{dz}|_{z=0} - a_y \frac{da_x^T}{dz}|_{z=0})[(a_x^*)^2 + (a_y^*)^2] \tag{3.10}$$

If the change in the polarisation state of the light is small then equations (3.10) may be rewritten as

$$\begin{aligned} \phi_r - \phi_i &= -\frac{\lambda \cos^2 2\phi_i}{2\pi S_{1i}^2} Im\{\frac{J^R}{1-n}\} \\ \eta_r - \eta_i &= -\frac{\lambda}{2\pi S_{0i}^2} Re\{\frac{J^R}{1-n}\} \end{aligned} \tag{3.11}$$

J^R may be obtained in terms of α_{ij} and β_{ij} and the Stokes vector of the incident light S_i by substituting equation (3.4) into (3.10)

$$\begin{aligned} J^R = \frac{i\pi n}{\lambda(1+n)}\{ & [\alpha_{yy} - \alpha_{xx} + (\beta_{yy} e^{-2i\varphi_y} - \beta_{xx} e^{-2i\varphi_x})](S_{0i}S_{2i} - iS_{1i}S_{3i}) \\ & + [\alpha_{yx} - \alpha_{xy} + (\beta_{yx} e^{-2i\varphi_x} - \beta_{xy} e^{-2i\varphi_y})](S_{0i}^2 - S_{3i}^2) \\ & + [\alpha_{yx} + \alpha_{xy} + (\beta_{yx} e^{-2i\varphi_x} + \beta_{xy} e^{-2i\varphi_y})](S_{0i}S_{1i} + iS_{2i}S_{3i})\} \end{aligned} \tag{3.12}$$

where $\varphi_{x,y} = \arg(a_{x,y})$.

The above is a general solution for the behaviour of a probe wave of arbitrary initial polarisation reflected from a nonlinear medium of arbitrary symmetry in the presence of a copropagating pump beam, also of arbitrary polarisation.

We now consider the specific case of the Specular Inverse Faraday effect. Although the SIFE is possible in media of arbitrary symmetry, we consider only the simplest case of an isotropic medium. In this case there are only two independent contributions to the third order susceptibility [Butcher, 90; Svirko, 94]:

$$\chi_{ijlm}^{(3)} = \chi_1(\delta_{ij}\delta_{lm} + \delta_{il}\delta_{jm} + \delta_{im}\delta_{jl}) + \chi_2\delta_{im}\delta_{jl} \tag{3.13}$$

Since $\chi_1 = \chi_{xxyy}$ has overall permutation symmetry, it is allowed in both absorbing and

absorptionless media. On the other hand, $\chi_2=\chi_{xyyx}-\chi_{xxyy}$ vanishes if frequency dispersion is negligible, and hence needs to be considered only in absorbing materials [Butcher, 90].

In the SIFE, the pump wave is circularly polarised: $S_{1p}=S_{2p}=0$, $S_{3p}=\pm S_{0p}$. If the incident probe wave is linearly polarised ($S_{3i}=0$, $S_{1i}^2 + S_{2i}^2 = S_{0,i}^2$):

$$J^R = \mp \frac{8\pi(\chi_{xxyy} - \chi_{xyyx} + \chi_{xxyy}e^{2i\psi})}{\lambda n|1 + n|^2(1 + n)} S_{0p}S_{0i}^2 \qquad (3.14)$$

where the + sign corresponds to a right-hand and the - sign corresponds to a left-hand circularly polarized pump wave and $\psi = (\varphi_p - \varphi)$ is the phase difference between the circularly polarized pump and linearly polarized probe waves. The formulae for polarization alterations in the reflected probe become

$$\frac{\phi_r - \phi_i}{\eta_r} = \pm \frac{32\pi I_p}{c|1 + n|^2} \, Im \, Re \, \frac{\chi_{xxyy} - \chi_{xyyx} + \chi_{xxyy}e^{2i\psi}}{n(1 - n^2)} \qquad (3.15)$$

where $I_p = cS_{0p}/8\pi$ is the intensity of the pump wave.

The term in equation (3.15) proportional to $\chi_2=\chi_{xyyx}-\chi_{xxyy}$ is independent of the relative phase of pump and probe, and hence represents the incoherent contribution to the SIFE. The term proportional to $\chi_1=\chi_{xxyy}$ is dependent on the relative phase of pump and probe ψ, and hence represent the coherent contribution to the SIFE. Since it depends on the value of χ_2, the coherent contribution is only significant in non-transparent media. Being dependent on the totally symmetric component χ_1, the coherent contribution may potentially be observed in both transparent and opaque media.

For a medium with instantaneous response, the experimentally observable value of probe polarisation rotation due to the SIFE is given by the convolution of the

instantaneous magnitude of induced rotation $\phi_{ind}(t)$ and the intensity of the probe $I_s(t)$, where the instantaneous value of $\phi_{ind}(t)$ is proportional to the instantaneous intensity of the pump $\phi_{ind}(t)=\mu I_p(t)$:

$$\phi_{ind}(\tau) \propto \int_{-\infty}^{+\infty} \phi_{ind}(t) I_s(t-\tau) dt \propto \int_{-\infty}^{+\infty} I_p(t) I_s(t-\tau) dt \qquad (3.16)$$

where τ is pump-probe delay. That is, if pump and probe pulses are produced by splitting a single laser beam, and material response is fast with respect to pulse duration, time-domain measurements of the SIFE return an autocorrelation function of intensity.

One can see that for coherent pump and probe the polarization effects on reflection are in fact polarization-sensitive versions of a degenerate four-wave-mixing process. What distinguishes the specular effects is that the nonlinear interaction takes place in a thin layer at the surface of the medium which is responsible for the reflection. In the case of strongly absorbing materials, the depth ℓ, of this skin layer may be estimated as the smaller of the wavelength or the light penetration depth.

3.4 Experimental Observation of the SIFE in Opaque Materials

In the experiments on $Cd_{0.6}Mn_{0.4}Te$ and $YBa_2Cu_3O_{7-\delta}$ the optical source was a frequency doubled mode-locked $Nd^{3+}YAG$ laser producing 80 picosecond pulses with 82 MHz repetition rate at wavelength $\lambda=532$ nm and with an output power of 200 mW. Experiments were conducted using the pump-probe reflective configuration polarimeter described in chapter 2. The pump beam was circularly polarised by a waveplate after passing through the birefringent prism polariser. The pump and probe beams were focused at the sample surface by a lens to a spot diameter of 20 μm. After losses in the polarimeter, the maximum attainable pump intensity at the sample surface was about 5 $MWcm^{-2}$.

For the experiments on GaAs and nickel, the light source was the Kerr-lens mode-

locked Ti:Sapphire laser described in chapter 2, producing 32 femtosecond pulses at wavelengths centred at λ=810 nm with output power ~500 mW. The polarisation of the pump beam was set as circular using a first order mica waveplate. This was a piece of mica of thickness ~40 μm. In the experiments with GaAs the dispersion in the polarimeter limited time resolution to ~70 femtoseconds, and the beams were focused on the sample by a lens to a spot diameter of 35 μm. Peak pump intensity at the sample surface was ~5 GW cm^{-2}. In the experiments on nickel, time resolution of 32 femtoseconds was achieved, by means of further reduction of dispersion in the polarimeter by the modifications described in section 2.4. The beams were focused by a parabolic mirror to a spot size of 35 μm. Peak pump intensity at the sample surface was ~10 GW cm^{-2}.

3.4.1 Study of the SIFE in the Diluted Magnetic Semiconductor $Cd_{0.6}Mn_{0.4}Te$

A diluted magnetic semiconductor is a semiconductor which has had a fraction of one of its constituent ions replaced by ions with a net magnetic moment. The most studied are $A^{II}B^{VI}$ hosts containing Mn^{2+} ions, which substitute for the cations A, so that the cation sublattice becomes a A-Mn alloy. Mn is used because it has a large magnetic moment, is electrically neutral in $A^{II}B^{VI}$ hosts (neither a donor or an acceptor), and can replace a large fraction of the cation A (up to 0.8 in $Cd_{1-x}Mn_xTe$) without significantly affecting crystal quality. These materials are of interest for several reasons. Their band structure and lattice parameters may be controlled by changing the fraction of Mn (this is also true of nonmagnetic ternary semiconductors). They also have various unusual magnetic properties. There has been much interest in the magneto-optical properties of dilute magnetic semiconductors because of their giant Faraday effects [Nikitin, 90]. These make them potentially attractive materials for magnetooptical devices (e.g. optical isolators or magnetic field sensors). The unusual feature of strong coupling of the free carrier spins with the lattice of magnetic ions was the motivation for investigation of optically induced magnetization [Ryabchenko,82; Awschalom, 87; 89; 91]. The nonlinear optical properties are also

unique, allowing for example easy observation of the light-intensity dependence of the Faraday effect in static magnetic fields [Frey, 92; 92a] and the inverse Faraday effect in transmission in the ferromagnetic phase [Afanas'ev, 75]. This made them an attractive target for study with the SIFE.

$Cd_{0.6}Mn_{0.4}Te$ was chosen in particular because it is a well-characterised zincblende structure material and its optical properties have been extensively studied. At 532nm $Cd_{0.6}Mn_{0.4}Te$ has reflectivity 26% and a penetration depth of $\sim$100 nm. The sample on which experiments were performed, which was supplied by D.E.Ashenford and B.Lunn of the University of Hull, consisted of a 2.2μm thickness layer of $Cd_{0.6}Mn_{0.4}Te$ deposited by molecular beam epitaxy on top of a 0.5μm thickness layer of CdTe, itself deposited on an InSb substrate. The surface of the sample was the (001) crystal plane. The probe beam was directed nearly normally to the (001) crystal plane with its initial polarization along the [110] direction, suppressing any contribution from specular gyrotropic linear dichroism (see chapter 4). The measurements were performed at room temperature. At room temperature the band-gap energy E_g for this alloy composition is approximately 2.1 eV and the spin-orbit splitting of the valence bands Δ_0 is about 0.9 eV [Lautenschlager, 85]. Since pump and probe wavelengths were 532nm (2.33 eV) carriers were excited only from the upper valence bands to the conduction band.

Figure 3.2 shows the pump-induced polarization rotation angle in $Cd_{0.6}Mn_{0.4}Te$ as a function of the relative pump-probe delay for left and right hand circularly polarized pump. As expected, the polarization azimuth rotation changes sign for opposite circular pump polarizations. One can see from figure 3.2 that the time dependence of the effect reproduces the pump-probe cross-correlation function, indicating that the response time is faster than the pulse duration of 80 picoseconds. Figure 3.3 shows the dependence of the magnitude of the effect on pump intensity in $Cd_{0.6}Mn_{0.4}Te$ and also in GaAs, measured for purposes of comparison. In both materials the effect is linear in pump power over the range studied; in $Cd_{0.6}Mn_{0.4}Te$ the constant of proportionality is 2 $x10^{-10}$ rad.cm^{2}W^{-1} while in GaAs it is $2x10^{-11}$ rad.cm^{2}W^{-1}.

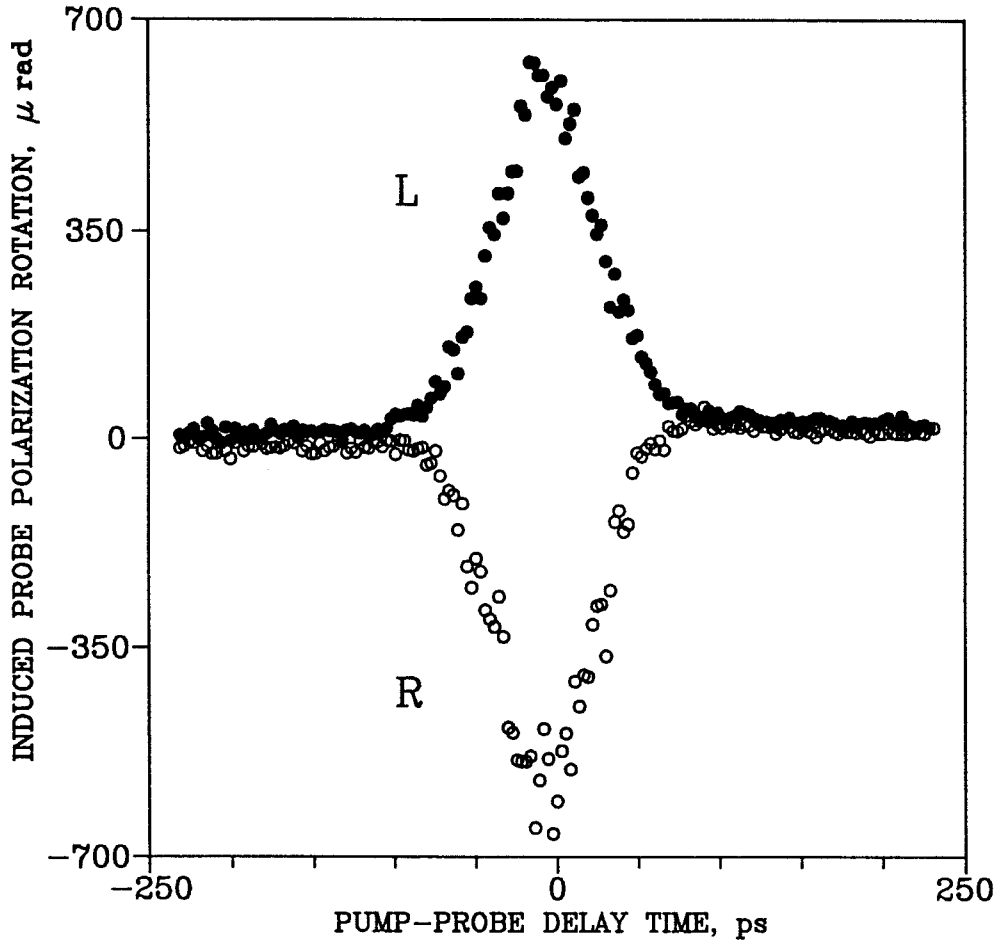

Figure 3.2 The SIFE in $Cd_{0.6}Mn_{0.4}Te$ as a function of relative pump-probe delay for left-hand (L) and right-hand (R) circularly polarised pump. I_p=3 MW cm^{-2}, λ=532 nm.

From equation (3.15) and given refractive index n=3.07, k=0.34 at 532nm [Lautenschlager, 85], one can deduce a value of χ_{xxyy} -χ_{xyyx} = 2.5 10^{-6} esu (3.5 10^{-14} SI) for $Cd_{0.6}Mn_{0.4}Te$ in comparison with χ_{xxyy} -χ_{xyyx} = 3 10^{-7}esu (4 10^{-15} SI) for GaAs. The value of χ in $Cd_{0.6}Mn_{0.4}Te$ is therefore high by comparison with non-resonant nonlinearities in a GaAs. However, later measurements by other members of our research group under identical circumstances gave a value of χ_{xxyy} -χ_{xyyx} = 2.3 10^{-6} esu (3.2 10^{-14} SI) in CdTe which is very similar to that for $Cd_{0.6}Mn_{0.4}Te$ [Bennett, 95a]. Therefore, it cannot necessarily be concluded that the magnetic ions have a significant effect on the SIFE in $Cd_{0.6}Mn_{0.4}Te$ at room temperature.

Only a tentative microscopic explanation is possible from this data. The optical excitation of 5 MW cm^{-2} creates a dense electron-hole plasma in the vicinity of the

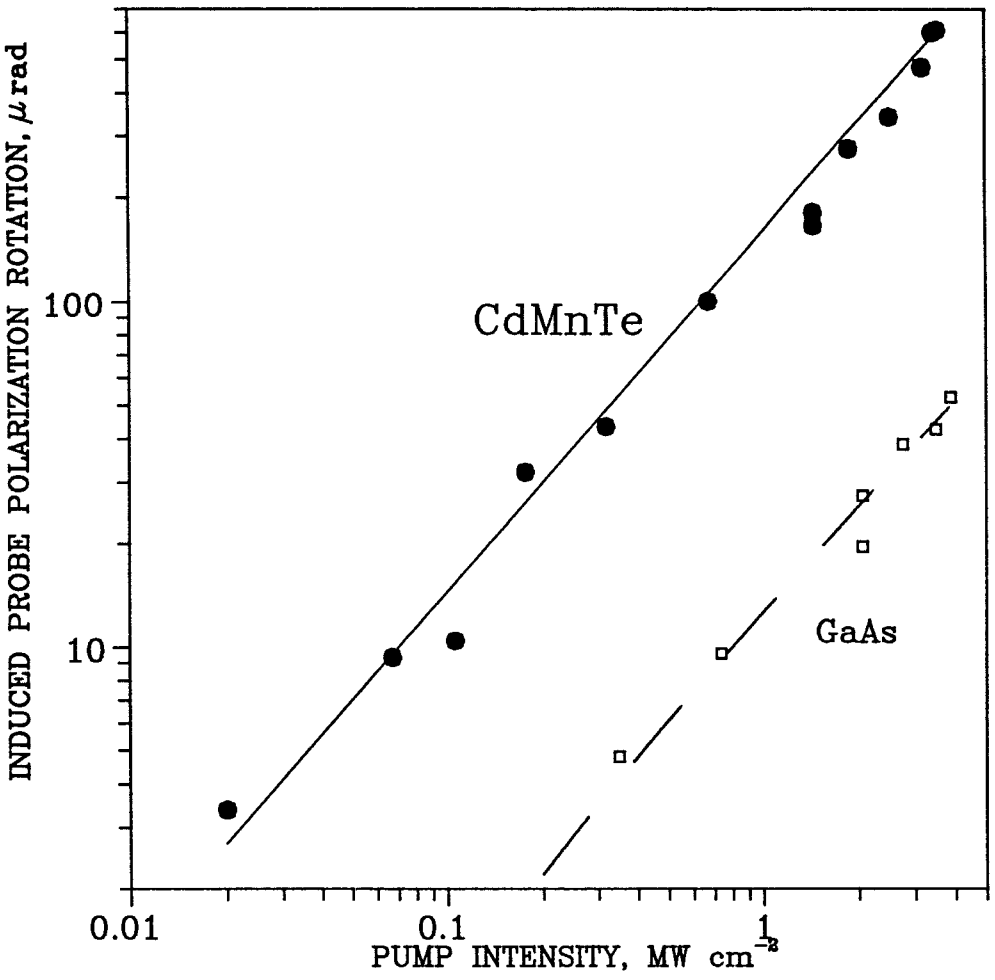

Figure 3.3 The SIFE in $Cd_{0.6}Mn_{0.4}Te$ and GaAs as a function of pump intensity, λ= 532 nm.

semiconductor surface whose density may be estimated as $N=10^{19}$-10^{20} cm^{-3} using the formula $N=(P_{pump}\times\alpha)/(\hbar\omega\times V\times L_{rep})$, where P_{pump} is the pump pulse energy, α is the absorption coefficient, V=penetration depth × the area of the spot and L_{rep} is the pulse repetition rate. With circularly polarized pumping the excited electron and hole populations are partially spin-polarised. At room temperature we may expect the polarised spins to relax on a picosecond time scale so that the fraction of spin polarised conduction electrons will follow the pump pulse envelope. In GaAs or CdTe, the population difference for states with opposite spins causes differential absorbtion of the right and left circularly polarized components of the linear probe giving polarization rotation [Popov, 94] (this is discussed in more detail in the section on femtosecond measurements in GaAs below.) In $Cd_{0.6}Mn_{0.4}Te$ the situation is more

complicated. Here the angular momentum in the conduction electron system is efficiently transferred to the paramagnetic ions by *s-d* exchange spin-flip processes. This spin-flip time has been estimated to be in the 1 picosecond range [Awschalom,87,89,91; Bastard, 92], comparable to the free carrier spin relaxation times. The Mn ion system will thus acquire a spin-polarisation which follows the optical pulse. Such Mn spin polarisation produces a very large splitting of the band gap for right and left circularly polarised light, roughly equivalent to a magnetic g-factor of 10^3. It might thus seem surprising that the SIFE in $Cd_{0.6}Mn_{0.4}Te$ not strongly enhanced with respect to CdTe. It should be noted that measurements of magnetisation due to the inverse Faraday effect also yielded small values [Nikitin,90]. This was attributed to decrease in magnetisation due to magnetic ion-hole interaction, and to strong depolarisation of electrons due to their excitation into states above the bottom of the conduction band.

Since the Faraday effect in $Cd_{1-x}Mn_xTe$ is known to exhibit a complicated temperature dependence, and magnetisation due to the inverse Faraday effect is stronger at low temperature, an interesting line of further research is to examine the temperature dependence of the SIFE in this material. This is being pursued by other members of the group.

3.4.2 Study of the SIFE in the High-T_c Superconductor $YBa_2Cu_3O_{7-\delta}$

High T_c superconductors such as $YBa_2Cu_3O_{7-\delta}$ are of interest both because of their potential technological usefulness and for their unusual and incompletely explained physics. In particular, attempts have been made by several groups to detect specular circular dichroism/birefringence in these materials, in a search for an optical manifestation of the hypothetical violation of time-reversality in these materials called for in some theories of the origin of their superconductivity [Lawrence, 92; Spielman,92; Lyons,93].

$YBa_2Cu_3O_{7-\delta}$ crystals are attributed to the orthorhombic crystal point group (4/mmm).

The structure consists of CuO_2 layers in the (001) plane, loosely joined by "fencelike" CuO_3 chains in the (100) plane [Beno, 87]. It is the (001) planes which conduct electricity in the superconducting state. The optical properties of $YBa_2Cu_3O_{7-\delta}$ crystals show a large anisotropy between excitations perpendicular to and parallel to the (001) plane. There is also a weaker anisotropy between the [100] and [010] directions, although this is often suppressed in measurement because $YBa_2Cu_3O_{7-\delta}$ samples generally display microtwinning with (110) and $(1\bar{1}0)$ as twinning planes. The domain sizes are generally on the order of $50\times50\mu$m [Petrov, 88; Koch, 89]. This means that measurements in the (001) plane often yield the average value for excitation along the [100] and [010] directions.

The experiments were performed with a sample of bulk $YBa_2Cu_3O_{7-\delta}$ at room temperature. The crystal had been grown by a method using a favourable flux from a SnO_2 crucible and then annealed in high purity flowing oxygen at 535°C for 2 weeks. Magnetisation measurements had shown that it had a sharp transition (within 1 K) to the superconducting state at 93 K [Lin, 92]. The crystal had a good quality mirror-like surface and a nearly perfect parallelepiped shape of approximately 2 mm by 3 mm by 100 μm. The sample surface was in the plane normal to the [001] direction. In these experiments, the polarisation of the probe beam was directed parallel to [100] (parallel to one of the edges of the crystal). Hence there was no rotation of the probe resulting from birefringence in the (001) plane. Since the anisotropy is small, we may assume that any orientationally dependent corrections to the SIFE will be small compared to the magnitude of the effect. Hence, we need not be concerned with the domain structure of the sample, since any differences in the induced rotation due to the orientation of the twinned microcrystals will be small.

The experiments were conducted at room temperature. At room temperature $YBa_2Cu_3O_{7-\delta}$ has a reflectivity for $\lambda=532$ nm of $\sim10\%$, which is roughly isotropic in the (001) plane [Koch, 89]. The light penetration depth is ~100 nm. Figure 3.4 shows the induced probe polarisation azimuth rotation as a function of pump-probe delay for the case of stimulation with a left hand (L) and right hand (R) circularly

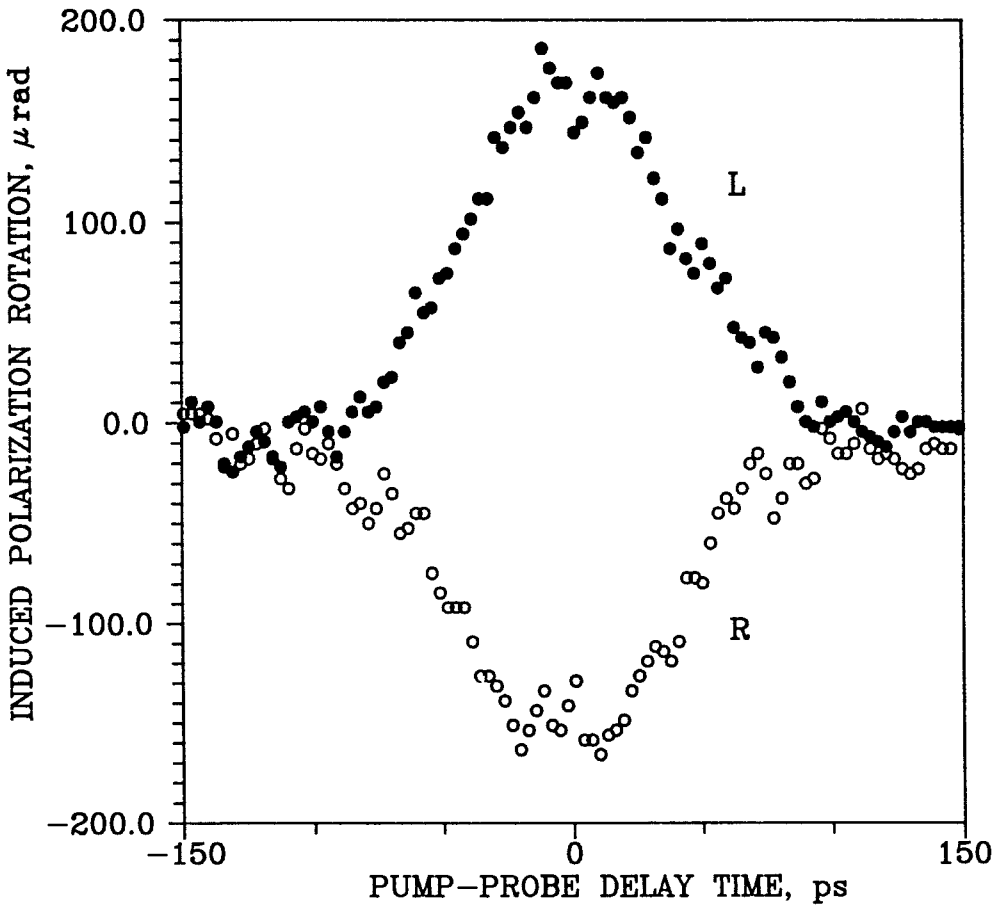

Figure 3.4 The SIFE in $YBa_2Cu_3O_{7-\delta}$ as a function of pump-probe delay. I_p=5 MW cm^{-2}, λ=532 nm.

polarised pump. Figure 3.5 shows the intensity dependence of the induced rotation over the range of intensities 0.2-8 MW cm^{-2}. The rotation due to the SIFE was linear in pump intensity up to 8 MWcm^{-2}, with constant of proportionality 2.2 10^{-11} rad.cm^2.W^{-1}.

From equation (3.15) and given refractive index n=1.8, k=0.4 at 532 nm [Koch,89], one can deduce values of χ_{xxyy} -χ_{xyyx} =8.4 10^{-9}esu (1.2 10^{-16}SI).

The following mechanisms may be responsible for SIFE in $YBa_2Cu_3O_{7-\delta}$: (a) Predominant spin polarization of the free electrons and holes due to circularly polarized pump which creates an effective magnetization. Here the relaxation of the nonlinearity is due to dephasing interaction of the carriers with each other and the

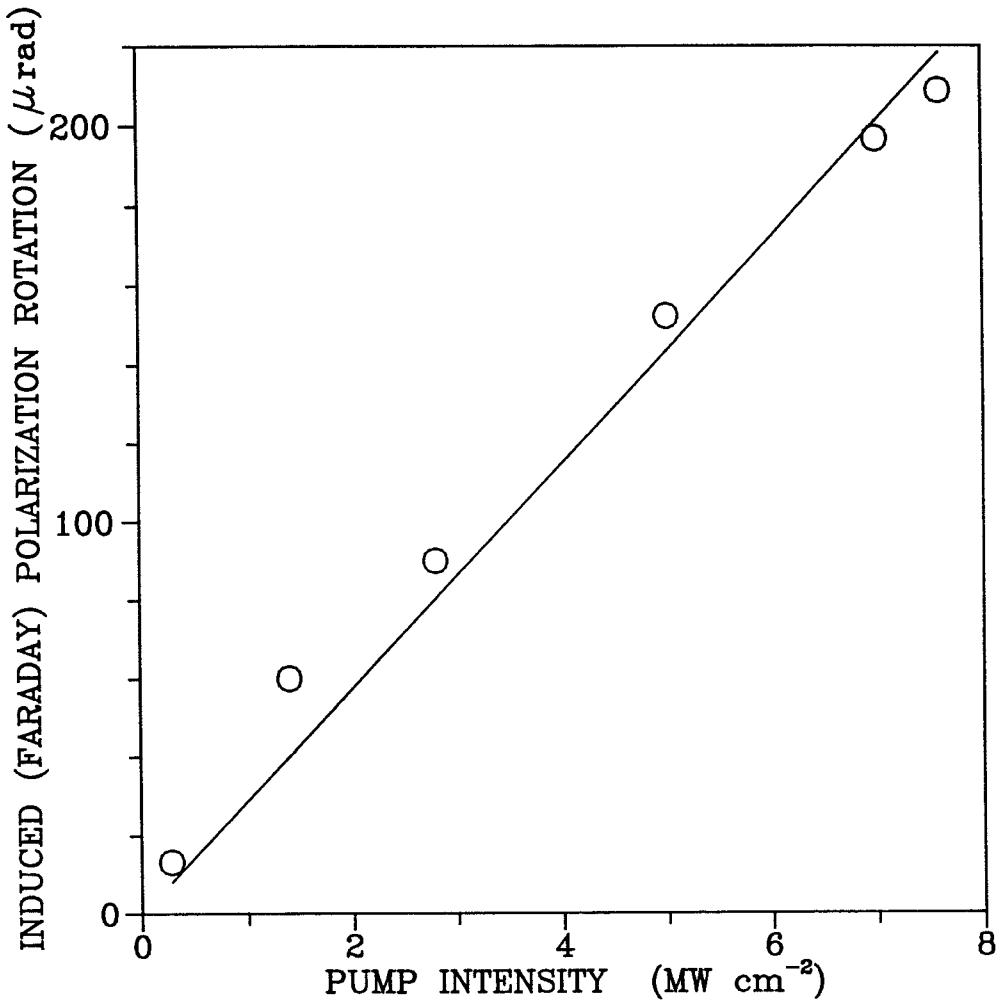

Figure 3.5 The SIFE in $YBa_2Cu_3O_{7-\delta}$ as a function of pump intensity. λ=532 nm

lattice; (b) Orientation of the Cu spins by polarized mobile carriers may also produce further magnetization. Spin polarization can relax through interaction with: (i) each other, (ii) phonons via spin-orbit interaction, (iii) free carriers. Given that the SIFE is due to light-induced magnetisation of a medium, it would be interesting to carry out low temperature experiments, where the Meissner effect should expel any field from the sample.

3.4.3 Study of the Ultrafast Dynamics of the SIFE in GaAs

The SIFE offers the possibility of optically investigating the spin relaxation and

thermalisation times of excited carriers in opaque materials. The first observations which resolved dynamics of the SIFE in GaAs were [Bungay,94], using a Ti:Sapphire laser producing 2-picosecond pulses (λ=750 nm). In this work two components of the incoherent SIFE were observed: a fast component whose decay was too fast to be resolved, and a more slowly decaying component of opposite sign, with a decay time of 11 ± 1 picosecond.

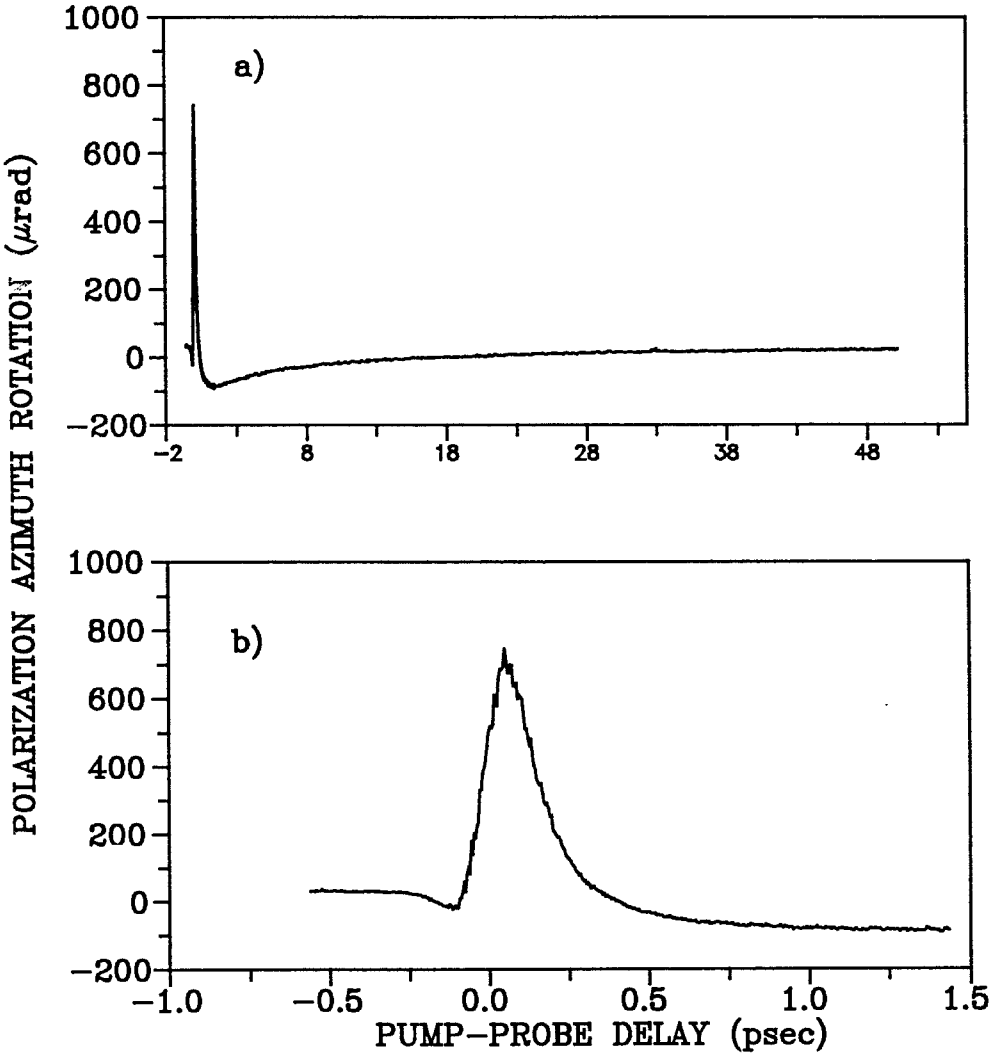

Figure 3.6 The SIFE in GaAs as a function of pump-probe relative delay for right-hand circularly polarised pump. I_p=4.8 GW cm-2, λ=810nm showing a) long tail, b) expansion of initial peak.

In the experiments described below, the transient SIFE was observed in bulk GaAs with ~70 femtosecond time resolution. The sample was a 4 mm × 8 mm × 1 mm

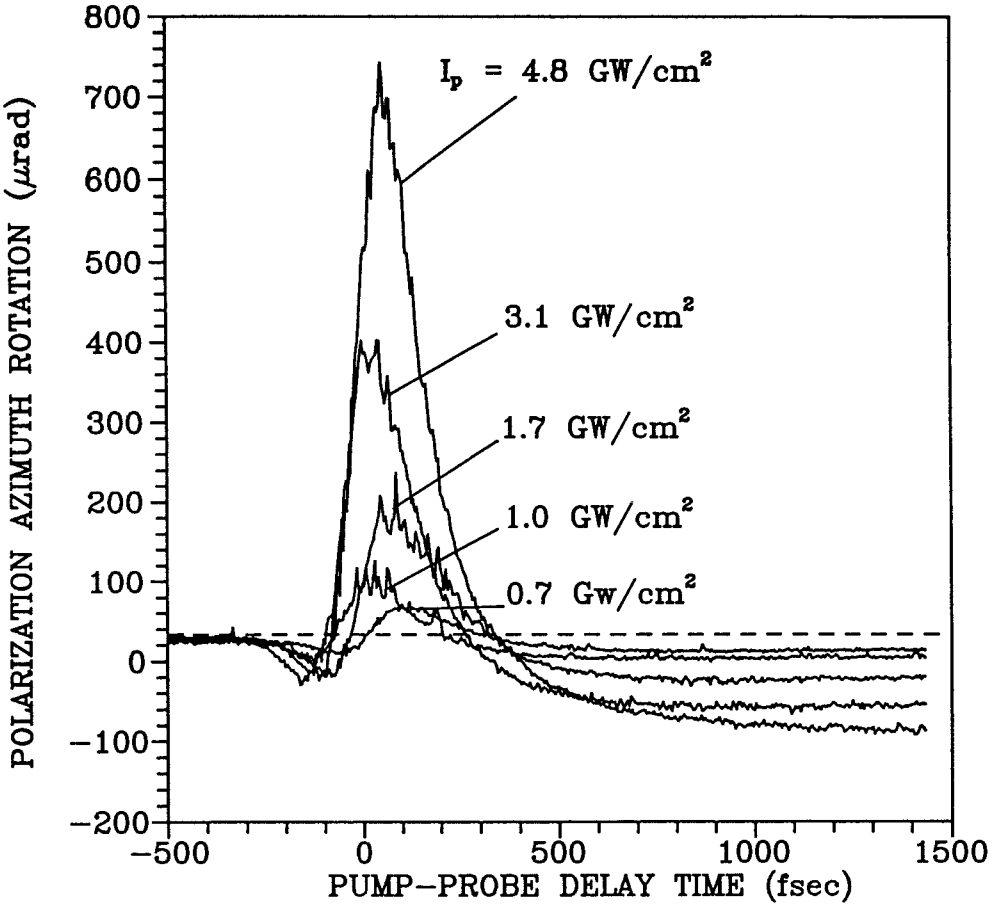

Figure 3.7 The SIFE in GaAs as a function of pump-probe delay for a variety of pump intensities, λ=810nm.

single crystal of GaAs. GaAs has a reflectivity of 32% at 810 nm. GaAs is opaque at 810 nm ($\hbar\omega$=1.53 eV) with light penetration depth of about 1 μm. This photon energy is 0.12 eV above the band gap, allowing excitation of electrons from the light and heavy hole bands but not from the split-off valence band. As in the experiments with $Cd_{0.6}Mn_{0.4}Te$, the sample was aligned such that the probe polarization azimuth was in the [110] direction, suppressing any contribution from specular gyrotropic linear dichroism. Pump intensities in the range from 0.7 - 5 GW cm^{-2} were used corresponding to estimated optically induced free carrier concentrations of up to 6.10^{18} cm^{-3}. The corresponding reflected probe polarization azimuth rotation and its behaviour in the time domain is shown in figure 3.6 for I_p = 5 GW cm^{-2}. The results shown in figures 3.6a and b were produced with a right-hand circularly polarised pump beam. Reversal of the pump chirality gave similar results but with the sign of

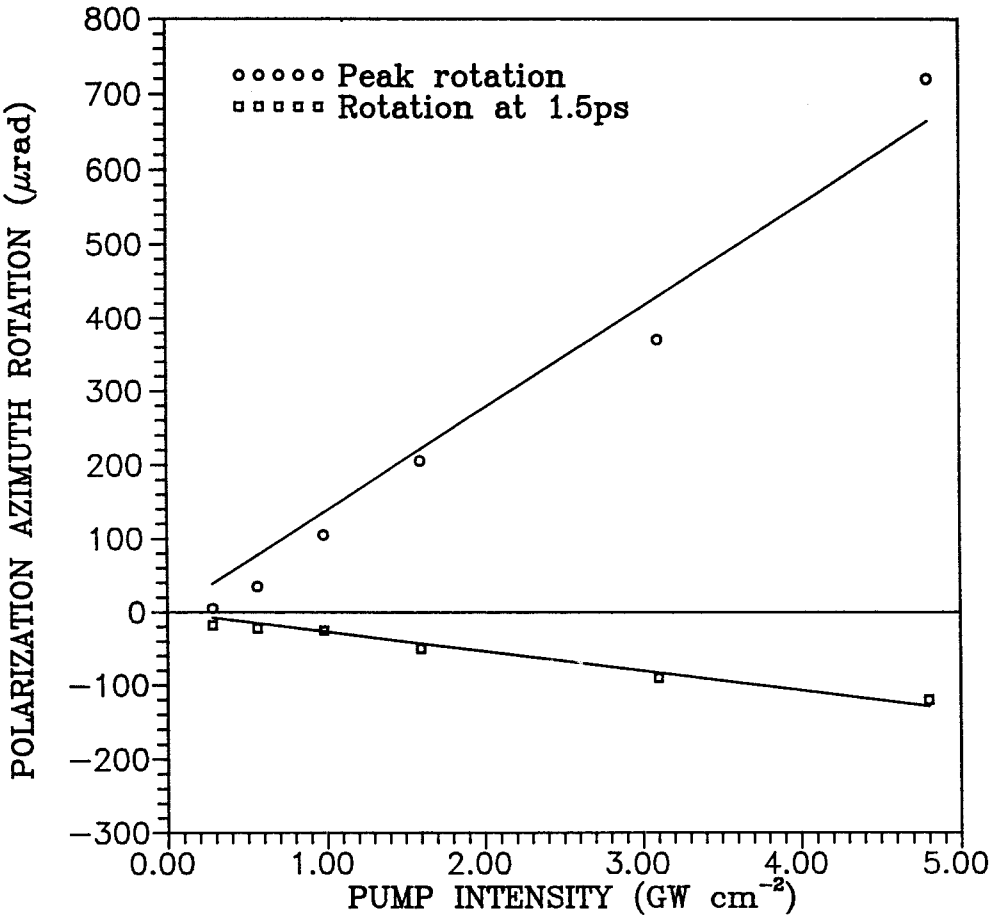

Figure 3.8 The magnitude of probe polarization azimuth rotation as a function of intensity; a) peak rotation, b) rotation at 1.5 ps pump-probe delay, λ=532 nm.

probe polarization rotation reversed. As expected, the results show a large positive rotation which decays over a few hundred femtoseconds, followed by a negative rotation which decays with a longer time constant.

The experiment was performed at a variety of pump intensities, as shown in figure 3.7. Figure 3.8 shows values of the polarisation azimuth rotation as a function of pump intensity at zero and 1.5 picosecond pump-probe delays. Probe polarisation azimuth rotation is a linear function of pump intensity at both time delays. The peak rotation has a constant of proportionality of 1.5 10^{-13}rad cm^{-2} W^{-1}, and the negative rotation peak at 1.5 picoseconds has a constant of proportionality of 2.7 10^{-14}rad cm^{-2} W^{-1}.

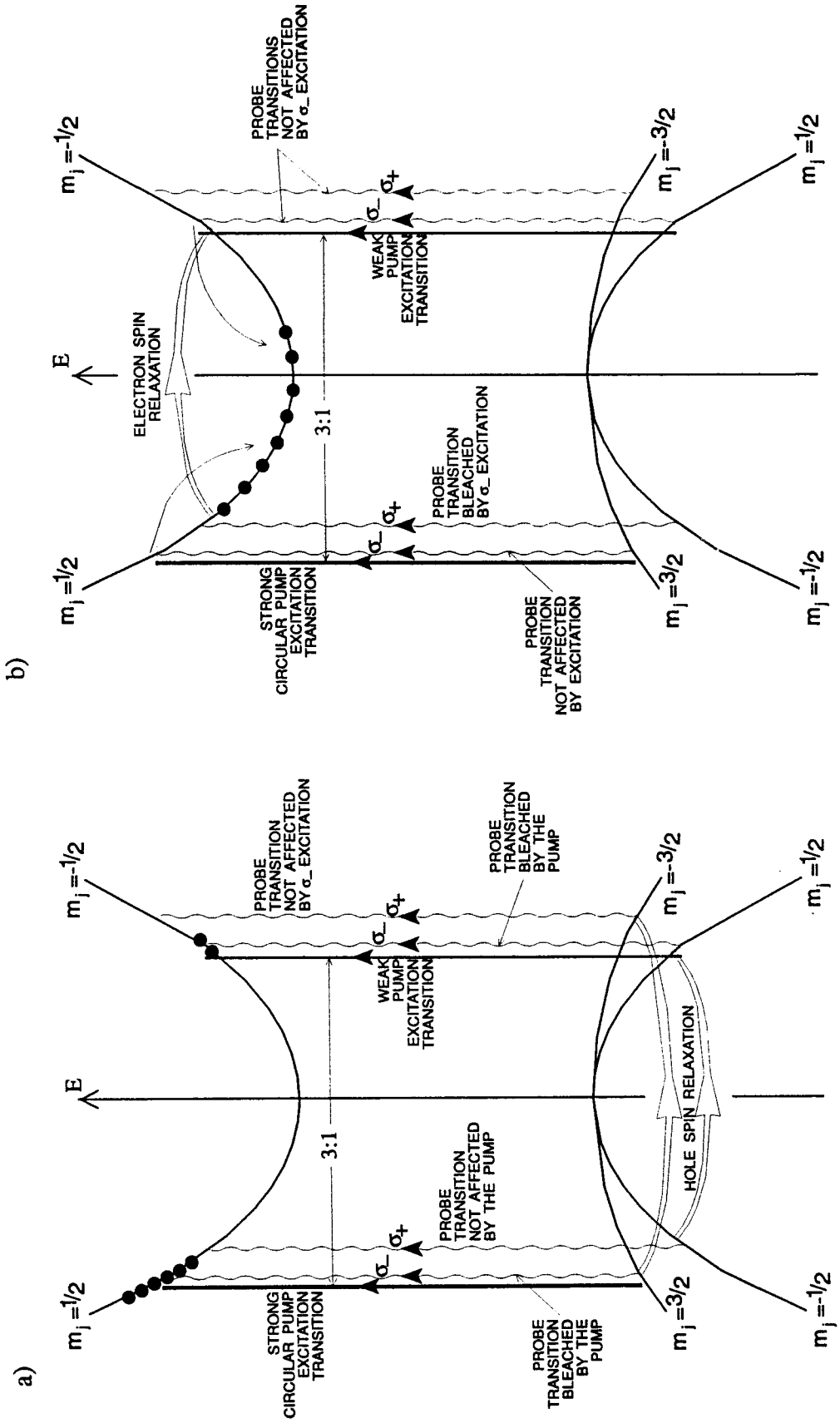

Figure 3.9 Model of Population Dynamics in GaAs by N.I.Zheludev, R.T.Harley and I.R.Shatwell. a) excitation by pump pulse, b) carrier relaxation

The long decay of the negative rotation feature is fit by a single exponential with a decay time of 10 picoseconds. The faster decaying positive rotation feature is well fit by a double exponential decay, one component having a decay time of 200-300 femtoseconds and the other a decay time in the region of 70 femtoseconds, although this is too short in comparison with the pulse length to be accurately determined.

A microscopic model explaining the time evolution of the SIFE in terms of the population dynamics of the optically created free carriers has been developed by N.I.Zheludev, R.T.Harley and I.R.Shatwell [Zheludev, 95a]. This is outlined below.

A 6-band model of the GaAs band-structure is adopted and rotation of the reflected light polarisation azimuth is considered to result from differential absorption of the left and right circularly polarised components of the linearly polarised probe light. The dynamics may be considered in two stages which are presented in figure 3.9.

In figure 3.9(a), the pump and probe pulses are coincident at the crystal surface, the left-hand circular polarised pump (σ_-) promotes carriers mainly from the heavy hole valence-band ($m_j^h = 3/2$) to the conduction band ($m_j^e = 1/2$). These transitions outweigh transitions from the light hole valence-band to the conduction band which have a reduced matrix element and a lower density of final states. These carriers occupy energy states close to the energy of the excitation and consequently bleach the absorption coefficient, α_-, associated with the σ_- pump leading to reflected probe polarisation azimuth rotation. This initial rotation relaxes due to two main processes: thermalisation of the electrons and holes towards the centre of the bands, which takes place on a 200 femtosecond timescale [Hunsche, 93; Knox, 86; Knox, 88] and hole spin relaxation on a timescale of 1 picosecond [Meier, 84].

The second stage of the population dynamics of the incoherent effect is shown in figure 3.9(b). The electrons and holes have thermalised towards the centre of the bands to form Boltzmann populations characterised by their excess energies [Hunsche,93], but the electron spins have not relaxed. The states occupied by

transitions from $m_j^h = 3/2$ to $m_j^e = 1/2$ have now emptied whilst the lower energy states corresponding to the light hole to conduction band transition ($m_j^h = -1/2$ to $m_j^e = 1/2$) are filled by the thermalised carriers. This transition corresponds to a σ_+ excitation and consequently the absorption, α_+, is more strongly bleached, reversing the sign of the observed polarisation azimuth rotation of the probe. The decay of the differential absorption is now controlled by the spin relaxation of the thermalised electrons in the conduction band which was measured to be 11 picoseconds by Bungay et. al. [Bungay, 94]. Recombination of the carriers is not considered, since this occurs on a sub-nanosecond timescale, and is too slow to be important in the interpretation of the SIFE.

Clearly, the theory outlined above is too simple to be expected to completely account for the response of GaAs, but it does show the main features in the observed dynamics of the SIFE, although the observed decay of the initial peak is faster than might be expected. Figure 3.10 compares a) experimental data on the SIFE in GaAs with b) a plot produced by a computer simulation created by I.R.Shatwell [Shatwell,95], based on the theory of the dynamics of the SIFE in GaAs described above. The simulation does not provide an absolute value for induced probe polarisation rotation, but the relative magnitude of the positive and negative rotation components should be accurate. The decay times for the electron and hole spin relaxations and thermalisation used to generate the plot were taken from values obtained by fitting exponential decays to the experimental data. The FWHM of the laser pulse was set at 70 femtoseconds. The model described above offers no explanation of the initial small negative rotation. This feature was also observed in the 2 picosecond experiments [Bungay, 94]. It may represent a nonlinearity with response time faster than the pulse length, so that it traces an autocorrelation of the pulse intensity. Such a contribution, superimposed on the slowly rising main peak arising from the population dynamics, and having opposite sign, could produce the initial dip observed. Such an effectively instantaneous response might arise from nonlinearity of bound electrons.

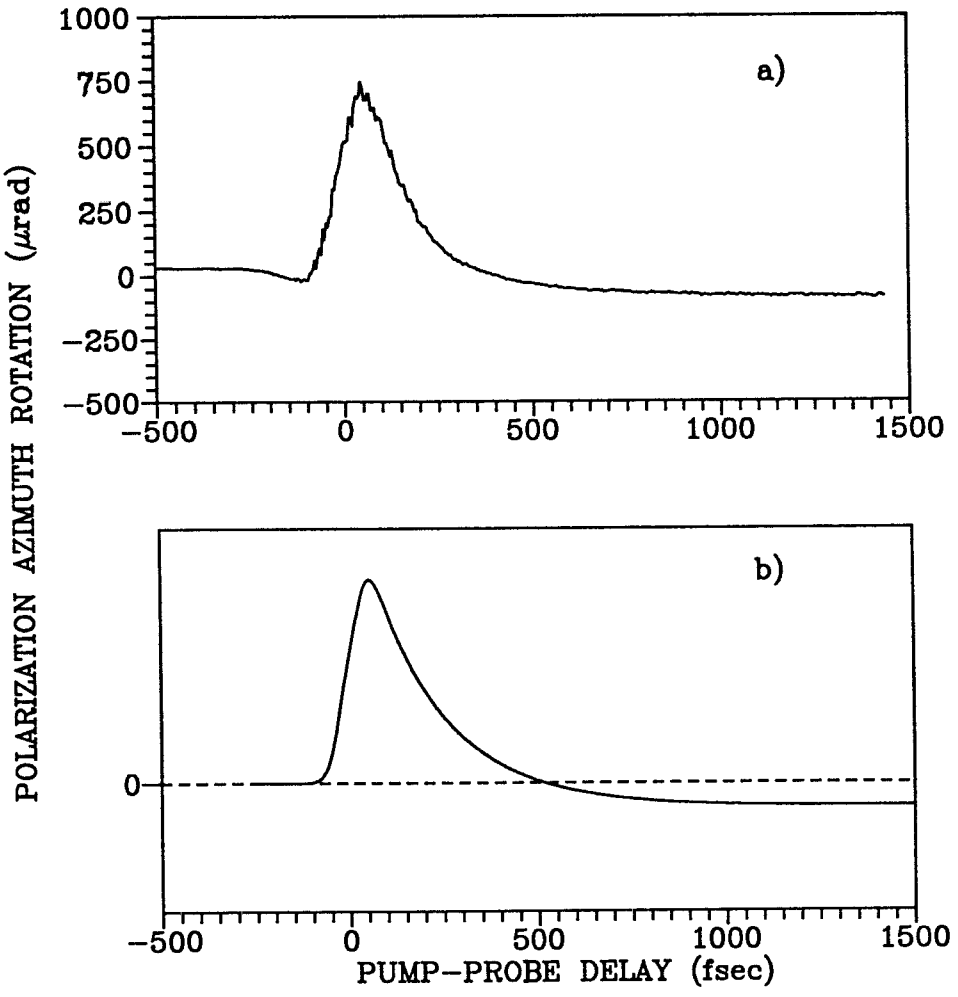

Figure 3.10 a) observed SIFE in GaAs, b) simulated SIFE in GaAs based on theoretical model.

3.4.4 Study of the SIFE in Nickel

Bulk metals might be expected not to have significant third order degenerate nonlinearity $\chi^{(3)}$ due to free electrons. Free electrons, the major agent in infrared absorption in metals, were expected to have no Kerr-type dipole nonlinearity unless they are confined in microparticles, and free-electron third-order multipole nonlinearities were estimated to be very small [Hache, 86; 88]. However, this does not take account of any spin-related processes.

The SIFE in gold was first observed by members of our group [Zheludev, 95] using a Cr:forsterite laser (λ=1260 nm) which produced 90 femtosecond pulses, and a number of other metals have also now been examined at this wavelength [Bennett,95]. All these metals showed instantaneous response on this timescale. The observed polarisation azimuth rotation in nickel was approximately an order of magnitude greater than in any of the other metals (800 μrad at pump intensity I_p=1 GWcm^{-2}).

The main mechanism of the nonlinearity in these materials is believed to be intraband free electron spin flipping [Zheludev, 95]. This is distinguishable from interband nonlinearities, for example those responsible for the coherent third-harmonic generation process [Burns, 71], and the major incoherent visible-range cubic optical nonlinearity which is due to resonant optical transitions from the d-states to the s-p conduction band in the vicinity of the Fermi level [Eesley, 86; Schoenlein, 87].

In [Zheludev, 95], the SIFE in metals is treated by use of a conventional metallo-optics approach. Light reflected from the surface of a metal undergoes a phase retardation $\alpha=tan^{-1}[2\kappa/(n^2-1+\kappa^2)]$, where n and κ are the real and imaginary parts of the refractive index. Rotation of the polarisation azimuth of the probe beam arises from pump-induced differential retardation of the left and right hand circularly polarised components of the probe. For $|\kappa| \gg |n|$, probe polarisation azimuth rotation is given by $\delta\alpha_r \approx -2\Delta\kappa/\kappa^2$, where $\Delta\kappa$ is the pump-induced difference between the values of κ for left and right hand circularly polarised light.

Conservation of energy and momentum requires that free-electron absorption occurs when an electron in the conduction band absorbs a photon and simultaneously emits/absorbs a phonon or scatters on an impurity, defect or boundary. In order for angular momentum to be conserved, the electron must reverse its spin state when it absorbs a photon. In SIFE measurements, absorption of photons from the circularly polarised pump beam gives rise to an imbalance in the populations of electrons with opposite projections of spin (m_J=1/2 and m_J=-1/2) along the propagation direction of the beam.

Since in the case considered the photon energy ($\hbar\omega$=1.5 eV) is much less than the Fermi energy (ε_F=9.2 eV) the induced circular dichroism may be treated by the standard quantum approach to free-carrier absorption [Dumke, 61], which is modified in [Zheludev, 95] to deal with spin-dependent processes. This analysis gives an expected value of rotation due to this spin-flipping mechanism of

$$\left|\frac{\delta\alpha_r}{\delta I}\right|_{theor} \propto \frac{8}{c\,\hbar\omega_p\,\rho(\varepsilon_F)\,\hbar\omega_L}\left(\frac{\tau_s}{\tau} - \frac{1}{2}\right) \qquad (3.17)$$

where ω_p is the plasma frequency, $\hbar\omega_L$ is the photon energy, $\rho(\epsilon_F) = 3N/(4\epsilon_F)$, N is the free electron density, ε_F is the Fermi energy, and (τ_s/τ) is the ratio between the relaxation time due to spin flipping processes and the relaxation time for electron momentum transfer due to all relaxation processes. This corresponds to values of $\chi^{(3)}$ in the region of 10^{-9} esu (10^{-17} SI).

It should be noted that although the expected value of $\chi^{(3)}$ is reasonably large, the observable effect of the SIFE is small, due to the high refractive index of metals, which acts on the observable rotation approximately as n^{-5} (see equation (3.15)). Hence the need for a highly sensitive polarimetric technique for its observation.

The metals other than nickel which were examined had observed values of rotation within the range that might be expected from equation (3.17). The enhancement of the effect in nickel may be due to spin correlation and exchange effects in this ferromagnetic material, as well as its relatively low Fresnel factor (n=2.50, k=4.20 at 810 nm) compared with other metals.

The relaxation time for this effect is estimated to be on the order of a few tens of femtoseconds. This provided a strong motivation to measure the SIFE in metals with the best possible time resolution, in order to resolve the relaxation time or place an upper limit on its value.

The nickel sample was produced by evaporating in a vacuum (7 10^{-6}mbar) a ~40 nm

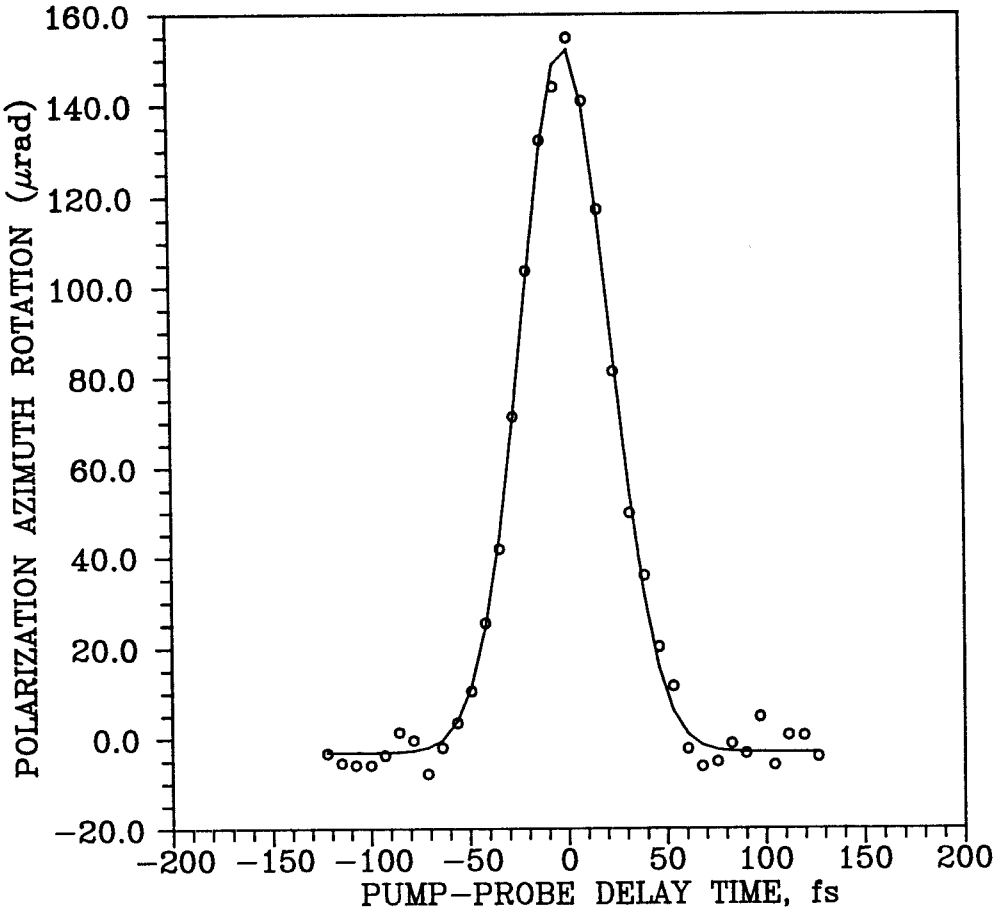

Figure 3.11 The SIFE in Nickel as a function of pump probe delay. I_p=10 MW cm^{-2}, λ=810 nm.

thickness layer of nickel of purity better than 99.99% onto a polished glass substrate. This is greater than the skin depth of nickel (δ=15 nm at λ=810 nm). It had a good, mirror-like surface of area 15 mm × 20 mm. Figure 3.11 shows probe polarisation azimuth rotation in nickel as a function of pump-probe delay. The data appears to be symmetrical about the zero delay position, i.e. the SIFE in nickel is effectively instantaneous with this time resolution. Treating the observed data as an autocorrelation function, we obtain a pulse length of 32 femtoseconds. The observed rotation has a magnitude of 155 μrad. Given n=2.5, k=4.2 (λ=810 nm) for a thin nickel film, this corresponds to a value of $\chi^{(3)}$ of 2 10^{-9} esu (2.7 10^{-17}SI). This is a fairly strong nonlinearity. In fact, in terms of speed and magnitude of nonlinear response, it is in the range required for all-optical switching applications, raising the possibility of important device applications. The possibility of using this nonlinearity

as the basis for an optical autocorrelator was discussed in chapter 2. With this in mind, it is intended that the nonlinear optical properties of bulk metals become a major research direction for our group.

3.5 Conclusions

The Specular Inverse Faraday effect has been observed in a variety of opaque materials, allowing the determination of components of $\chi^{(3)}$ in these materials. With the use of a femtosecond modelocked laser, the time evolution of the SIFE in GaAs has been observed, allowing measurement of carrier relaxation times. Strong and very fast (not more than 32 femtoseconds relaxation time) nonlinearity was observed in nickel, raising the possibility of use of this material in optical switching, or as an interaction medium in a fast autocorrelator.

The effectiveness of the SIFE as a tool of nonlinear spectroscopy of opaque materials has been demonstrated. As a spectroscopic technique, the SIFE has several advantages. Since it is a reflective phenomenon, it may be used to study opaque materials. The time resolution of the method is limited only by the pulse length of the laser used. These advantages have been clearly demonstrated in the work on metals, where very fast nonlinearity of bulk metals has been observed.

3.6 References

[Afanas'ev, 75] Afanas'ev M.M, Zakharchenya B.P, Kompan M.E. et. al. Soviet Physics JETP Lett., **21**, (1975), 224.

[Arutyunyan, 75] Arutyunyan V.M, Papazyan T.A, Adonts G.G, Karmenyan A.V, Ishkhanyan S.P. and Khol'ts L, Sov. Phys. JETP, **41**, (1975), 22.

[Atkins, 68] Atkins P.W. and Miller M.H, Mol. Phys., **15**, (1968), 503.

[Awschalom, 87] Awschalom D.D, Warnock J. and von Molnar S, Phys. Rev. Lett., **58**, (1987), 812.

[Awschalom, 89] Awschalom D.D. and Warnock J, IEEE J.Q.Electronics **25** (1989), 2570.

[Awschalom, 91] Awschalom D.D. and Freeman M.R, Physica B, **169**, (1991), 285.

[Bar-Ad, 91] Bar-Ad S. and Bar-Joseph I, Phys. Rev. Lett., **66**, (1991), 2491.

[Bar-Ad, 92] Bar-Ad S. and Bar-Joseph I, Phys. Rev. Lett., **68**, (1992), 349.

[Bastard, 92] Bastard G and Ferreira R, Surface Science, **267**, (1992), 335

[Bennet, 95] Bennet P.J, Loh H, Popov S.V, Shatwell I.R, Svirko Yu.P, Zheludev N.I, 12-th UK National Quantum Electronics Conference, Southampton, 4-8 Sep 1995, paper 8-2

[Bennet, 95a] Bennet P.J, Loh H, Popov S.V, Shatwell I.R, Svirko Yu.P, Zheludev N.I, Kamalov V.F. and Slobodchikov E.V, Paper QWA8, QELS 95, Baltimore, Maryland, May 1995.

[Beno, 87] Beno M.A, Soderholm L, Capone D.W, Appl. Phys. Lett. **51**, (1987), 57.

[Bungay, 94] Bungay A.R, Popov S.V, Shatwell I.R, Zheludev N.I, European Quantum Electronics Conference, Amsterdam, Aug 28-Sep 2, 1994.

[Burns, 71] Burns K.W and Blombergen N, Phys. Rev. B **4**, (1971), 3437.

[Butcher, 90] Butcher P.N. and Cotter D, "The Elements of Nonlinear Optics", C.U.P., 1990.

[Damen, 91] Damen T.C, Leo K, Jagdeep Shah and Cunningham J.E, Appl. Phys. Lett., **58**, (1991), 1902.

[Dumke, 61] Dumke W.P, Phys. Rev., **124**, (1961), 1813.

[Eesley, 86] Eesley G.L, Phys. Rev. B **33**, (1986), 2144.

[Fishman, 77] Fishman G. and Lampel G, Phys. Rev. B., **16**, (1977), 820.

[Frey, 92] Frey J, Frey R, Flytzanis C, Triboulet R, J. Opt. Soc. Am. B, **9**, (1992), 132.

[Frey, 92a] Frey J, Frey R, Flytzanis C, Phys. Rev. B, **45**, (1992), 4056.

[Golubkov, 90] Golubkov A.A. and Makarov V.A, Opt. Spectrosc., **69**, (1990) 369.

[Hache, 86] Hache F, Ricard D, and Flytzanis C, J. Opt. Soc. Am. B **3**, (1986) 1647.

[Hache, 88] Hache F, Ricard D, Flytzanis C and Kreibig U, Appl. Phys. A **47**, 347 (1988).

[Hunsche, 93] Hunsche S, Heesel H, Ewertz A. and Kurz H, Phys. Rev. B., **48**, (1993), 17818.

[Kawazoe, 93] Kawazoe T, Masumoto Y. and Mishina T, Phys. Rev. B., **47**, (1993), 10452.

[Knox, 88] Knox W.H, Chelma D.S, Livescu G, Cunningham J.E. and Henry J.E, Phys. Rev. Lett., **61**, (1988), 1290.

[Knox, 86] Knox W.H, Hirlimann C, Miller D.A.B, Shah J, Chelma D.S. and Shank C.V, Phys. Rev. Lett., **56**, (1986), 1191.

[Koch, 89] Koch B, Geserich H.P, Wolf T.H, Sol. State. Comm., **71**, (1989), 495.

[Krenn, 85] Krenn H, Zawadski W. and Bauer G, Phys. Rev. Lett., **55**, (1985), 1510.

[Kuwata, 84] Kuwata M, J. Phys. Soc. Japan, **53**, (1984), 4456.

[Kuwata, 87] Kuwata M, J. Lum., **38**, (1987), 247.

[Lautenschlager, 85] Lautenschlager P, Logothetidis S, Vina L, Cardona M, Phys. Rev. B, **32**, (1985), 3811.

[Lawrence, 92] Lawrence T.W, Szöke A, Laughlin R.B, Phys. Rev. Lett., **69**, (1992), 1439.

[Lin, 92] Lin C.T, Zou W, Liang W.Y, Schonherr E, Bender H, Physica C, **195**, (1992), 291.

[Lyons, 93] Lyons K.B, Dillon J.F, Duclos S.J et. al., Phys. Rev. B, **47**, (1993), 8195.

[Meier, 84] Meier F. and Zakharchenia B.P (Editors), "Optical Orientation", North Holland, 1984.

[Nikitin, 90] Nikitin P.I, Savchuk A.I, Sov.Phys.Usp., **33**, (1990), 974.

[Petrov, 88] Petrov M.P, Grachev A.I, Krasin'kova M.V. et. al. Sol. State. Comm., **67**, (1988), 1197.

[Popov, 94] Popov S.V, Svirko Yu.P, Zheludev N.I, Optics Letters, **19**, (1994), 13.

[Popov, 96] Popov S.V, Svirko Yu.P, Zheludev N.I, accepted by J. Opt. Soc. Am. A.

[Rana, 94] Rana R.S, Eunsoon Oh, Chua K, Ramdas A.K, Nolte D.D, Phys. Rev. B, **49**, (1994), 7941.

[Roussignol, 92] Roussignol P, Rolland P, Ferreira R, Delalande C. and Bastard G, Surf. Sci., **267**, (1992), 360.

[Ryabchenko, 82] Ryabchenko, S.M, Semenov, Yu.G, Terletskii, O.V, Sov. Phys. JETP, **55**, (1982), 557.

[Saiki, 92] Saiki T, Takeuchi K, Kuwata-Gonokami M, Mitsuyu T. and Ohkawa K, Appl. Phys. Lett., **60**, (1992), 192.

[Schoenlein, 87] Schoenlein R.W, Lin W.Z, Fujimoto J.G, and Eesley G.L, Phys. Rev. Lett. **58**, (1987), 1680.

[Sham, 93] Sham L.J, J.Phys: Condens. Matter, **5**, (1993), A51.

[Shen, 94] Shen Y.R, Surface Science, **229**, (1994), 551.

[Spielman, 92] Spielman S, Dodge J.S, Lombardo L.W et. al., Phys. Rev. Lett., **68**, (1992), 3472.

[Stark, 92] Stark J.B, Knox W.H. and Chelma D.S, Phys. Rev. Lett., **68**, (1992), 3080.

[Svirko, 94] Svirko Yu.P. and Zheludev N.I, JOSA B, 11, (1994), 1388.

[Takeuchi, 90] Takeuchi A, Muto S, Inata T. and Fujii T, Appl. Phys. Lett., **68**, (1990), 3080.

[Van de Zeil, 65] Van der Zeil J.P, Pershan P.S. and Malmstron L.D, Phys.Rev.Lett. **15**, (1965), 190.

[Wieman, 76] Wieman A, Hänsch T.W, Phys.Rev.Lett. **36**, (1976), 1170.

[Zerrouati, 88] Zerrouati K, Fabre F, Bacquet G, Bandet J. and Frandon J, Phys. Rev. B, **37**, (1988), 1334.

[Zheludev, 95] Zheludev N.I, Bennett P.J, Loh H, Popov S.V, et.al., Optics Letters, **20**, (1995), 1368.

[Zheludev, 95a] Zheludev N.I, Shatwell I.R. and Harley R.T, Private communication.

Chapter 4

Observation of Natural and Pump-Induced Specular Gyrotropic Linear Dichroism

4.1 Synopsis

The work in this chapter forms part of ongoing research into optical effects which we attribute to time-nonreversality in the optical response of noncentrosymmetric materials. The results of investigations into natural and induced gyrotropic linear dichroism in zincblende semiconductors are presented. These effects are interpreted as being the result of lack of time-reversal symmetry in the interaction of light with non-centrosymmetric media. Section 4.2 describes the restraints that Onsager symmetry places on the optical susceptibilities of materials as a result of time-reversality of the light-matter interaction process, and gives examples of materials in which reversality of the light-matter interaction may not be valid. Section 4.3 shows how time-nonreversality in zincblende symmetry crystals may manifest itself as nonreciprocal light-matter interaction. Section 4.4 extends the theory of specular reflective phenomena given in section 3.3 to include linear and nonlinear nonlocal terms. Section 4.5 describes experimental observation of linear and induced gyrotropic linear dichroism in zincblende structure semiconductors and section 4.6 interprets these results in terms of a simple band structure model of the materials.

4.2 Onsager Symmetry and Time-Nonreversality

In thermodynamics, certain symmetry relations for macroscopic kinetic coefficients

may be derived from the fluctuation-dissipation theorem under the condition that the microscopic processes involved are time-reversible [Onsager, 31; Landau, 84]. Specifically, if X_i are some displacements of the system from thermodynamic equilibrium, and f_i are the forces producing such displacements, such that $X_i=L_{ij}f_j$, the Onsager relations state that L_{ij} is symmetric, i.e. $L_{ij}=L_{ji}$. The principle of the symmetry of the kinetic coefficients may be applied in optics [Landau, 84]. If the light-matter interaction is time-reversible, restrictions can be derived on the allowed components of the optical susceptibilities. If we use the material equation of the form

$$D_i = \varepsilon_{ij}E_j + \nabla_n(\gamma_{ijn}E_j) \tag{4.1}$$

where $\boldsymbol{D}$ is the electric displacement vector, $\boldsymbol{E}$ is the electric field strength of the electromagnetic wave and ∇ is the gradient operator, the restrictions on ϵ and γ are

$$\varepsilon_{ij} = \varepsilon_{ji} \quad , \quad \gamma_{ijk} = -\gamma_{jik} \tag{4.2}$$

These restrictions are independent from and additional to any symmetry restrictions imposed on ϵ and γ by the material point group.

Since the Onsager relations arise from the fluctuation dissipation theorem, there is no reason to suppose that they are valid for systems which are far from thermodynamic equilibrium. Such a departure from equilibrium might be produced by stimulation of a medium by an intense transient optical pulse, as in some of the experiments described below. In such a case the system is obviously not time reversible, since the decay of the excited state provides a clear distinction between past and future. Hence, one may expect the restrictions (4.2) to be lifted in a crystal excited to a non-equilibrium state.

However, even for low intensity steady state stimulation there are circumstances in which the Onsager relations do not apply, namely where microscopic time-reversal symmetry is violated. The case of an externally applied magnetic field is mentioned by Onsager. Other examples are atoms which are time-non-reversible because they possess net electronic angular momentum [Hamaguchi, 80] and the hypothetical

timenonreversible state in some superconductors which would arise from the existence of particles with fractional spin statistics [Wen, 89; March-Russell, 88]. As first suggested by [Lifshitz, 81] and comprehensively investigated in [Barron, 87;94;94a], chemical interactions involving chiral molecules are not necessarily symmetrical with respect to time-reversal, leading to violation of thermodynamic principles based on microscopic reversibility. The question of the possible existence of non-reciprocal electromagnetic "Tellegen" media has recently attracted controversy [Weiglhofer, 95; Sihvola, 95].

Let us consider an example described in [Belinicher, 80], where microscopic electronic scattering processes in a medium lacking inversion symmetry (P-odd) are not symmetrical with respect to time reversal. This is illustrated in figure 4.1 which represents particles interacting in a noncentrosymmetric potential represented by a wedge. In 4.1a) the particles have initial momenta κ_1, κ_2 and final momenta κ'_1, κ'_2. In 4.1b), the time-reversed scenario, the initial momenta of the particles are reversed $(-\kappa_1,-\kappa_2)$, but the final momenta are $\kappa''_1 \neq -\kappa'_1$ and $\kappa''_2 \neq -\kappa'_2$. Belinicher and Sturman showed that in such a system even a small perturbation leads to the generation of a unidirectional flow of particles. A system in which such a flow occurs is clearly not at thermodynamic equilibrium and the Onsager relations cannot be expected to apply.

Svirko and Zheludev [Svirko, 95] have recently shown that time-nonreversality is a general feature of nonlocal light-matter interactions in noncentrosymmetric media. The time-nonreversible terms arise in particular from the spin-orbit terms in the crystal Hamiltonian.

The rules for transformation of crystal properties and electromagnetic fields under space (P) and time (T) inversion [e.g. Berestetskii, 82; Lax, 74] may be summarised as follows. Under space inversion P: spatial coordinates $r \Rightarrow -r$, gradients $\nabla \Rightarrow -\nabla$, electron momenta $p \Rightarrow -p$, electrostatic potential of crystal $V(r) \Rightarrow V(r)$, electron angular momenta and spin $L \Rightarrow L$, $\sigma \Rightarrow \sigma$, electric field strength $E(r,t) \Rightarrow -E(-r,t)$, magnetic induction $B(r,t) \Rightarrow B(-r,t)$, vector potential $A(r,t) \Rightarrow -A(-r,t)$. Under time-reversal T: $r \Rightarrow r$,

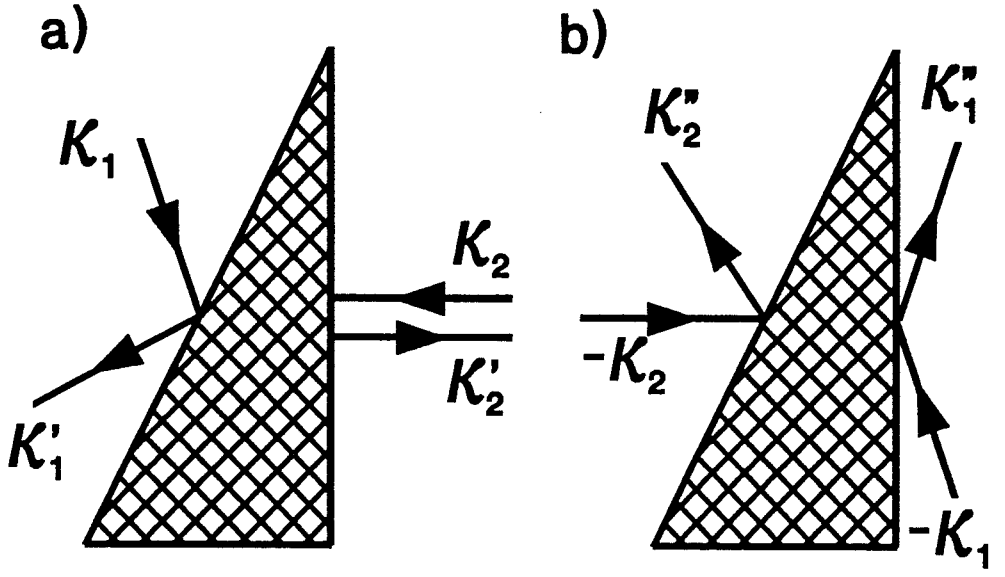

Figure 4.1 Representation of particles interacting in a non-centrosymmetric potential. a) "direct" scenario, b) time-reversed scenario.

$\nabla \Rightarrow \nabla, p \Rightarrow -p, V(r) \Rightarrow V(r), L \Rightarrow -L, \sigma \Rightarrow -\sigma, E(r,t) \Rightarrow E(r,-t), B(r,t) \Rightarrow -B(r,-t), -A(r,t) \Rightarrow -A(r,-t).$

The Hamiltonian of an electron in a crystal may be given by

$$H = \frac{p^2}{2m} + eV - \frac{e\hbar^2}{8m^2c^2}\nabla^2 V - \frac{e\hbar}{4m^2c^2}[\nabla V \times p]\cdot\sigma \qquad (4.3)$$

where p and σ are the momentum and spin of the electron and V represents the internal potential of the crystal. This Hamiltonian is always symmetrical with respect to time inversion (T) and space inversion (P). The Hamiltonian representing the interaction between the crystal and a light wave is given by

$$H_{int} = -\frac{e}{mc}p\cdot A(r,t) - \frac{e^2}{2mc^2}A^2(r,t) - \frac{e^2\hbar}{4m^2c^2}[\nabla V \times A(r,t)]\cdot\sigma - \mu\cdot B(r,t) \qquad (4.4)$$

where $A(r,t)$ is the vector potential of the wave, $B(r,t)$ is its magnetic induction and $\mu = (e\hbar/2mc)\sigma$. For a linearly polarised wave of frequency ω and wave-vector k, $A(r,t) = A^{(0)}cos(\omega t - kr)$. There are a number of time-non-reversible terms in the interaction Hamiltonian. Some of these terms are even functions of coordinate, and will therefore have zero matrix elements for transitions between states of opposite

parity (optical transitions). However, there are terms arising from the spin-orbit interaction and the part of the crystal potential which is an odd function of coordinate, which are T-odd and P-odd (i.e. they change sign under either the P or T operations):

$$\Delta H_{int,odd} = -\frac{e^2\hbar}{2m^2c^3}\{(r\cdot[k\times A^{(0)}]) - (r\cdot\sigma)(\nabla V_{odd}\cdot[k\times A^{(0)}])\}\sin(\omega t) \qquad (4.5)$$

where V_{odd} is the component of the crystal potential which is an odd function of coordinate (and may therefore exist only in a noncentrosymmetric medium). The interaction Hamiltonian is invariant under the combined operation PT, as must be the case, since optical interactions are even with respect to charge conjugation (C), and all physical interactions are even with respect to the combined operation CPT. The T-noninvariant contributions to the interaction Hamiltonian are linear in the wavevector of the light wave. Hence T-odd interactions will manifest themselves in first order spatial dispersion phenomena only. This means that the restrictions imposed on the nonlocality tensor γ_{ijk} by the optical consequences of the Onsager relations are not necessarily valid in a noncentrosymmetric material with a significant spin-orbit contribution to its Hamiltonian.

4.3 Reciprocity in Nonlocal Optics

As shown below, the optical phenomena associated with the symmetric part of the nonlocality tensor γ^s may be distinguished from the conventional circular birefringence and dichroism associated with the antisymmetric part of the nonlocality tensor γ^a by the fact that, while polarisation effects associated with γ^a (e.g. optical activity) will cancel on retroreflection of the light wave through the medium, polarisation effects associated with γ^s will add.

Determining whether optical effects will add or cancel on reflection back through a medium requires comparison of waves propagating in the forward and backwards directions. In order to do this consistently, the calculations in this section will be

performed in one laboratory Cartesian coordinate system. This frame is oriented such that the z-axis is along the forward (positive) direction of propagation and the xy-plane is perpendicular to it.

An electromagnetic wave at frequency ω may be represented by $E = \xi A e^{i(\omega/c)nz}$, where ξ is the polarization vector, $(\xi.\xi^*)=1$, and n is the complex refractive index, whose real and imaginary parts are responsible for refraction and absorption. In the laboratory frame, the wave propagating in the forward direction (say, from 0 to $+z$), denoted below by the subscript "$\rightarrow$", has $Re\{n_{\rightarrow}\}>0$ and $Im\{n_{\rightarrow}\}>0$, while the wave propagating in the backwards direction (say, from 0 to $-z$), denoted by subscript "$\leftarrow$", has $Re\{n_{\leftarrow}\}<0$ and $Im\{n_{\leftarrow}\}<0$. In order to be exposed to the same absorption and retardation two counter-propagating eigenwaves must have opposite refractive indices: $n_{\rightarrow} = - n_{\leftarrow}$. Since elliptical polarization handedness is determined with respect to the propagation direction, two eigenwaves propagating in opposite directions with polarization vectors $\xi_{\rightarrow}$ and $\xi_{\leftarrow}$, have the same polarizations if $\xi_{\rightarrow} = \xi_{\leftarrow}^*$. Two waves with polarization states different only by a phase factor $e^{i\alpha}$, such as ξ and $\xi e^{i\alpha}$, should be considered as having the same polarization. The reciprocity conditions for the eigenwaves may now be formulated in the following analytical way:

$$\begin{aligned} n_{\rightarrow} &= - n_{\leftarrow} \\ \xi_{\rightarrow} &= (\xi_{\leftarrow})^* e^{i\alpha} \end{aligned} \qquad (4.6)$$

Below, for simplicity, we will consider light propagation along a non-birefringent direction, presuming $\epsilon_{xx}=\epsilon_{yy}=\epsilon$. This allows us to concentrate on the effects arising from the nonlocality tensor. The spatial evolution of the components E_x and E_y of a transverse electromagnetic wave is governed by the wave equation:

$$\frac{d^2E_i}{dz^2} + \frac{\omega^2}{c^2}\left(\epsilon E_i + \gamma_{ijz}\frac{dE_j}{dz}\right) = 0 \; ; \quad i = x,y, \;\; j = x,y \qquad (4.7)$$

Substitution of the wave solution $E = \xi A e^{i(\omega/c)nz}$ into (4.7) gives us the characteristic equation which leads to the following refractive coefficients and corresponding

polarization states of the eigenwaves:

$$n_{1,3} = \pm i\nu_+ + \nu \pm \sqrt{\epsilon + (i\nu_+ \pm \nu)^2}$$
$$n_{2,4} = \pm i\nu_+ - \nu \pm \sqrt{\epsilon + (i\nu_+ \mp \nu)^2} \qquad (4.8)$$

$$\xi_{1,3} = \frac{\{\mp\nu_- + i\nu,\ \nu_a \mp \nu_s\}}{\sqrt{|\nu_a \mp \nu_s|^2 + |\nu_- \mp i\nu|^2}}$$
$$\xi_{2,4} = \frac{\{\nu_s \pm \nu_a,\ -\nu_- \pm i\nu\}}{\sqrt{|\nu_s \pm \nu_a|^2 + |\nu_- \mp i\nu|^2}} \qquad (4.9)$$

Here $\nu = (\nu_a^2 - \nu_s^2 - \nu_-^2)^{1/2}$, $\nu_{a,s} = (\omega/4c)(\gamma_{xyz} \mp \gamma_{yxz})$, $\nu_{+,-} = (\omega/4c)(\gamma_{xxz} \pm \gamma_{yyz})$. Here, we use the prescription for treatment of the symmetric and anti-symmetric components of the nonlocality tensor γ outlined in [Birss, 67]. The anti-symmetric components of the nonlocality should be treated as *i*-tensors, which do not change sign with reversal of the direction of propagation, while the symmetric components should be treated as *c*-tensors, which reverse sign with reversal of the direction of propagation. For a realistic situation $|\epsilon| \gg |\nu|$ and $Re\{n_{1,2}\} > 0$; $Im\{n_{1,2}\} > 0$ while $Re\{n_{3,4}\} < 0$; $Im\{n_{3,4}\} < 0$. That is, indices "1" and "2" denote waves propagating in the forward direction while "3" and "4" denote waves propagating in the reverse direction.

Let us consider two different optical effects dependent on the nonlocality tensor:

(i) Light propagation in an isotropic gyrotropic medium. Here by symmetry $\gamma_{xyz} = -\gamma_{yxz}$ and $\gamma_{xxz} = \gamma_{yyz} = 0$. Therefore, the eigenvalues of the refractive index and the corresponding eigenpolarisations are

$$n_{1,3} = \frac{\omega\,\gamma^a}{2c} \pm \sqrt{\epsilon + (\frac{\omega\,\gamma^a}{2c})^2}, \quad \xi_{1,3} = \frac{1}{\sqrt{2}}\{1, -i\}$$
$$n_{2,4} = -\frac{\omega\,\gamma^a}{2c} \pm \sqrt{\epsilon + (\frac{\omega\,\gamma^a}{2c})^2}, \quad \xi_{2,4} = \frac{1}{\sqrt{2}}\{1, -i\} \qquad (4.10)$$

The eigenwaves are left and right circularly polarised (see figure 4.2a). From here we can easily arrive at the familiar result that rotation of polarisation azimuth due to optical activity is compensated on reflection.

(ii) Light propagation along a cubic axis in a crystal of $\bar{4}3m$ point group. Here by symmetry the dielectric tensor is isotropic $\epsilon_{xx} = \epsilon_{yy} = \epsilon_{zz} = \epsilon$, $\gamma_{xyz} = \gamma_{yxz}$ and $\gamma_{xxz} = \gamma_{yyz} = 0$. The eigenvalues of the refractive index and the corresponding eigenpolarisations are

$$n_{1,4} = \pm i\frac{\omega\,\gamma^s}{2c} \pm \sqrt{\epsilon - (\frac{\omega\,\gamma^s}{2c})^2}, \quad \xi_{1,4} = \frac{1}{\sqrt{2}}\{1, 1\}$$
$$n_{2,3} = \mp i\frac{\omega\,\gamma^s}{2c} \pm \sqrt{\epsilon - (\frac{\omega\,\gamma^s}{2c})^2}, \quad \xi_{2,4} = \frac{1}{\sqrt{2}}\{1, -1\} \qquad (4.11)$$

Reversing the direction of propagation preserves the refractive coefficients of the two eigenwaves (see figure 4.2b). The eigenwaves are two orthogonal linearly polarized waves.

A wave of arbitrary polarization propagating through the crystal in the positive direction may be decomposed as

$$E_{\rightarrow}(z) = \xi_1 A_1 e^{in_1\frac{\omega}{c}z} + \xi_2 A_2 e^{in_2\frac{\omega}{c}z} \qquad (4.12)$$

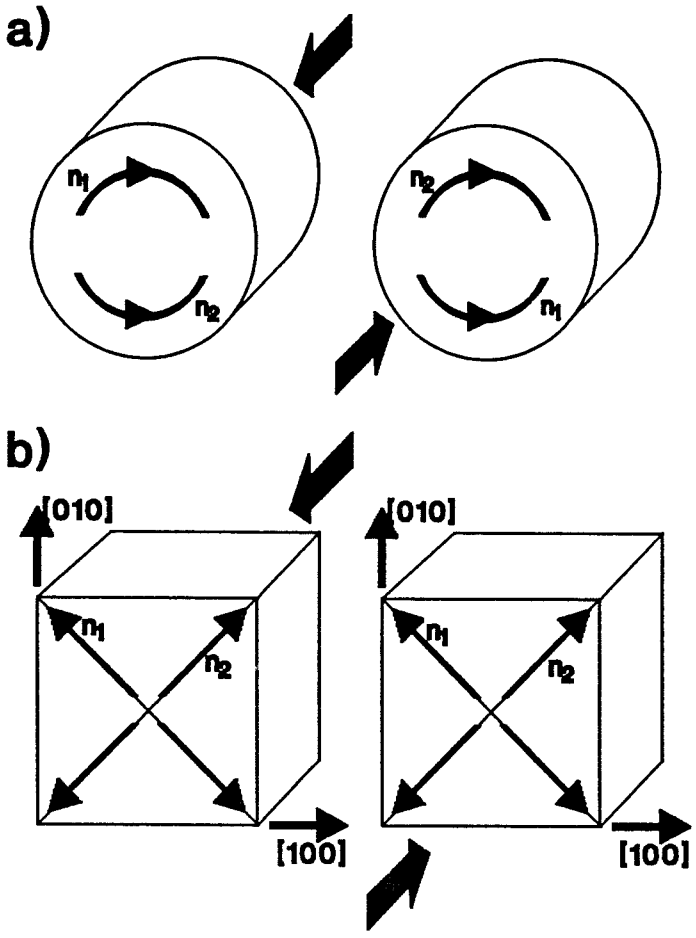

Figure 4.2 Eigenpolarisations and refractive indices for counter-propagating beams in a) isotropic gyrotropic medium ($\gamma_{xyz}=-\gamma_{yxz}$), b) $\bar{4}3m$ crystal ($\gamma_{xyz}=\gamma_{yxz}$)

where $A_{1,2}$ determine the magnitudes of the projections on the eigenwaves at $z=0$. For a typical situation where the nonlocal response is a small correction to the local response

$$E_{\rightarrow}(L) = \{\xi_1 A_1(1 - \frac{\omega^2}{2c^2}\gamma^s L) + \xi_2 A_2(1 + \frac{\omega^2}{2c^2}\gamma^s L)\} e^{i\frac{\omega}{c}n_0 L} \qquad (4.13)$$

where $n_0 = \epsilon^{1/2}$. If, say $Re\{\gamma^s\}<0$, the polarization azimuth of a linearly polarized wave $E_{\rightarrow}$ with real A_1 and A_2 tends towards eigenwave ξ_1. For an initially linearly polarized wave small rotation of the polarization azimuth is given by

$$\delta\phi = -\frac{\omega^2}{2c^2} Re(\gamma^s) L \cos(2\phi) \qquad (4.14)$$

where ϕ is the polarization azimuth of the incident wave with respect to the [100] direction. Similarly, for a wave propagating in the opposite direction, say from zero to *-L*

$$E_{\leftarrow}(z) = \xi_1 A_1 e^{-in_1\frac{\omega}{c}z} + \xi_2 A_2 e^{-in_2\frac{\omega}{c}z} \tag{4.15}$$

and we have

$$E_{\leftarrow}(L) = \{\xi_1 A_1(1 - \frac{\omega^2}{2c^2}\gamma^s L) + \xi_2 A_2(1 + \frac{\omega^2}{2c^2}\gamma^s L)\} e^{-i\frac{\omega}{c}n_0 L} \tag{4.16}$$

Here, again, for $Re\{\gamma^s\} < 0$ the polarization azimuth of the linearly polarized wave $E_{\leftarrow}$ with real A_1 and A_2 tends towards ξ_1. That is, polarization azimuth rotation is doubled on the way back through the crystal. This polarization effect, which is due to the symmetric part of the nonlocality tensor, is known as gyrotropic linear dichroism. This analysis should also apply to reflective phenomena arising from γ^s, with the result that waves of the same initial polarisation incident on opposite sides of the crystal will experience polarisation azimuth rotation of opposite sign with respect to their direction of propagation.

4.4 Nonlocal Specular Polarisation Effects in Materials with Instantaneous Response

In section 3.3 a general formula was quoted for the change in polarisation state of a probe wave reflected from the surface of a medium in the presence of a strong pump wave, taking account of local linear and third-order terms only. The value of the polarisation azimuth rotation and induced ellipticity of the reflected probe was obtained for the specific case of a circularly polarised pump (the Specular Inverse Faraday effect), a linearly polarised probe, and neglecting any anisotropy of the material tensors. In order to deal with the polarisation effects discussed in this chapter we must extend the treatment in section 3.3 to deal with linear and third-order nonlocalities. As in section 3.3, the treatment presented is that of [Popov, 96].

The material equation (3.1) now needs to be modified to deal with the effects of nonlocality, i.e. gradient terms must be included:

$$D_i^{(3)}(r) = (\varepsilon_{ij} + ik_n\gamma_{ijn} + \nabla_n\gamma_{ijn})E_j e^{ik.r} + [\chi_{ijlm} + ik_n\Gamma^b_{ijlmn} + \frac{1}{2}\nabla_n(\Gamma^b_{ijlmn} - \Gamma^s_{ijlmn})]E_jE_lE_m^* e^{ik.r} \tag{4.17}$$

where

$$\chi_{ijkl} = \chi^{(3)}_{ijkl}(\omega,\omega,\omega,-\omega) + \chi^{(3)}_{ijlk}(\omega,\omega,-\omega,\omega) + \chi^{(3)}_{ilkj}(\omega,-\omega,\omega,\omega) \tag{4.18}$$

and

$$\Gamma^b_{ijlmn} = \Gamma^{(3)}_{ijlmn}(\omega,\omega,\omega,-\omega,\ r) + \Gamma^{(3)}_{iljmn}(\omega,\omega,-\omega,\omega,\ r) - \Gamma^{(3)}_{imjln}(\omega,-\omega,\omega,\omega,\ r)$$
$$\Gamma^s_{ijlmn} = -\Gamma^{(3)}_{ijlmn}(\omega,\omega,\omega,-\omega,\ r) - \Gamma^{(3)}_{iljmn}(\omega,\omega,-\omega,\omega,\ r) - \Gamma^{(3)}_{imjln}(\omega,-\omega,\omega,\omega,\ r) \tag{4.19}$$

We will see below that Γ^b_{ijlmn} describes nonlocality of the bulk nonlinear response, while Γ^s_{ijlmn} is significant at the boundary of the medium.

If we proceed as in section 3.3, the equation for the evolution of the electric field of the light wave becomes

$$2ik\frac{dE_i^T}{dz} + \frac{\omega^2}{c^2}(\varepsilon_{ij} + ik\gamma_{ijz} - n^2\delta_{ij})E_j^T = -\frac{\omega^2}{c^2}(\chi_{ijlm} + ik\Gamma^b_{ijlmz})E_j^T E_l^T E_m^{T*} \tag{4.20}$$

and the magnitude of the transmitted probe is

$$\frac{da_i^t}{dz} = \frac{ik}{2}(\alpha_{ij}a_j^t + \beta_{ij}a_j^{t*}) \tag{4.21}$$

where the indices i,j cover the x,y directions and α and β are now

$$\alpha_{ij} = -\delta_{ij} + \frac{\omega^2}{(kc)^2}[(\varepsilon_{ij} + ik\gamma_{ijz}) + 2(\chi_{ijlm} + ik\Gamma^b_{ijlmz})A^t_l A^{t*}_m]$$
$$\beta_{ij} = \frac{\omega^2}{(kc)^2}(\chi_{ilmj} + ik\Gamma^s_{ilmjz})A^t_l A^t_m \qquad (4.22)$$

where the amplitudes A^t_i are, in general, functions of the coordinate z and satisfy equation (4.20).

As with purely local effects, α is independent of the phase of the wave, while β depends on the phases as well as the intensities of the polarisation components of the pump wave. Inclusion of nonlocal terms modifies the boundary conditions for the probe wave at the surface of the medium. The boundary equation for the electric field vector remains unchanged, but there is an extra term in the boundary equation for the magnetic field vector:

$$\boldsymbol{a}^t(z=0) - \boldsymbol{a}^i(z=0) - \boldsymbol{a}^r(z=0) = 0$$
$$\boldsymbol{b}^t(z=0) - \boldsymbol{b}^i(z=0) - \boldsymbol{b}^r(z=0) = \frac{i\omega}{c}[z \times \boldsymbol{d}^s] \qquad (4.23)$$

where d^s_i determines the surface contribution to the nonlocal response and is associated with induced surface current.

$$d^s_i = \gamma_{ijz}a^t_j + (\Gamma^b_{ijlmz} - \Gamma^s_{ijlmz})A^t_l A^{t*}_m a^t_j + \frac{1}{2}(\Gamma^b_{ilmjz} - \Gamma^s_{ilmjz})A^t_l A^t_m a^{t*}_j \qquad (4.24)$$

where $\boldsymbol{A}^t$ and $\boldsymbol{a}^t$ are taken at $z=0$. In terms only of the electric field strength the boundary conditions are

$$\boldsymbol{a}^T - \boldsymbol{a}^R - \boldsymbol{a} = 0$$
$$n\boldsymbol{a}^T + \boldsymbol{a}^R - \boldsymbol{a} = \frac{ic}{\omega}\left(\frac{d\boldsymbol{a}^T}{dz}\Big|_{z=0} + \frac{\omega^2}{c^2}\boldsymbol{d}^s\right) \qquad (4.25)$$

giving

$$a^T(z=0) = \frac{2}{1+n}a + \frac{ic}{\omega(1+n)}\left(\frac{da^T}{dz}\Big|_{z=0} + \frac{\omega^2}{c^2}d^s\right)$$
$$a^R = \frac{1-n}{1+n}a + \frac{ic}{\omega(1+n)}\left(\frac{da^T}{dz}\Big|_{z=0} + \frac{\omega^2}{c^2}d^s\right) \qquad (4.26)$$

The polarisation azimuth orientation and ellipticity of the reflected probe is given by

$$\tan 2\phi^r = \tan 2\phi^i - \frac{\lambda}{\pi S_{1i}^2} Im\left\{\frac{J^R}{1-n}\right\}$$
$$\sin 2\eta^r = \sin 2\eta^i - \frac{\lambda}{\pi S_{0i}^2} Re\left\{\frac{J^R}{1-n}\right\} \qquad (4.27)$$

or, for small changes in polarisation state

$$\phi_r - \phi_i = -\frac{\lambda \cos^2 2\phi_i}{2\pi S_{1i}^2} Im\left\{\frac{J^R}{1-n}\right\}$$
$$\eta_r - \eta_i = -\frac{\lambda}{2\pi S_{0i}^2} Re\left\{\frac{J^R}{1-n}\right\} \qquad (4.28)$$

where J_R is now

$$J^R = \left[\left(a_x\frac{da_y^T}{dz}\Big|_{z=0} - a_y\frac{da_x^T}{dz}\Big|_{z=0}\right) + \frac{\omega^2}{c^2}(a_x d_y^s - a_y d_x^s)\right]\left[(a_x^*)^2 + (a_y^*)^2\right] \qquad (4.29)$$

In terms of the Stokes parameters of the incident probe wave J^R is

$$J^R = \frac{i\pi n}{\lambda(1+n)}\{[\alpha'_{yy} - \alpha'_{xx} + (\beta'_{yy}e^{-2i\varphi_y} - \beta'_{xx}e^{-2i\varphi_x})](S_{0i}S_{2i} - iS_{1i}S_{3i})$$
$$+ [\alpha'_{yx} - \alpha'_{xy} + (\beta'_{yx}e^{-2i\varphi_x} - \beta'_{xy}e^{-2i\varphi_y})](S_{0i}^2 - S_{3i}^2)$$
$$+ [\alpha'_{yx} + \alpha'_{xy} + (\beta'_{yx}e^{-2i\varphi_x} + \beta'_{xy}e^{-2i\varphi_y})](S_{0i}S_{1i} + iS_{2i}S_{3i})\} \qquad (4.32)$$

where $\varphi_{x,y} = arg(a_{x,y})$ and α' and β' are

$$\alpha'_{ij} = \alpha_{ij} - \frac{\omega^2}{(kc)^2} 2ik(\gamma_{ijz} + (\Gamma^b_{ijlmz} - \Gamma^s_{ijlmz})A_l A^*_m)$$
$$\beta'_{ij} = \beta_{ij} - \frac{\omega^2}{(kc)^2} ik(\Gamma^b_{ijlmz} - \Gamma^s_{ilmjz})A_l A_m \qquad (4.33)$$

We consider the case of a single low intensity beam incident on the surface of a crystal of $\bar{4}3m$ point group, where the crystal surface is perpendicular to a cubic direction in the crystal [001], as in the propagation problem discussed in the previous section. The beam is initially linearly polarised at some angle ϕ to the [100] direction (S_{3i}=0, $S_{1i}^2 = S_{0i}^2 cos2\phi$, $S_{2i}^2 = S_{0i}^2 sin2\phi$). Since there is no pump beam, terms in $\chi^{(3)}$ and $\Gamma^{(3)}$ are zero. By symmetry $\epsilon_{xx} = \epsilon_{yy} = \epsilon_{zz} = \epsilon$, $\gamma_{xyz} = \gamma_{yxz}$ and $\gamma_{xxz} = \gamma_{yyz} = 0$. Therefore, J^R is given by

$$J^R = \frac{2\pi^2}{\lambda(1+n)} \gamma_{xyz} s_0^2 \cos 2\phi_i \qquad (4.34)$$

and the formula for the alteration of the polarisation of the reflected wave is

$$\frac{\phi^R - \phi}{\eta^R} = -\frac{4\pi}{\lambda} \cos 2\phi_i \; Im \; Re \; \frac{\gamma_{xyz}}{(1 - n^2)} \qquad (4.35)$$

The imaginary component of γ^s causes the plane of polarisation of the reflected light to rotate, while the real component induces ellipticity. We may call this effect specular gyrotropic linear dichroism/birefringence.

Now we add an intense pump beam, also linearly polarised in the same plane as the probe beam. The effect of the pump beam on the probe may be considered via the tensor component Γ^s_{xxyz}, which represents the modification to γ_{xyz} induced by the pump. Since the pump is linearly polarised with the same polarisation as the probe the polarisation state of the probe cannot be modified as a result of the optical Kerr effect or the inverse Faraday effect. The formula for J^R is now

$$J^R = -\frac{32\pi^2\Gamma^s_{xxyz}(1 + \frac{1}{2}e^{i\Psi})}{\lambda^2|1+n|^2(1+n)} S_0 s_0^2 \cos 2\phi \qquad (4.36)$$

and the formulae for the alteration of the polarisation of the reflected wave are

$$\begin{matrix}\phi_r - \Phi \\ \eta_r\end{matrix} = \frac{128\pi^2 I_p}{\lambda|1+n|^2} Im \frac{\Gamma^s_{xxyz}}{n(1-n^2)}(1 + \frac{1}{2}e^{i\Psi})\cos 2\phi \qquad (4.37)$$

where $I_p = cS_{0p}/8\pi$ is the intensity of the pump wave. We can see that both the linear and pump induced effects have a $cos2\phi$ dependence on crystal orientation. Of course, if the response time of the material is longer than the excitation time, this formula is not strictly applicable, but it is useful for revealing the symmetry of the effect.

4.5 Observation of Linear and Pump-Induced Gyrotropic Linear Dichroism in Zincblende Semiconductors

A detailed examination of gyrotropic linear dichroism/birefringence in the $A^{III}B^{V}$ zincblende semiconductor GaAs has been conducted by Bungay et.al.. $A^{III}B^{V}$ semiconductors with zincblende symmetry are particularly appropriate materials in which to search for the ***k***-linear time-nonreversible effects described above, because the $\bar{4}3m$ point-group permits the symmetric nonlocality tensor component ($\gamma^s_{ijk}=\gamma^s_{jik}$) and the spin-orbit interaction plays an important role in the band structure [Kane, 57]. Also, within the scope of linear optics, crystals of the $\bar{4}3m$ point group are isotropic ($\epsilon_{ij}=\epsilon\delta_{ij}$) and show no optical activity ($\gamma^a=0$). Hence, only γ^s may lead to alteration of the polarisation state of a light wave interacting with the crystal. Bungay et.al. observed polarisation azimuth rotation of linearly polarised light reflected from the (001) surface of a sample of GaAs, which displayed the characteristic $cos2\phi$ orientational dependence of the time-nonreversible effect [Bungay, 93]. Also, in a thin (20μm) sample of GaAs, using a tunable laser they performed wavelength dependent reflection experiments above the band gap and transmission experiments just below

the band gap, including double pass experiments where the laser light was reflected back through the sample [Bungay, 94, 94a]. They found that the rotation in the case of the double pass experiments was twice that observed in the single pass experiments, confirming the bulk, nonreciprocal nature of the effect.

In the experiments described below, study of specular gyrotropic linear dichroism is extended to two new materials of the same zincblende symmetry. A nonlinear effect with the same *cos 2φ* orientational dependence is also studied, which we interpret as a light-induced modification to the linear effect. Such an effect was first observed as a result of excitation of GaAs by an intense laser pulse by Zheludev and Paraschuk [Zheludev, 90].

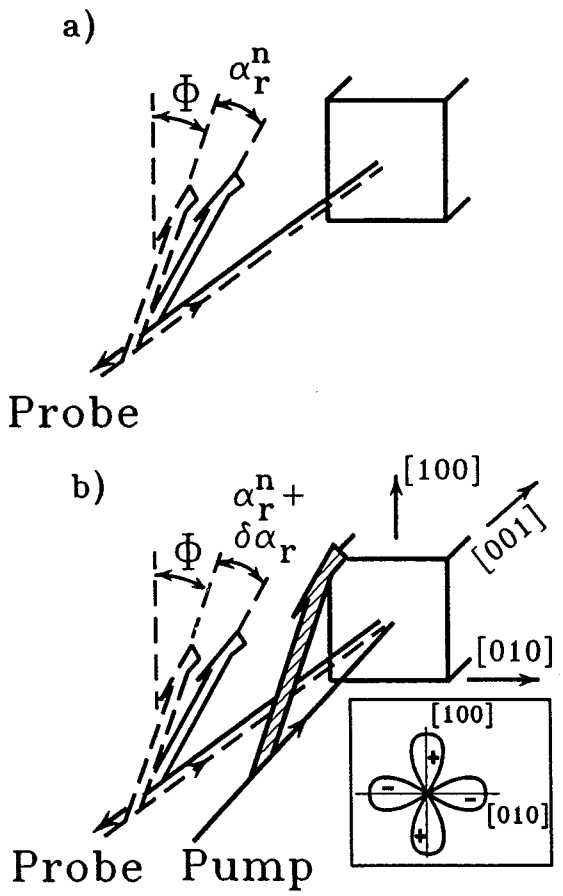

Figure 4.3 Experimental arrangement for observation of a) natural and b) pump-induced gyrotropic linear dichroism. Inset shows expected dependence of polarisation azimuth rotation on crystal orientation.

The experimental arrangement was essentially similar to that employed in the experiments described in chapter 3, except that the incident pump beam was linearly polarised. Figure 4.3 shows the experimental arrangement for measurement of natural (figure 4.3a) and pump-induced (figure 4.3b) probe polarisation azimuth rotation. The pump and probe were identically polarised, ensuring the absence of any contribution from the Optical Faraday or Kerr effects. The inset in figure 4.3 illustrates the expected dependence of the effect on the orientation of the polarisation azimuth of the light with respect to the crystal axes. The optical source used in these experiments was a frequency doubled mode-locked Nd^{3+}YAG laser producing 80 picosecond pulses with 82 MHz repetition rate at wavelength $\lambda = 532$ nm and output power of 200 mW. The pump and probe beams were focused at the sample surface by a lens to a spot diameter of 20 μm. After losses in the polarimeter, the maximum attainable pump intensity at the sample surface was about 5 $MWcm^{-2}$. The samples being examined were attached to a rotating mount in order to allow measurements of the dependence of the observed effect on crystal orientation. The tilt of the front face of the mount was adjustable, allowing the orientation of the face of the sample to be set precisely perpendicular to the axis of rotation of the mount, so that the direction of the beam reflected from the sample did not change when the sample was rotated. The beam was reflected at normal incidence to an accuracy of better than 1°, and with a change in the direction of the beam during orientation dependence experiments of less than 0.1°.

The samples examined were the zincblende ($\bar{4}3m$) structure semiconductors GaAs and InSb and the zincblende structure semimagnetic semiconductor $Cd_{0.6}Mn_{0.4}Te$.

4.5.1 Observation of Linear and Pump-Induced Gyrotropic Linear Dichroism in InSb and GaAs

The experiments were performed with good substrate quality bulk GaAs and InSb samples cut and polished normally to [001]. At 532 nm GaAs has a reflectivity of 38% and a light penetration depth of ~130 nm, and InSb has a reflectivity of 46%

and a penetration depth of ~20 nm.

The natural (pump-independent) rotation of a normally reflected probe beam was measured in both GaAs and InSb as a function of crystal orientation. The magnitude of the polarization azimuth rotation was 6.5×10^{-4}rad in GaAs (figure 4.4) and 3.2×10^{-4} rad in InSb (figure 4.5). In both cases the rotation had the $\cos2\phi$ dependence on the orientation of the crystal expected for the time-nonreversible effect (equation 4.35). The rotation observed in GaAs coincides closely with that observed in [Bungay, 93] in GaAs with light of wavelength 543 nm. These rotations give values of γ^{s}_{xyz} *(natural)* $=4.6\times10^{-8}$cm for GaAs and γ^{s}_{xyz} *(natural)* $= 2.7\times10^{-8}$cm for InSb. Here values of $n=4.18$, $k=0.326$ for GaAs and $n=3.977$, $k=2.14$ for InSb (λ = 532nm) are used [Seraphin, 67].

In both crystals pump-induced polarization plane rotation on a scale of 10^{-4} - 10^{-5} rad was detected in the reflected probe. In both GaAs (figure 4.6) and InSb (figure 4.7) the induced rotation had the same sign as the natural rotation (i.e. it increased the natural effect). In GaAs the induced rotation was found to increase proportionally to the pump at the rate of 1.1×10^{-11} rad cm^2W^{-1} within the measured range of intensity (figure 4.8). In InSb in the range of pump intensity up to 1 MW cm^{-2} the induced rotation scaled linearly with the pump with a constant of 4.3×10^{-11}rad cm^2W^{-1} and tended to saturate at higher intensities (figure 4.9). From the pump-probe delay dependencies one can see that induced polarization rotation appeared immediately after excitation. In GaAs (figure 4.10), at pump intensity 5 MW cm^{-2}, approximately 50% of the rotatory power disappeared with the pump pulse. Another 25-30% decayed with a time constant of approximately 180 ps. There was also an offset of about 20% of the total rotation which did not disappear between the excitation pulses spaced by 12 ns but at the same time responded to the chopper pump modulation with period of 0.83 ms. In InSb (figure 4.11) the relaxation picture was very similar except that the fast "tail" of the decay dependence was shorter and had relaxation time of approximately 60 ps and there was also a much longer second relaxation time which was impossible to identify accurately since it was longer than the range of our

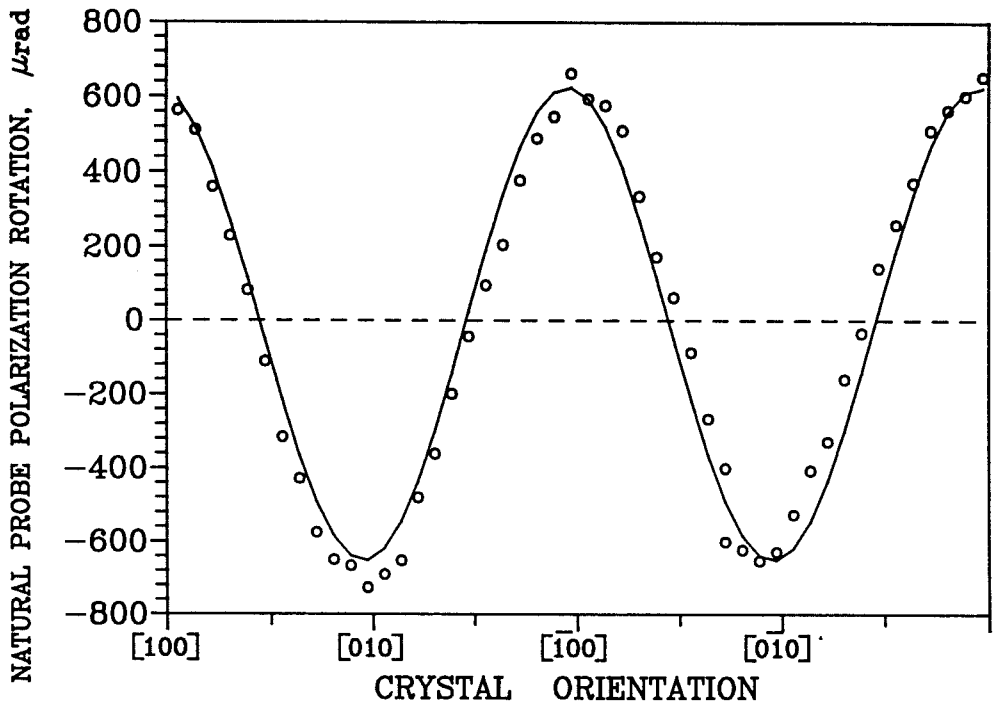

Figure 4.4 Natural probe polarisation azimuth rotation in GaAs as a function of crystal orientation. λ=532 nm.

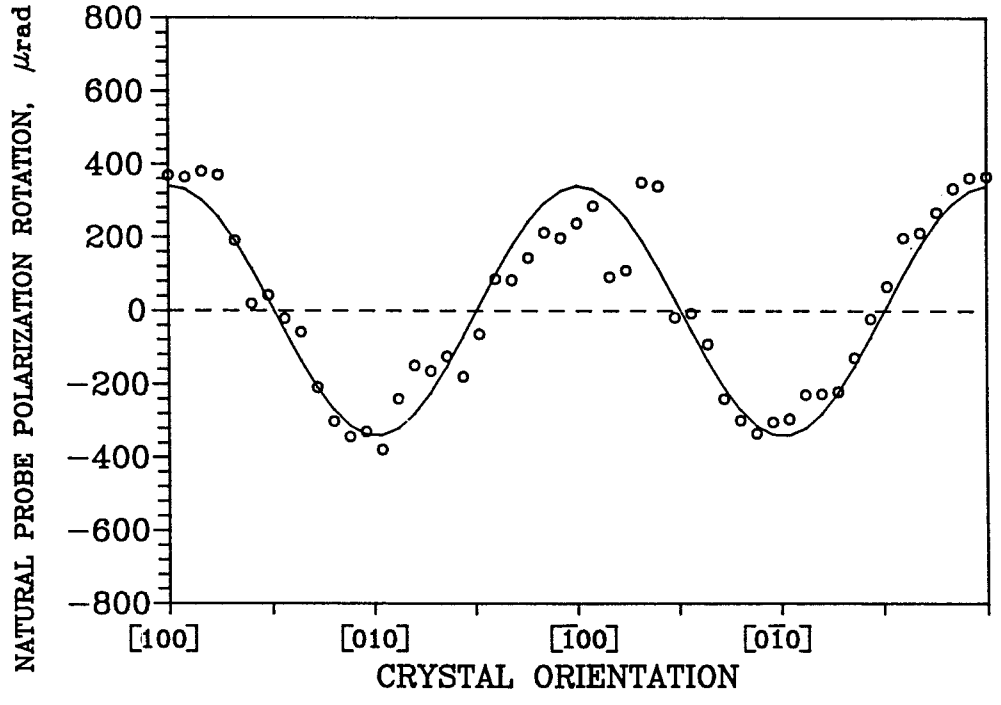

Figure 4.5 Natural probe polarisation azimuth rotation in InSb as a function of crystal orientation. λ=532 nm.

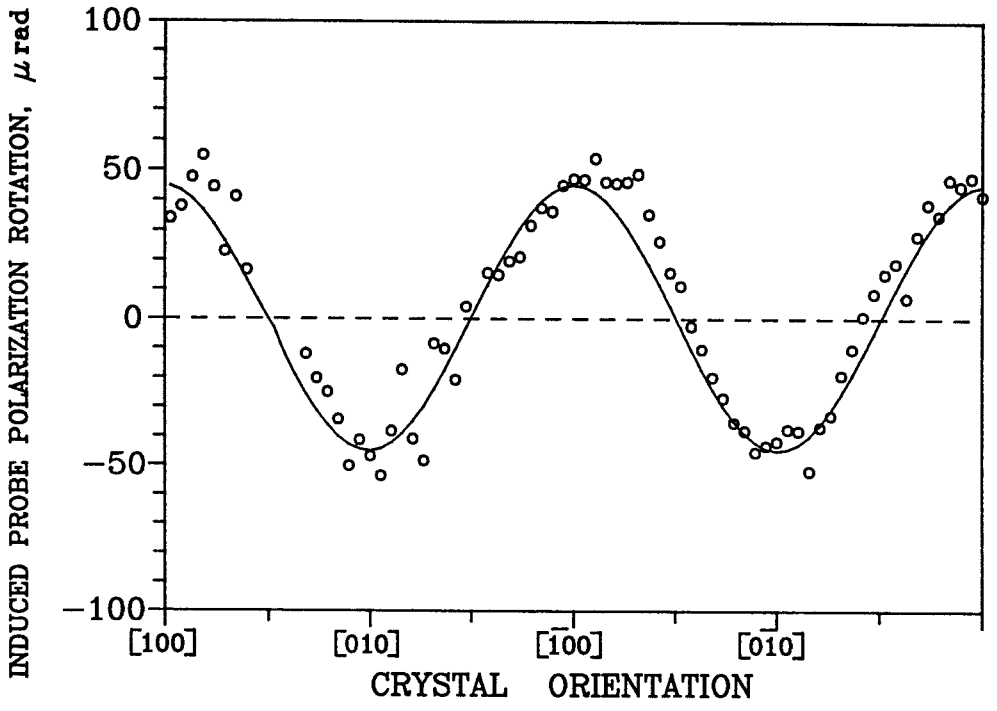

Figure 4.6 Pump-induced probe polarisation azimuth rotation in GaAs as a function of crystal orientation at zero pump-probe delay for pump intensity I_p= 5 MW cm^{-2}, λ=532 nm.

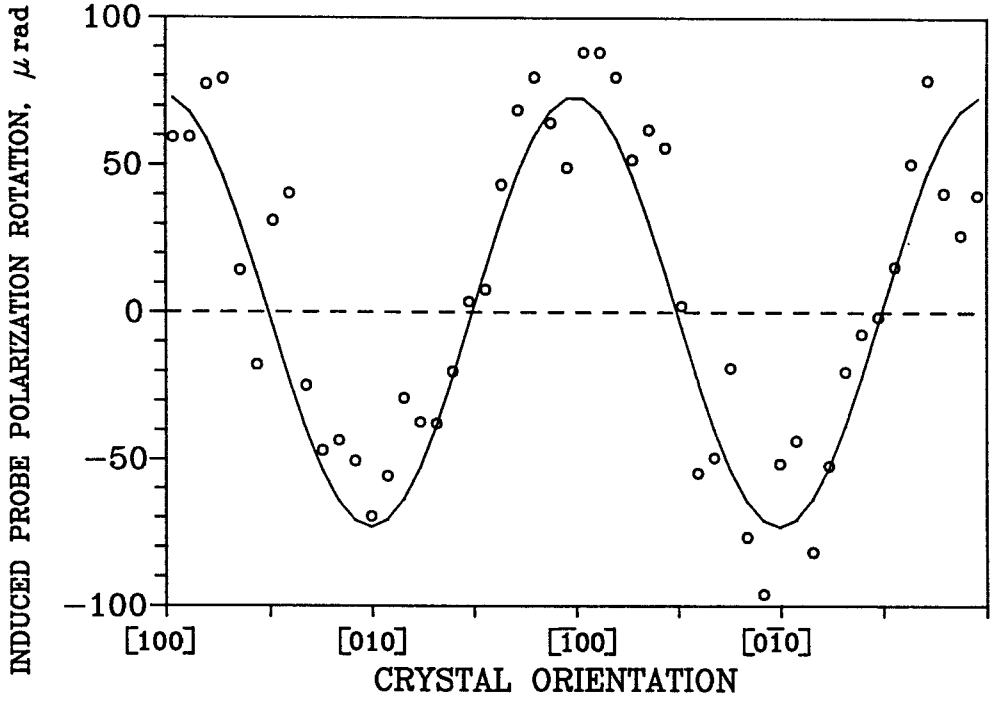

Figure 4.7 Pump-induced probe polarisation azimuth rotation in InSb as a function of crystal orientation at zero pump-probe delay for pump intensity I_p= 5 MW cm^{-2}, λ=532 nm.

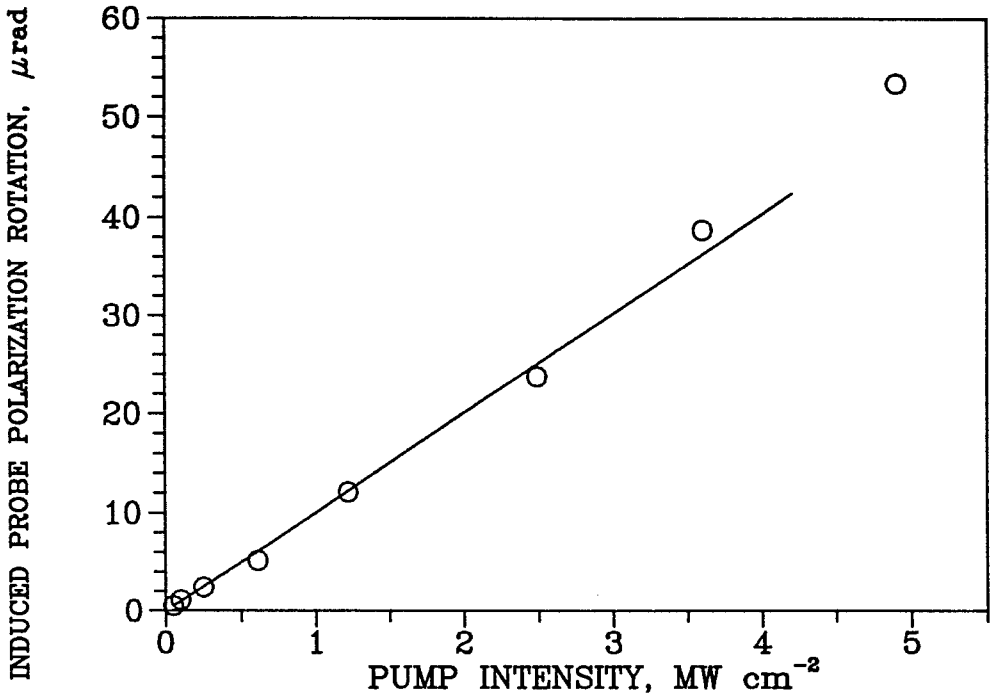

Figure 4.8 Induced probe polarisation azimuth rotation in GaAs as a function of pump intensity. λ=532 nm.

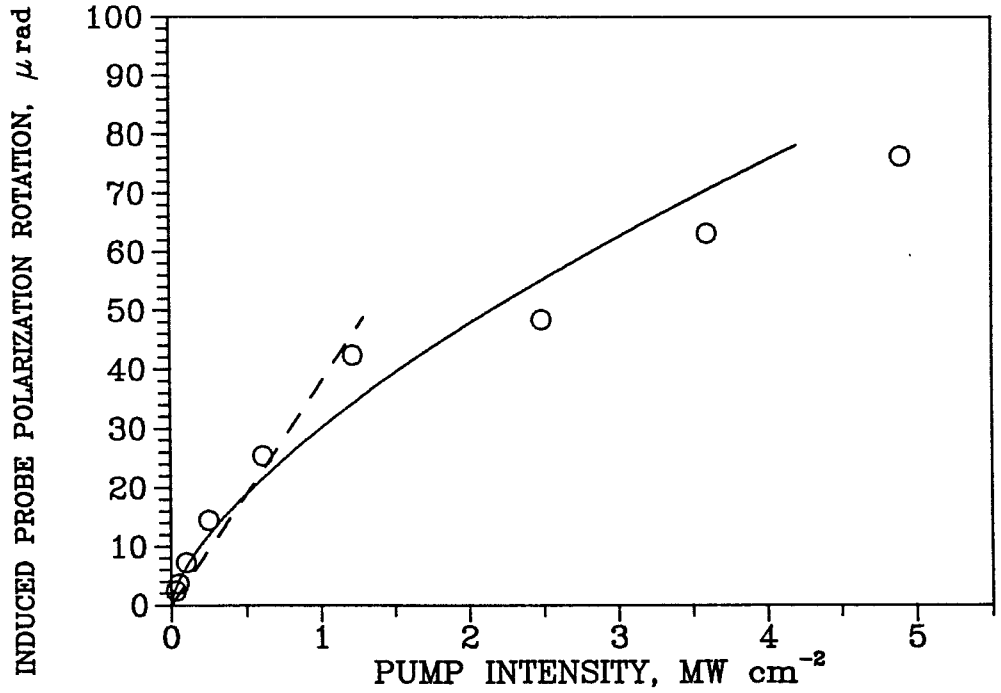

Figure 4.9 Induced probe polarisation azimuth rotation in InSb as a function of pump intensity. λ=532 nm.

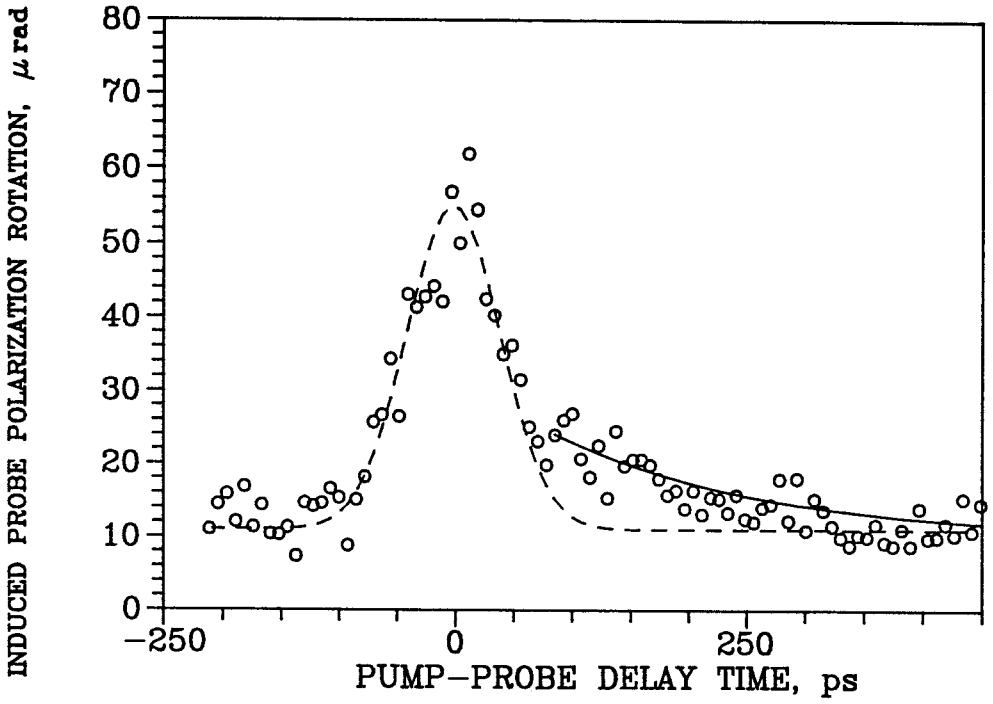

Figure 4.10 Induced probe polarisation azimuth rotation in GaAs as a function of pump-probe delay. I_p=5 MW cm^{-2}, λ=532 nm.

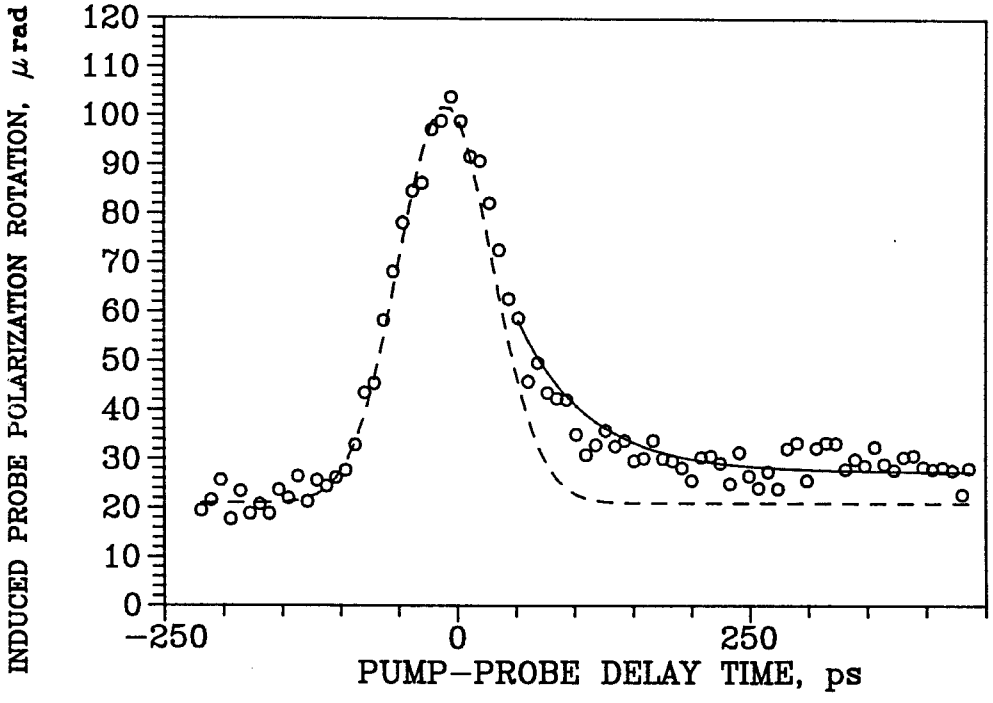

Figure 4.11 Induced probe polarisation azimuth rotation in InSb as a function of pump-probe delay. I_p=5 MW cm^{-2}, λ=532 nm.

delay line, though shorter than the excitation pulse repetition period of 12 ns (see figure.4b). The "non-decaying" component was also observed in InSb. In the entire intensity range the value and sign of the induced polarization rotation both in GaAs and InSb depended on the sample orientation exactly as predicted by (3) (figure.3b). The "non-decaying" contribution also obeyed cos2ϕ orientational dependence.

The value of the induced nonlocality tensor component at $I_p = 1$ MW.cm^{-2} may be estimated via formula (4.32) as γ^s_{xyz} *(induced)*$= 7.5\times10^{-10}$ cm for GaAs and γ^s_{xyz} *(induced)* $= 3.7\times10^{-9}$ cm for InSb.In both materials, the observed effects were found to be nonreciprocal. That is, when the sample was rotated by 180° about one of the cubic axes of the crystal which were parallel to the plane of the sample surface (i.e. [100] or [010]) and illuminated on the opposite face, the sign of the observed polarisation plane rotation was reversed.

4.5.2 Observation of Linear and Pump-Induced Gyrotropic Linear Dichroism in $Cd_{0.6}Mn_{0.4}Te$

The experimental arrangement for the experiments on $Cd_{0.6}Mn_{0.4}Te$ was identical to that for the experiments on GaAs and InSb described in section 4.5.1 above. The same sample of $Cd_{0.6}Mn_{0.4}Te$ was used in these experiments as in the specular inverse Faraday effect experiments described in section 3.4.1. Natural rotation on a scale of $\delta\alpha_r = 5\ 10^{-4}$rad was observed in the single-beam experiment (figure 4.12). The orientational dependence of the effect meets with high accuracy the cos 2ϕ dependence given in formula (4.32). Given n=3.07, k=0.34 at 532nm [Lautenschlager, 85], this allows us to estimate the value of γ^s_{xyz}*(natural)* $= 2\ 10^{-8}$cm.

Additional pump-induced polarization plane rotation on reflection on a scale of 10^{-4}rad was observed with a pump of intensity 4 MWcm^{-2}. The orientational dependence of the effect when the sample was rotated around [001] was identical to that of the linear effect (figure 4.13). Here the solid line represents the effect as it would appear in accordance with formula (5) for γ^s_{xyz}*(induced)*$= 2.5\ 10^{-9}$cm. The

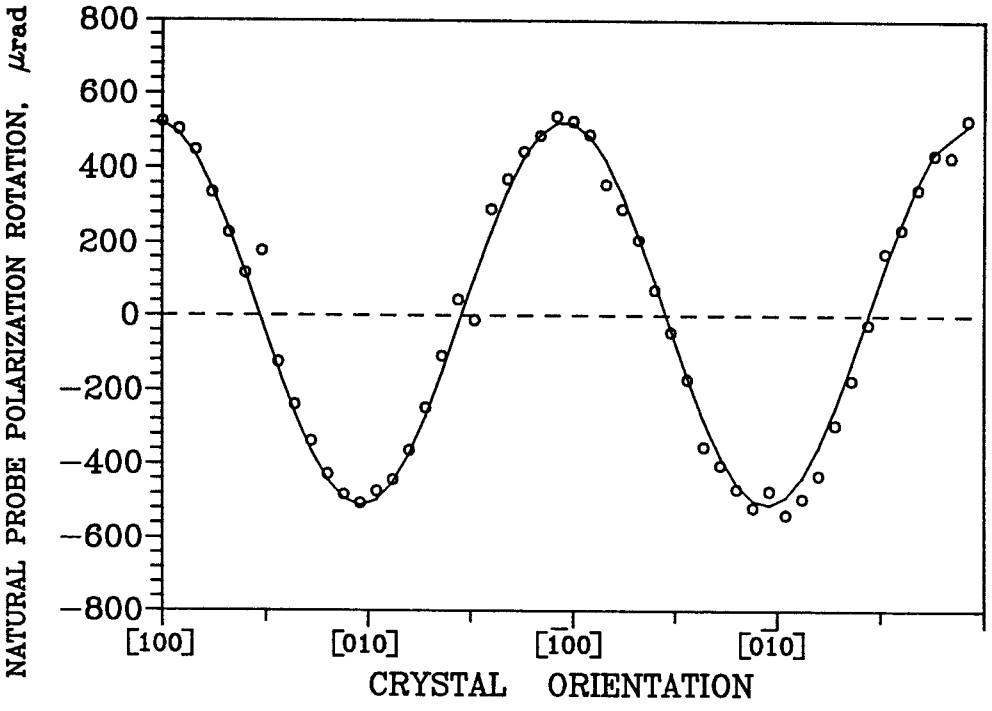

Figure 4.12 Natural probe polarisation azimuth rotation in $Cd_{0.6}Mn_{0.4}Te$ as a function of crystal orientation.I_p=5 MW cm^{-2}, λ=532 nm.

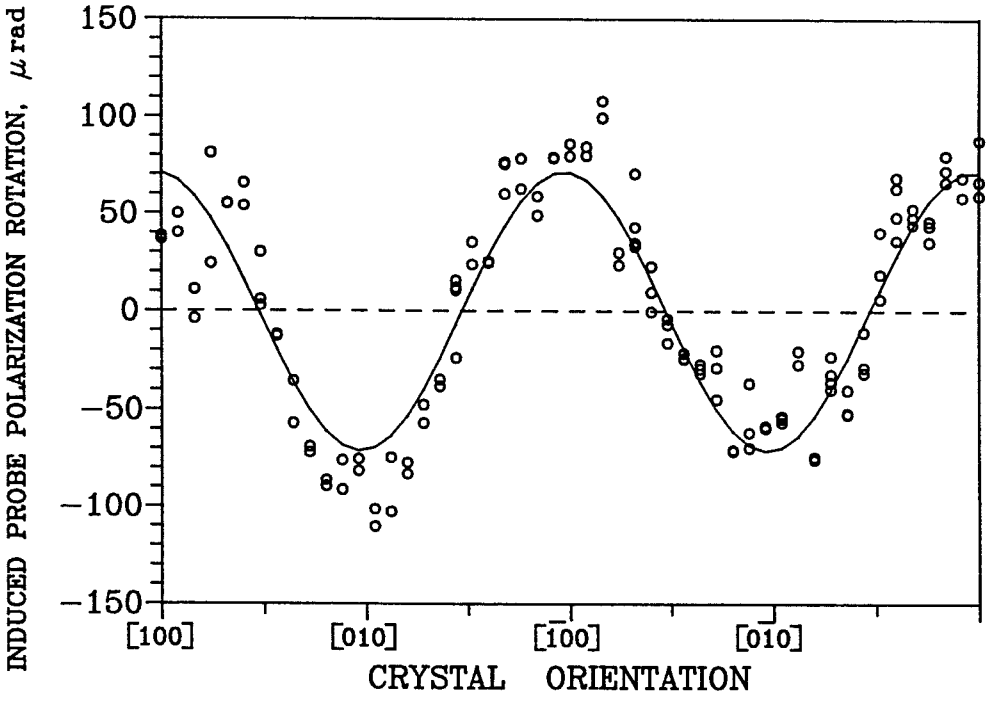

Figure 4.13 Pump-induced probe polarisation azimuth rotation in GaAs as a function of crystal orientation at zero pump-probe delay for pump intensity I_p= 5 MW cm^{-2}, λ=532 nm.

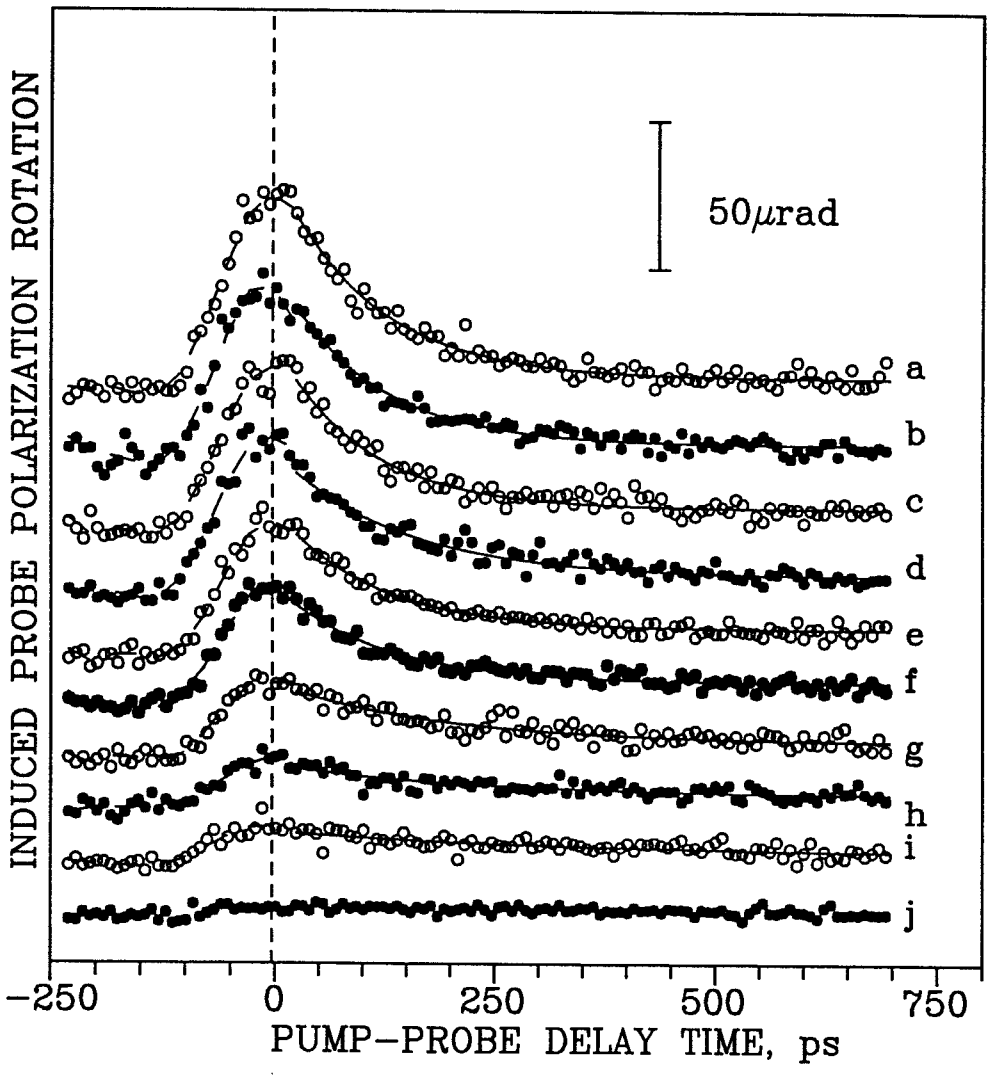

Figure 4.14 Induced probe polarisation azimuth rotation in GaAs as a function of pump-probe delay for pump intensities I_p a)4.8 b)4.5 c)3.5 d)2.6 e)2 f)0.95 g)0.45 h)0.25 i)0.065 j)0.03 MWcm^{-2}.

induced polarisation azimuth rotation is shown as a function of pump-probe delay for various pump intensities in figure 4.14. In the range of pump intensity up to about 1 MW cm^{-2} the induced rotation was found to increase proportionally to the pump at a rate of 6 10^{-11} rad cm^{2}W^{-1} and tended to saturate at higher intensities (figure 4.15). However, its relaxation rate strongly depended on the intensity of optical stimulation. The rotatory power relaxation fits reasonably a single-exponential model. The decay time decreased with the excitation level as shown in figure 4.16 where the dashed line is an empirical best fit $\tau \propto I_{pump}^{-0.4}$.

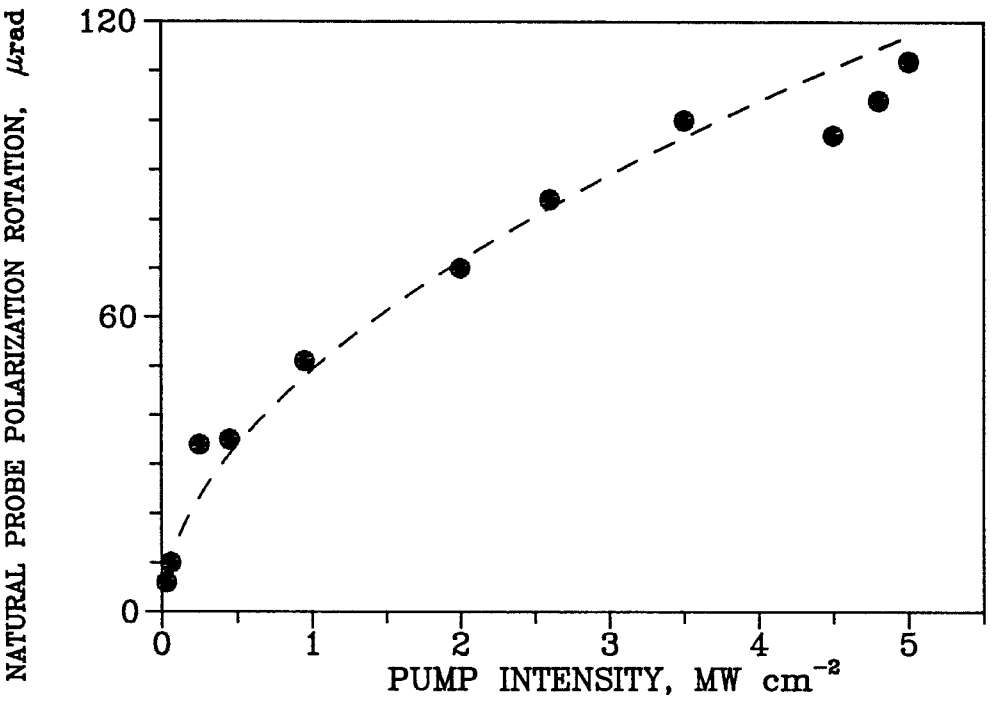

Figure 4.15 Induced probe polarisation azimuth rotation in $Cd_{0.6}Mn_{0.4}Te$ as a function of pump intensity, λ=532 nm.

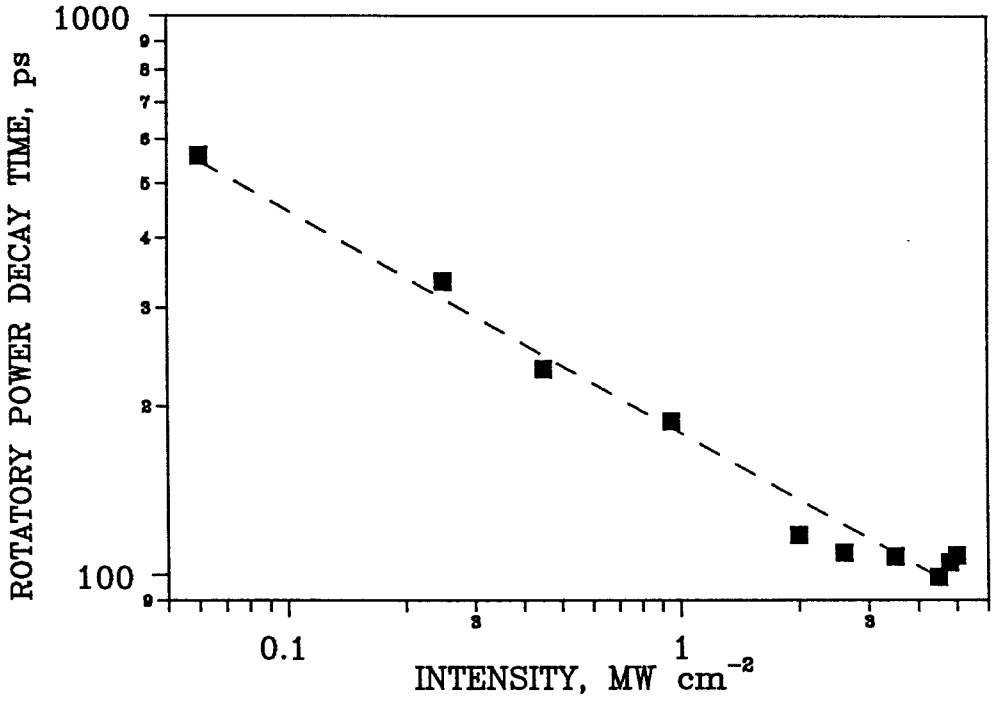

Figure 4.16 Decay time of induced probe polarisation rotation in $Cd_{0.6}Mn_{0.4}Te$ as a function of pump intensity, λ=532 nm.

4.6 Origin of Linear and Pump-Induced Gyrotropic Linear Dichroism/ Birefringence in Zincblende Semiconductors

Below a microscopic picture of the observed effect is outlined, explaining the appearance of k-linear terms in the optical response and its time-non-reversible nature. This picture, which involves examination of transitions promoted by left and right circularly polarised photons, is not directly comparable with the phenomenological description in section 4.3, where the eigenpolarisations in a zincblende symmetry material with nonlocal response were shown to be linear, but we believe that it is applicable as long as we assume that any changes in the polarisation state of the light are small.

For the sake of simplicity we limit ourselves to considering a simple two-band structure in GaAs which is pictured in figure 4.17. It represents the lowest electron band and the heavy hole band. A similar picture might be presented for the light hole band. We assume that the conductivity band is parabolic and degenerate with respect to the projection of the total electron angular momentum **J**. This spin degeneracy holds in all centro-symmetric structures. The situation is different for structures which lack a centre of inversion, such as zinc-blend crystals, where taking account of the spin-orbit interaction, including relativistic corrections, leads to terms linear in q (where q is the wave vector of the electron) [Bir, 74; Pikus, 84; Cardona, 88]. In the heavy-hole band only Δ-directions ($q \parallel$ [100]) remain degenerate. All other directions including the L-direction ($q \parallel$ [111]) and X-direction ($q \parallel$ [110]) become non-degenerate. We take account of this splitting in the valence band of our model. However, even taking account of the spin-orbit interaction *the crystal itself remains time-reversible* [Svirko, 95] and the band structure obeys the rule requiring a state with angular momentum m_J at a general q point to have the same energy as the opposite state at $-q$: $E(q, m_J) = E(-q, -m_J)$ (see, for example [Bir, 74; Lax, 74]). The q-odd splitting is on a scale of only a few meV and may be ignored in the majority of calculations. However, it is crucial when k-linear optical effects are considered and leads to time-non-reversible optical interaction with the crystal.

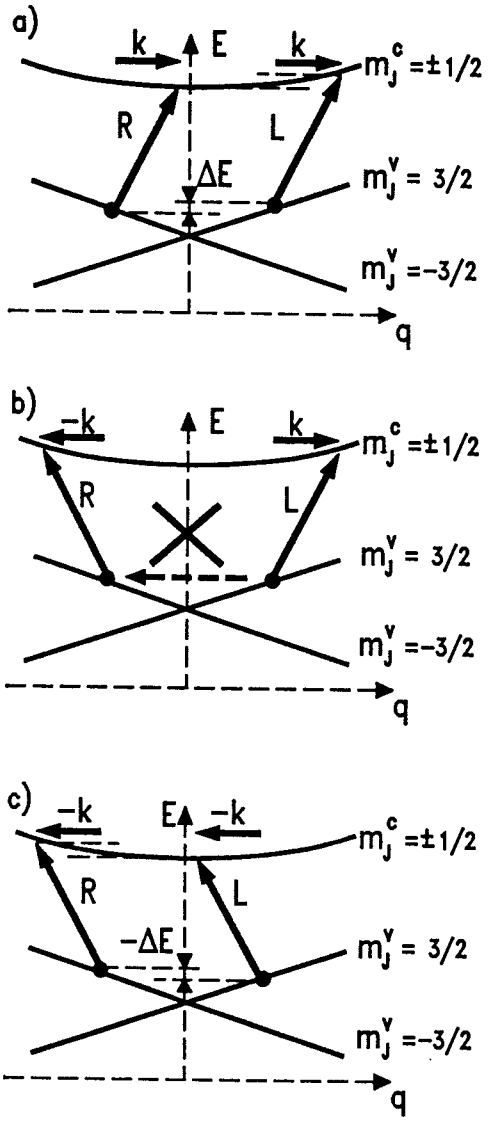

Figure 4.17 Simple band structure model for GaAs and interaction of light with the crystal showing a) wave vector dependence of transitions, b) time-non-reversality of interaction, b) non-reciprocity of interaction

As follows from the law of conservation of momentum, optical transitions from the valence band to the conductivity band are not exactly vertical: $q_v = q_c + k$. One can see that, taking account of the valence band splitting and the finite value of the wave vector k of the photon involved, the transitions $m_J^v = -3/2 \Rightarrow m_J^c = -1/2$ and $m_J^v = 3/2 \Rightarrow m_J^c = 1/2$ promoted by left and right polarised light (L and R in figure 4.17) of the same quantum energy begin and end at energy levels which differ by ΔE on the dispersion curve (figure 4.17a). This means that absorption and refractive

coefficients for left and right handed polarised light are different, due to the finite value of the k-vector of the optical excitation. This differential absorbtion/refraction, however, does not result in the conventional *time-reversible effect of optical activity* described by the *anti-symmetric* part of the nonlocality tensor $\gamma^a_{ijk} = -\gamma^a_{jik}$. This tensor component is forbidden by the crystal point group and vanishes in microscopic calculation of optical response as a result of summation over all available initial q-states [Blank, 91]. In fact the interaction of light with this structure is time-non-reversible. This may be seen from the following simple analysis.

Let us reverse the scenario of light-matter interaction with respect to time. Electron and photon momenta and spin are odd with respect to time inversion ($T \Rightarrow -T$: $k \Rightarrow -k$; $q \Rightarrow -q$, $\sigma \Rightarrow -\sigma$) [Lax, 74]. For example, the transition which is time-conjugated to $m_J^v = 3/2 \Rightarrow m_J^c = 1/2$, should appear in the time reversed scenario as pictured in figure 4.17b. In fact this time-reversed transition does not occur, since due to angular momentum conservation it requires the opposite handedness of light polarization: $m_J^v = -3/2 \Rightarrow m_J^c = -1/2$ must be promoted by R-polarized light. However, time reversal does not affect the handedness of light polarization. "Direct" and "time-reversed" scenarios are not equivalent, the light-matter interaction is time non-reversible. This is due to the spin-orbit interaction induced splitting of the hole bands in a crystal lacking P-symmetry.

Figure 4.17c. shows how the excitation diagram figure 4.17a appears if we reverse time not for the whole system, which includes the light beam and the crystal, but only for the excitation, i.e. where we reverse the direction of light propagation. This is the test for reciprocity of the effect. Inversion of the wave vector of the light symmetrically swaps the positions in the band structure of the transitions for right- and left-hand polarized components. Now, what was positive right-left birefringence (dichroism) becomes negative and vice versa. This will lead to change of the sign of the polarization plane rotation, as was experimentally observed. This effect is described by the *symmetric* part of the nonlocality tensor $\gamma^s_{ijk} = \gamma^s_{jik}$ and manifests itself as k- *linear* birefringence/dichroism for linearly polarized light.

In order to make a theoretical estimate of the value of the optical nonlocality tensor γ on the basis of the above model, we must evaluate the **q**-odd spin splitting in the band structure of GaAs in the conditions of the experiments described above (estimates are not produced for the other materials because of the narrow gap of InSb and the necessity of accounting for higher bands and non-parabolicity affects which are beyond the scope of this model, and because consideration of $Cd_{0.6}Mn_{0.4}Te$ would require understanding of the possible role of the Mn^+ admixture ions). The following parameters for GaAs will be used: E_g = 1.435eV, m_{hh}=0.57; m_{hl} =0.082; m_c=0.067. The value of the q-vector of the electron involved in the direct optical valence-conductivity band transition may be estimated in the parabolic approximation

$$q^2 = 2m_h m_c(\hbar\omega - E_g)/((m_c+m_h)\hbar^2) \qquad (4.38)$$

where m_h is equal to the mass of heavy hole m_{hh} or light hole m_{hl} for heavy-hole or light-hole to electron state transitions correspondingly. If the *hh-c* transition is promoted by a quantum of energy $\hbar\omega$=2.33 eV (λ=532 nm), q = 1.2 10^9 m^{-1}. Spin dependent terms cubic in q appear in the conduction band Hamiltonian in the following manner [Pikus, 84]: $\delta_3 E = (\hbar/2)\sigma.\Omega(q)$ where σ are the Pauli matrices, and Ω is a vector such that

$$\Omega_x(q) = \alpha\hbar^2 q_x(q_y^2 - q_z^2)/[m_c(2m_c E_g)^{1/2}] \qquad (4.39)$$

(cyclic permutation of the indices x,y,z is presumed, $\alpha \sim 6\ 10^{-2}$). The vector Ω is always perpendicular to the electron quasimomentum. In the experimental situation described above the splitting in the X direction is $\delta_3 E$ = 26 meV. The q-linear terms are mainly produced by bilinear second-order perturbation terms consisting of the $q.p$ and the spin-orbit terms

$$E_{so} = (\hbar/4m^2c^2)\{[(\nabla V_0)\times p]\cdot\sigma + [(\nabla V_0)\times q]\cdot\sigma\} \qquad (4.40)$$

(here V_0 is the periodic potential of the crystal). The strongest q-linear correction to the band structure appears in the heavy-hole band [Bir, 74; Cardona, 88]. It is given by $\delta_1 E = -2\sqrt{2}\ C_q\ q$ and by $\delta_1 E = 3/2\sqrt{3}\ C_q\ q$ for the L and X directions correspondingly. Here $C_q \sim -3.4\ 10^{-13}$ eVm for GaAs. From these figures one can

see that in both non-degenerate directions the value of splitting is of order 1 meV.

Since the k-linear contribution to the dielectric tensor $\epsilon(\omega, k) \approx \epsilon(\omega) + \gamma k$ appears as the result of q-odd corrections in the band structure $E(\omega, k) = E(\omega) + \delta_{1,3}E$, we can decompose $\epsilon = \epsilon(E(\omega)) + (\partial\epsilon/\partial E)\,\delta_{1,3}E$ and attribute the nonlocal response to the second term . Thus $(\partial\epsilon/\partial E)\,\delta_{1,3}E = \gamma k$. Here the partial derivative depends on the frequency dispersion of the dielectric tensor, but for the purpose of a rough estimate we may take it as equal to ϵ/E_g, thus $|\gamma| = (\epsilon\,\delta_{1,3}E)/(k\,E_g)$. By neglecting the conductivity electron mass in comparison with the hole mass and by rounding the numerical coefficients this formula become for q-linear terms:

$$|\gamma| \approx (\varepsilon\lambda C_q m_c^{1/2}/\hbar E_g)(\hbar\omega - E_g)^{1/2} \qquad (4.41)$$

and for q-cubic terms:

$$|\gamma| \approx (\varepsilon\lambda\alpha/2\pi)[(\hbar\omega - E_g)/E_g]^{3/2} \qquad (4.42)$$

The above formula for the q-linear contribution gives an estimated value of $\gamma \sim 2\times10^{-7}$ cm at 532 nm, which is reasonably similar to the observed $\gamma^{exp} = 4.5\times10^{-8}$cm. The formula for q-cubic terms gives, however, the much larger estimated value of $\gamma \sim 4\times10^{-6}$cm. The question of which of the two q-odd contributions considered above actually produces k-linear terms in the optical response is not resolved by this simple qualitative analysis. The q-linear and q-cubic terms have slightly different symmetry: the first has lower symmetry and lifts degeneracy along the P-odd (polar) L-direction [111] whilst the second does not. This, together with the large estimate of the value of γ which we obtain due to q-cubic terms in the band structure, probably indicates that the q-linear terms are responsible for the k-odd birefringence. However more comprehensive microscopic and symmetry analysis is required to demonstrate this conclusively.

A possible explanation of the observed intensity-dependent effect, i.e. increase of the value of γ^{s}_{ijl} of approximately 2% by excitation at 1 MW cm^{-2}, is re-normalization of the band structure. Excitation of 1 MW cm^{-2} produces free carriers with a density

of about 2 $10^{18}cm^{-3}$ leading to squeezing of the band structure of several percent [Blank, 91] and promotion of electrons by the probe wave to states with a higher value of the wave vector and consequently to the enhancement of the q-odd contributions. The relaxation rate of this nonlinearity is controlled by the recombination of the conductivity electrons which is on a sub-nanosecond timescale and would explain the observed decay tails.

If this is the mechanism involved, we would expect that the nonlinear effect will be observable for any polarisation of pump beam, since the density of generated free carriers is the important factor. Some confirmation that this is in fact the case comes from recent experiments by S.V.Popov, which are presented here (figure 4.18), although the author was not involved in their production. They show induced polarisation azimuth rotation of a linearly polarised probe beam (λ=1260 nm) on reflection from a sample of InSb as a function of crystal orientation in the presence of a strong circularly polarised pump. The sharp peak at zero delay is due to the specular inverse Faraday effect, which has a very fast response time in this material. In addition to this peak, there is a slowly decaying tail which displays the characteristic $cos2\phi$ orientational dependence of the nonreciprocal effect. In contrast to the specular inverse Faraday effect, the tail shows the same sign of rotation for left- and right-hand circularly polarised pump. This confirms that the effect is observable with at least three different types of pump polarisation and suggests that it can indeed be produced by a pump of any polarisation state.

In competition with the transient time-nonreversible mechanism described above, one may consider some others which are also transient, but not necessarily time-non-reversible. For example, the creation of the dense electron-hole plasma leads to excitation of a strong acoustical pulse arising mainly due to the concentration-deformation mechanism leading to the effect of piezo-gyrotropy [Lax, 74]. The relaxation time of this effect is determined by the typical time of sound propagation over the absorbtion layer, which is on the order of tens of picoseconds. Another mechanism may be a longitudinal electrooptic effect caused by the Dember field

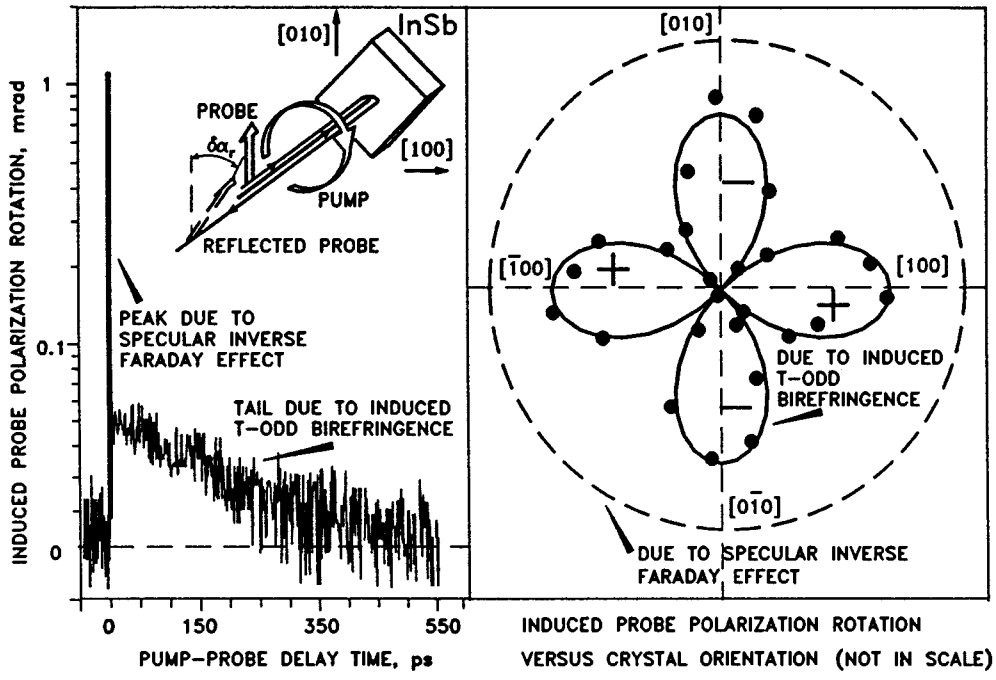

Figure 4.18 Specular Gyrotropic Linear Dichroism induced by a circularly polarised pump in InSb at λ=1260 nm (reproduced by permission of S.V.Popov)

[Seeger, 91]. This surface field appears due to the difference of the electron and hole diffusivity and is directed normally to the surface. The relaxation time here is close to the characteristic time of ambipolar diffusion which is on a scale of 10 picoseconds. Neither of these mechanisms seems a likely explanation of the observations described above, where decay times longer than the pulse length of 80 picoseconds are found in all the materials studied, and, of course, they do not explain the natural effect. Crystal surface anisotropy [Aspnes, 85] may be another reason for an alteration of the polarization state of the reflected probe light and its alteration induced by the pump may in principle give rise to the polarization-affecting phenomenon observed here. However, the experiments [Bungay, 94a] combining reflection, single and forward-backward transmission measurements of gyrotropic linear dichroism in GaAs and investigation of its spectral dependence give backing to the importance of the bulk nonlocal contribution to specular rotatory power, but not of the anisotropic surface contribution. In GaAs and InSb a "non-decaying" component was observed which had the same orientational dependence as the other components of the induced effect, but a relaxation time which was longer than the

pulse repetition rate, but faster than the chopping frequency. This "non-decaying" component might be attributed to alteration of the "natural" rotation resulting from heating of the sample by the intense pump pulse.

A topic of interest is any possible role of the Mn^{+} admixture ions in $Cd_{0.6}Mn_{0.4}Te$ in the observed effect. As mentioned in chapter 3, the strong coupling of free carrier spins with the lattice of magnetic ions is responsible for many of the unusual properties of diluted magnetic semiconductors. Whether they enhance the spin-orbit splitting on which the effect described in this chapter depends, is a possible subject for further research. The results obtained above show that the polarisation azimuth rotation in $Cd_{0.6}Mn_{0.4}Te$ is on the same scale of magnitude of that observed in the nonmagnetic semiconductors. Since the magnetic properties of CdMnTe are strongly temperature dependent, a possible topic of further research might be comparison of the temperature dependence of the natural and induced effects as a function of temperature.

4.7 Conclusions

The effect of specular gyrotropic linear dichroism (first observed in GaAs [Bungay,93]) was studied in two new materials (InSb and $Cd_{0.6}Mn_{0.4}Te$) and a pump induced effect with the same orientational dependence as the linear effect was observed in GaAs, InSb and $Cd_{0.6}Mn_{0.4}Te$. This induced effect is interpreted as being an enhancement to the linear effect produced by renormalisation of the band gap in these materials due to the creation of a dense electron hole plasma. Theoretical backing for the existence of this effect comes from studies of the light-matter interaction Hamiltonian for non-centrosymmetric materials and consideration of the nonreciprocal nature of the predicted optical consequences of these time-nonreversible terms.

4.8 References

[Aspnes, 85] Aspnes D.E. and Studna A.A, Phys. Rev. Lett., **54**, (1985), 1956.

[Barron, 87] Barron L.D, Chem. Phys. Lett., **135**, (1987), 1.

[Barron, 94] Barron L.D, Chem. Phys. Lett., **221**, (1994), 311.

[Barron, 94a] Barron L.D, Science, **266**, (1994), 1491.

[Belinicher, 80] Belinicher V.I, Sturman B.I, Sov. Phys. Usp., **23**, 199 (1980).

[Berestetskii, 82] Berestetskii V.B, Lifshitz E.M, Pitaevskii L.P, "Quantum Electrodynamics", Pergamon, Oxford, (1982).

[Bir, 74] Bir G.L, Pikus G.E, "Symmetry and Strain-Induced Effects in Semiconductors", John Willey, (1974).

[Birss, 67] Birss R.R, Shrubsall R.G, Philos. Mag., **15**, (1967), 687.

[Blank, 91] Blank R, Haug H, Phys.Rev.B, **44**, (1991), 10513.

[Buckingham, 79] Buckingham A.D, Phil. Trans. R. Soc. Lond. A, **293**, (1979), 239.

[Bungay, 93] Bungay A.R, Kugler N, Zheludev N.I, Physics Letters A, **174**, (1993), 335.

[Bungay, 94] Bungay A.R, Pointel Y, Zheludev N.I, Jnl. of Luminescence, **60**, (1994), 36.

[Bungay, 94a] Bungay A.R, Popov S.V, Svirko Yu.P, Zheludev N.I, Chem. Phys. Lett., **217**, (1994), 249.

[Cardona, 88] M.Cardona, N.E.Christensen, G.Fasol. Phys.Rev. B, **38**, 1806 (1988).

[Hamaguchi, 80] Hamaguchi H, Buckingham A.D, Kakimoto M, Opt. Lett., **5**, (1980), 114.

[Kane, 57] Kane E.O, J. Phys. Chem. Solids, **1**, (1957), 249.

[Landau, 84] Landau L.D, Lifshitz E.M, Pitaevskii L.P, "Electrodynamics of Continuous Media", 2nd ed., Pergamon, Oxford, 1984.

[Lautenschlager, 85] Lautenschlager P, Logothetidis S, Vina L, Cardona M, Phys. Rev. B **32**, (1985), 3811.

[Lax, 74] Lax M, "Symmetry Principles in Solid State and Molecular Physics", John Willey & Sons, (1974).

[Lifshitz, 81] Lifshitz E.M, Pitaevskii L.P, "Physical Kinetics", Pergamon, Oxford, 1981.

[March-Russell, 88] March-Russell J, Wilczek F, Phys. Rev. Lett., **61**, (1988), 2066.

[Onsager, 31] Onsager L, Phys. Rev., **37**, (1931), 405; **38**, (1931), 2265.

[Pikus, 84] Pikus G.E, Titkov A.N, in "Optical Orientation", Eds. Meier F and Zakharchenia B.P, Elsevier Science Publishers B.V., (1984).

[Popov, 95] Popov S.V, Svirko Yu.P, Zheludev N.I, "Susceptibility Tensors for Nonlinear Optics", IoP Publishing, Bristol, 1995.

[Popov, 96] Popov S.V, Svirko Yu.P, Zheludev N.I, accepted by J. Opt. Soc. Am. A.

[Seeger, 91] Seeger K, "Semiconductor Physics", Springer, NY, 1991.

[Seraphin, 67] Seraphin B.O, Bennett H.E in "Semiconductors and Semimetals", Vol.3, Ed. Willardson R.K, Beer A.C, Academic Press Ltd., (1967).

[Sihvola, 95] Sihvola A, IEEE Antennas and Propagation Magazine, **37**(3), (1995), 32.

[Svirko, 95] Svirko Yu.P, Zheludev N.I, Opt. Lett., **20**, (1995), 1809.

[Wen, 89] Wen X.G, Zee A, Phys. Rev. Lett., **62**, (1989), 2873.

[Weiglhofer, 95] Weiglhofer W.S, Lakhtakia A, IEEE Antennas and Propagation Magazine, **37**(3), (1995), 32.

[Zheludev, 90] Zheludev N.I, Paraschuk D.Yu, JETP Lett., **52**, (1990), 32.

Chapter 5

Simulation of Evolution of Partially Polarised Light in Nonlinear Media

5.1 Synopsis

The work described in this chapter was motivated by papers by Zheludev and Svirko [Svirko, 94; 94a] on the evolution of partially polarised light in linear and nonlinear media. Of particular interest was the idea of using partially polarised light as a diagnostic of broken time-reversibility. It was decided to use a statistical simulation approach to this problem, rather than the analytical perturbation calculations performed by Zheludev and Svirko. The development of this approach and some preliminary results are presented in this chapter. Section (5.2) discusses previous research into partially polarised light and "depolarisation" of light waves. Section (5.3) describes a program developed to simulate the evolution of the polarisation state of partially polarised light in nonlinear media. Section (5.4) describes the results obtained by the program in the case of an isotropic nonlinear medium and section (5.5) compares the results obtained with analytical predictions.

5.2 Introduction

In recent years there has been much interest in polarisation instability and chaos [for reviews: Zheludev, 89; David, 90]. A chaotic distribution of light polarisation was predicted for two counter-propagating waves in a nonlinear medium, leading to depolarisation of the light. However, there are also mechanisms not involving chaos

which can have the effect of "depolarising" light. Crosignani et.al. [Crosignani, 86] dealt theoretically with the case of fully polarised light whose instantaneous intensity had an exponential distribution, such as might be generated by a (non-modelocked) multi-mode laser. They showed that elliptically polarised light with these statistics undergoes depolarisation in an isotropic nonlinear medium, due to autorotation of the polarisation ellipse [Maker, 64; Crosignani, 85]. Chernov and Zon [Chernov, 93] dealt with the behaviour of the same type of light in an anisotropic nonlinear medium. The use of laser-noise-induced polarisation fluctuations in a nonlinear medium as a spectroscopic tool has been theoretically investigated [Walser, 94].

Another case of interest is where the initial polarisation state of the light has some random component i.e. the light is initially only partially polarised. Svirko and Zheludev have dealt with the case of light which is a mixture of a totally polarised component and a totally unpolarised random component with gaussian statistics by means of analytical perturbation calculations. This might represent the output of a single mode laser operating close to threshold, where the polarisation state undergoes random fluctuations due to spontaneous emission. In [Svirko, 94], the use of partially polarised light in detecting broken time reversibility in linear optical interaction with solids was discussed. In [Svirko, 94a], the interaction of partially polarised light with nonlinear media was discussed. In this paper, it was predicted that in an absorptionless medium with isotropic nonlinear response (and linear response of arbitrary symmetry), no intensity dependent change of the degree of polarisation should occur. However, Crosignani et.al. [Crosignani, 86] have calculated that an elliptically polarised beam with a random intensity profile of *arbitrary* distribution propagating in an isotropic nonlinear medium will tend asymptotically (for long propagation lengths) to a value of degree of polarisation which is equal to the degree of ellipticity of the input light. This is a practically important case, since isotropic nonlinearity is a widely accepted model for fibre optics. This seemed an appropriate starting point of investigation for a computer simulation of the behaviour of partially polarised light.

5.3 Simulation of the Evolution of the Stokes' Vector of Partially Polarised Light

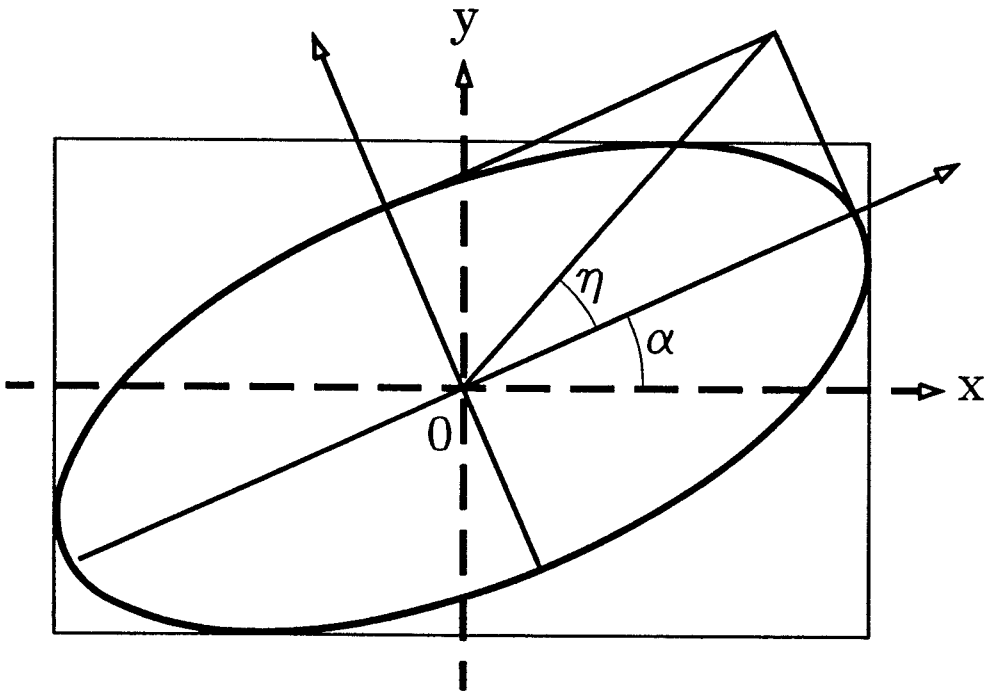

Figure 5.1 Polarisation ellipse of a light beam; α: polarisation azimuth angle, η: ellipticity angle

The polarisation state of light may be represented by the polarisation azimuth angle α, the ellipticity angle η and the degree of polarisation r. The definitions of α and η in terms of the polarisation ellipse of the light are shown in figure 5.1. α is the angle of the semi-major axis of the polarisation ellipse to the x-direction, η is $\tan^{-1}(A/B)$ where A and B are the semi-major and semi-minor axes of the polarisation ellipse respectively. The degree of polarisation r is the ratio between the total intensity of the light beam and the intensity of the polarised component of the light beam.

In [Svirko, 94a] and here, the intensity and polarisation state of a light beam are described via the quaternion representation, i.e. in terms of the Stokes' vector. The components of the Stokes' vector are defined by

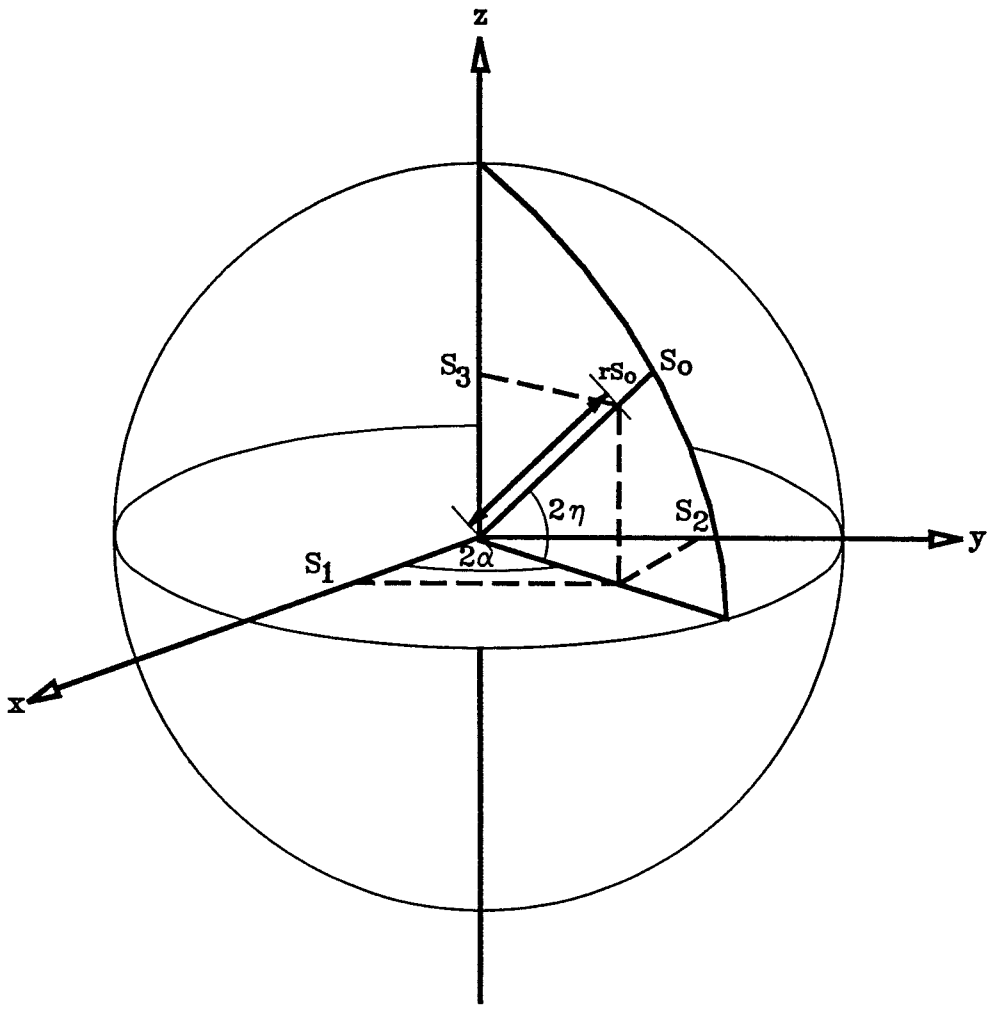

Figure 5.2 Relationship between α, η, r and S_0, S_1, S_2, S_3

$$S_\alpha = \langle \sigma_{ij}^{(\alpha)} E_i^* E_j \rangle \quad (\alpha = 0,1,2,3) \tag{5.1}$$

where $\sigma^{(\alpha)}$ are the Pauli matrices

$$\sigma^{(0)} = \begin{pmatrix} 1 & 0 \\ 0 & 1 \end{pmatrix}, \ \sigma^{(1)} = \begin{pmatrix} 1 & 0 \\ 0 & -1 \end{pmatrix}, \ \sigma^{(2)} = \begin{pmatrix} 0 & 1 \\ 1 & 0 \end{pmatrix}, \ \sigma^{(3)} = \begin{pmatrix} 0 & -i \\ i & 0 \end{pmatrix} \tag{5.2}$$

and $\langle . \rangle$ denotes averaging over time [Born, 80]. The Stokes' vector contains all information about the state of the light except its absolute phase, which is arbitrary. The Stokes' vector approach to the evolution equation of a light wave was first used in the context of polarisation dynamics in [Kubo, 80, 81]. It was first used to deal with nonlinear polarisation dynamics in [Sala, 84], and generalised to absorbing and

nonlocal nonlinear media in [Zheludev, 90]. It has been very widely used in studying polarisation phenomena [for reviews: Zheludev, 89; David, 90]. Figure 5.2 represents the polarisation state of the light in terms of the Stokes' vector components on the Poincare sphere, and shows the relationship between the Stokes vector components and α, η and r.

In terms of the Stokes' vector components α, η, r are:

$$\alpha = \frac{1}{2}\tan^{-1}\left(\frac{S_2}{S_1}\right)$$

$$\eta = \frac{1}{2}\sin^{-1}\left(\frac{S_3}{\sqrt{S_1^2+S_2^2+S_3^2}}\right) \qquad (5.3)$$

$$r^2 = \frac{S_1^2+S_2^2+S_3^2}{S_0^2}$$

To deal with the evolution of partially polarised light in a nonlinear medium the approach of [Svirko, 94a] (i.e. use of the quaternion representation for the light polarisation, material and wave equations) was applied to totally polarised light, but the evolution of partially polarised light was simulated numerically (by randomly generating instantaneous polarisation states for the unpolarised component of the light and averaging the results of the evolution of many such states), rather than being derived analytically.

To model the propagation of light in nonlinear media we start from the equation for a light wave $\mathscr{E}(r)=Ee^{ik.z-\omega t}$ with slowly-varying amplitude E, frequency ω and wave number k, propagating along the z direction in a medium with cubic nonlinearity

$$\frac{dE_i}{d\zeta} = i\,(u_{ij}E_j + \kappa_{ijkl}\,E_jE_kE_l^*)$$
$$\zeta = \frac{2\pi\omega^2}{kc^2}z \qquad (5.4)$$

where u_{ij} and κ_{ijkl} are determined by the dielectric tensor ϵ_{ij}, the linear nonlocal optical response tensor $\gamma^{(1)}_{ijz}$, and tensors of the local $\chi^{(3)}_{ijkl}$ and nonlocal $\Gamma^{(3)}_{ijklz}$ cubic nonlinearity of the medium

$$u_{ij} = \frac{\epsilon_{ij} - n^2\delta_{ij}}{4\pi} + ik\gamma^{(1)}_{ijz}$$
$$\kappa_{ijkl} = (\chi^{(3)}_{ijkl} + ik\Gamma^{(3)}_{ijklz}) \qquad (5.5)$$

Use of equation (5.4) presumes that the light spectrum remains a narrow band around the central frequency.

The field strength components may be converted to the following quadratic form which we will call the *s*-vector: $s^\alpha = \sigma^{(\alpha)}_{ij}E_i^*E_j$ $(\alpha=0,1,2,3)$, where $\sigma^{(\alpha)}$ are the Pauli matrices. This is similar to the Stokes' vector $\boldsymbol{S}$, except that s represents the instantaneous value of the polarisation of the light, while the Stokes' vector is defined for *steady state stochastical processes* and thus involves averaging over time, i.e. $\boldsymbol{S}=\langle s\rangle$. In terms of s the evolution equation of the light (5.4) becomes

$$\frac{ds_\alpha}{d\zeta} = -Im(\Omega_0 s_\alpha + \Omega_\alpha s_0) - Re\,(e_{\alpha\beta\gamma}\Omega_\beta s_\gamma)\,, \quad \alpha=1,2,3 \qquad (5.6)$$

$$\frac{ds_0}{d\zeta} = -Im(\Omega_\alpha s_\alpha + \Omega_0 s_0)\,, \quad \alpha=1,2,3. \qquad (5.7)$$

where $e_{\alpha\beta\gamma}$ is the Levi-Civita symbol,

$$\begin{aligned} v^{\alpha} &= \sigma_{ji}^{\alpha} u_{ij}; \quad u_{ij} = \frac{1}{2} v^{\alpha} \sigma_{ij}^{(\alpha)} \\ w^{\alpha\beta} &= \sigma_{ji}^{(\alpha)} \kappa_{ijkl} \sigma_{kl}^{(\beta)}; \quad \kappa_{ijkl} = \frac{1}{4} w^{\alpha\beta} \sigma_{ij}^{(\alpha)} \sigma_{lk}^{(\beta)} \end{aligned} \tag{5.8}$$

and $\Omega_{\alpha} = v^{\alpha} + \frac{1}{2} w^{\alpha\beta} s_{\beta}$; $\alpha,\beta = 0...3$. All single-beam linear and third order degenerate nonlinear optical propagation effects may be described by means of equations (5.6, 5.7).

Equations (5.6, 5.7) may be used to deal with the evolution of the Stokes' vector $\boldsymbol{S}$ of partially polarised light if time averaging is replaced by ensemble averaging, in accordance with the ergodic theorem [Goodman, 85]. The conditions for a process to be considered ergodic are:

a) the ensemble is strictly stationary i.e. the k-th order joint probability density function is independent of the time origin for all k

b) the ensemble contains no strictly stationary sub-ensembles which have probability other than zero or one.

Both these conditions are met by thermal light. The evolution of the polarisation state of a single wave, taking account of linear and third-order nonlinear terms, is always described by a continuous and single-valued function of the initial conditions [Tratnik,87]. Hence, a single region in the Poincare sphere may change shape but will not split into two or more separate regions during propagation. Therefore, if condition b) is met at the input to the medium, it will be met at any point during propagation through the medium [Svirko, 94a]. Hence, the polarization state of the light may be found in terms of the Stokes vector $\boldsymbol{S}$ by taking the average value of s for a large number of randomly generated cases.

A computer program was written in order to model the behaviour of partially

polarized light propagating through a medium. The program was written in Pascal, using double precision variables (15 significant figures). The program allows the user to input the components of the material tensors ϵ_{ij}, $\gamma^{(1)}{}_{ijz}$, $\chi^{(3)}{}_{ijkl}$ and $\Gamma^{(3)}{}_{ijklz}$, and the length of propagation of the light through the medium. The user may also specify the intensity I and the polarisation state of the light, either by specifying polarization ellipse azimuth angle α, ellipticity angle η and degree of polarisation r, or in terms of the components of the Stokes' vector.

As in [Svirko, 94; 94a] we consider incident light as consisting of a totally polarized part E_0 and an unpolarized part δE: $E=E_0+\delta E$. This might represent a single mode laser with spontaneous emission noise. This partially polarized light is simulated by adding a randomly generated component with Gaussian statistics (representing the unpolarized component) to a fixed polarization component. A random polarization state is generated as 2 orthogonal $(\delta E_x, \delta E_y)$ independent phasor field components. A circular gaussian random phasor $v_1+i.v_2$ (i.e. a number composed of 2 independent gaussian random variables with zero means and equal variances) is generated by applying the Box-Muller transformation [Box, 58] to a pair of uniform deviates (u_1, u_2) in the range $0 \le u \le 1$:

$$\begin{aligned} v_1 &= \sqrt{S_0(1-r)/2}\sqrt{-2\ln u_1}\cos(2\pi u_2) \\ v_1 &= \sqrt{S_0(1-r)/2}\sqrt{-2\ln u_1}\sin(2\pi u_2) \end{aligned} \qquad \textbf{(5.9)}$$

The real and imaginary parts of each field component have gaussian probability distributions with equal variances. Hence, the probability distribution of the phase of each field component is uniform in the range $0<\phi<2\pi$ and the amplitude has an exponential distribution. The random polarization component therefore has the statistical properties of unpolarized thermal light, which, since it is composed of a very large number of independent randomly phased contributions, has zero mean circular gaussian statistics [Mandel, 63; Goodman, 85]. The variance of the gaussian distribution is chosen to match the specified magnitude of the unpolarized component.

The uniform deviates u_1, u_2 were generated using a linear congruential generator whose output was shuffled [Press, 86]. A linear congruential generator produces a sequence of (pseudo-)random numbers according to a formula of the form $u_i = X_i/m$, $X_{i+1} = (aX_i + c),\ mod\ m$. The values output by the linear congruential generator are stored in an array. In the first call to the random number routine, another randomly generated number is used to select one of the stored numbers as the output of the routine. In subsequent calls to the routine, the previously output number is used to select a stored number. A new random number is generated by the congruential generator to refill the entry in the array that has been used. The shuffling was performed to avoid the pathology associated with combining linear congruential generators with the Box-Muller transformation [Bratley, 87]. Since it involves periodic functions, applying the Box-Muller transform to the output of a linear congruential generator will produce a distribution of v_1, v_2 all of which fall on a spiral. Shuffling the numbers generated removes sequential correlations between them, removing this problem. In general, it is difficult to be sure that there are no problems associated with applying the output of a particular random number generator to a particular problem. A simple way to be confident of the results obtained is to compare the results of applying a generator based on a different principle to the same problem. Substitution of a random number generator based on a subtraction method [Press, 86] did not affect the results obtained in section 5.4 below. The phasor components $E_{0,x}$, $E_{0,y}$ of the fixed polarization component are calculated from the values of S_1, S_2, S_3 which were input by the user. These are added to the randomly generated component to create the instantaneous polarization state.

In general, the differential equations (5.6, 5.7) are solved numerically by means of the fourth-order Runge-Kutta method [Press, 86]. However, for the specific case of an isotropic nonlinear medium, an analytical solution was used (see section 5.4 below), greatly increasing the speed of the program.

The computer program was tested for accuracy by comparing the results obtained with analytical solutions to the evolution of the polarisation state for a variety of

simple cases such as linear birefringent or optically active media and for the case of fully polarised light in an isotropic nonlinear medium. The generated results agreed with the analytical solutions to an accuracy of 10^{-10}.

5.4 Evolution of Partially Polarised Light in an Isotropic Nonlinear medium

An important aim of developing the program described above was to test the predictions made in [Svirko, 94a]. It was decided to concentrate on the simplest possible example of a nonlinear medium. The case of a dissipationless isotropic medium with cubic nonlinearity and no nonlocality or dissipation was examined: $Re\{\epsilon_{xx}\}=Re\{\epsilon_{yy}\}$, $Im\{\epsilon\}=0$, $\gamma=0$, $Re\{\chi^{(3)}_{xxxx}\}=3Re\{\chi^{(3)}_{xxyy}\}$, $Im\{\chi^{(3)}\}=0$. This has the advantage that there exists an analytical solution to the evolution equations of the s-vector. Hence, time-consuming numerical solutions of the evolution equations need not be found, allowing a large number of runs to be performed in a relatively short time. In terms of the s-vector, using equations (5.6, 5.7) above, we find that the evolution equations for this case are:

$$\frac{ds_0}{d\zeta} = 0 \quad , \quad \frac{ds_1}{d\zeta} = -2\chi s_3 s_2 \quad , \quad \frac{ds_2}{d\zeta} = 2\chi s_3 s_1 \quad , \quad \frac{ds_2}{d\zeta} = 0 \qquad \textbf{(5.10)}$$

Solving the simultaneous differential equations we obtain:

$$\begin{aligned} \frac{d^2 s}{d\zeta^2} &= -(2\chi s_3)^2 s_1 \\ \frac{d^2 s}{d\zeta^2} &= -(2\chi s_3)^2 s_2 \end{aligned} \qquad \textbf{(5.11)}$$

It can be seen that while s_3 remains constant s_1 and s_2 oscillate in phase quadrature with a frequency proportional to χs_3. This is equivalent to the instantaneous polarization azimuth direction of the light $\alpha=(1/2)tan^{-1}(s_2/s_1)$ rotating

$$\delta\alpha = \chi s_3 \zeta \qquad \textbf{(5.12)}$$

The final values of the Stokes vector components after propagation are

$$
\begin{aligned}
s_0 &= s_{0,init} \\
s_1 &= s_{0,init} \frac{\sqrt{s_{0,init}^2 - s_{3,init}^2}}{s_{0,init}} \cos\left(\tan^{-1}\left\{\frac{s_{2,init}}{s_{1,init}}\right\} + 2\chi s_{3,init}\zeta\right) \\
s_2 &= s_{0,init} \frac{\sqrt{s_{0,init}^2 - s_{3,init}^2}}{s_{0,init}} \sin\left(\tan^{-1}\left\{\frac{s_{2,init}}{s_{1,init}}\right\} + 2\chi s_{3,init}\zeta\right) \\
s_3 &= s_{3,init}
\end{aligned}
\qquad \textbf{(5.13)}
$$

The effect of propagation through this medium on the averaged polarization vector S was obtained for light with polarization $S_1 = rS_0$, $S_2 = S_3 = 0$, for a variety of initial values of degree of polarization r. To obtain the values of S for each case the results of calculations of the evolution of s for 10^5 randomly generated polarization states were averaged. It was found that the effect of isotropic $\chi^{(3)}$ is to decrease the degree of polarization of the light, the speed of the decay depending on the initial value of r. Figure 5.3 shows the change in r for various initial values of r as a function of the dimensionless constant $(d/\lambda)\chi^{(3)}S_0$ where d is crystal length. These results may be explained as follows:

The effect on the instantaneous polarization state is to produce a rotation of the orientation of the linear polarization component of light proportional to the magnitude of the circular polarization component s_3. Since partially polarized light has a spread of values of s_3, the distribution of the instantaneous azimuth direction of the polarization is broadened as it passes through the medium: instantaneous polarization states with positive s_3 have the direction of their polarization ellipse rotated in one sense, while those with negative s_3 are rotated in the opposite sense. If we view the polarization state of the light by plotting it in the space defined by s_1, s_2, s_3, then as the light wave passes through the medium, the distribution of polarization states becomes an increasingly tightly wound spiral wrapped around the s_3 axis (figure 5.4).

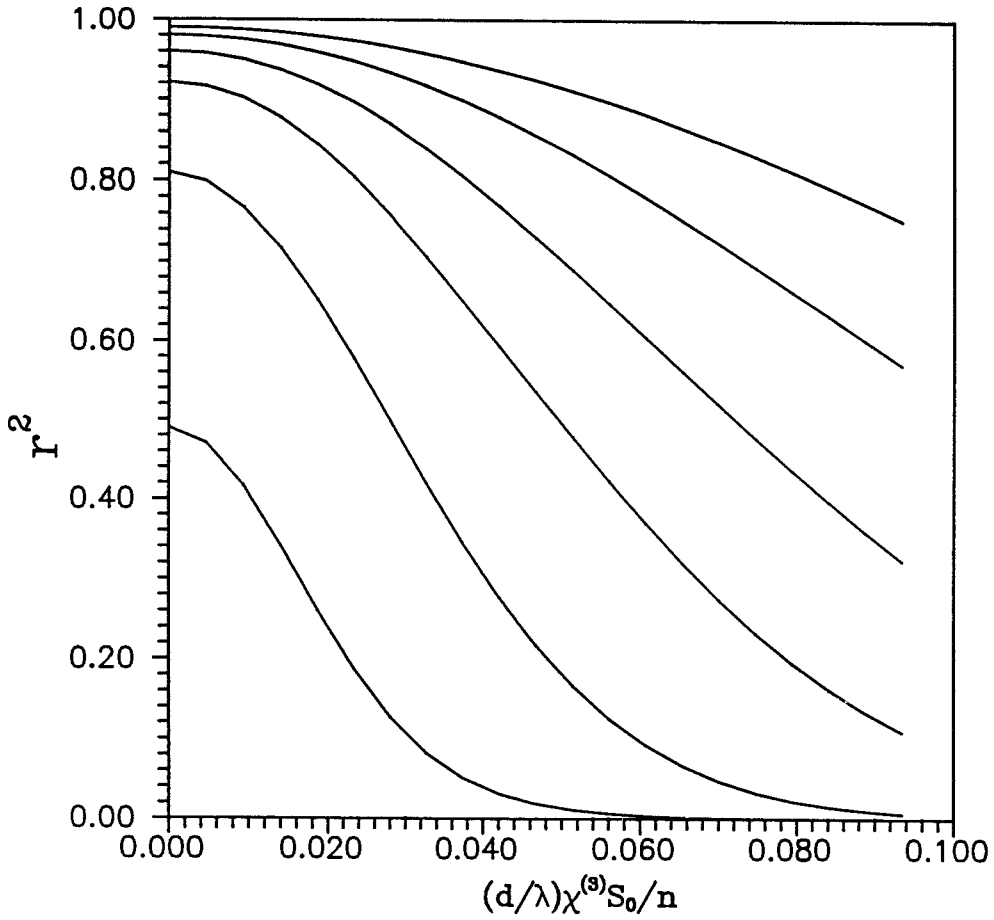

Figure 5.3 Evolution of the degree of polarisation r of initially linearly polarised light in an isotropic nonlinear medium as a function of a dimensionless constant

This causes the averaged value S_1 to decrease as the beam propagates through the nonlinear medium, tending to zero for long distances. Since for the case we are considering S_2 and S_3 are zero (and remain zero during propagation) this means that r decreases. The speed at which this decay occurs depends on the variance of s_3 and hence on the average intensity of the randomly polarized component of the light.

It is important to note that, although r becomes small, there remains a relationship in the output light between the instantaneous value s_3 and the instantaneous values s_1, s_2. This clearly distinguishes the output light from conventional unpolarized light. The initial high value of r could be restored by passing the output light through another medium with the opposite value of isotropic $\chi^{(3)}$. For light with the same value of r,

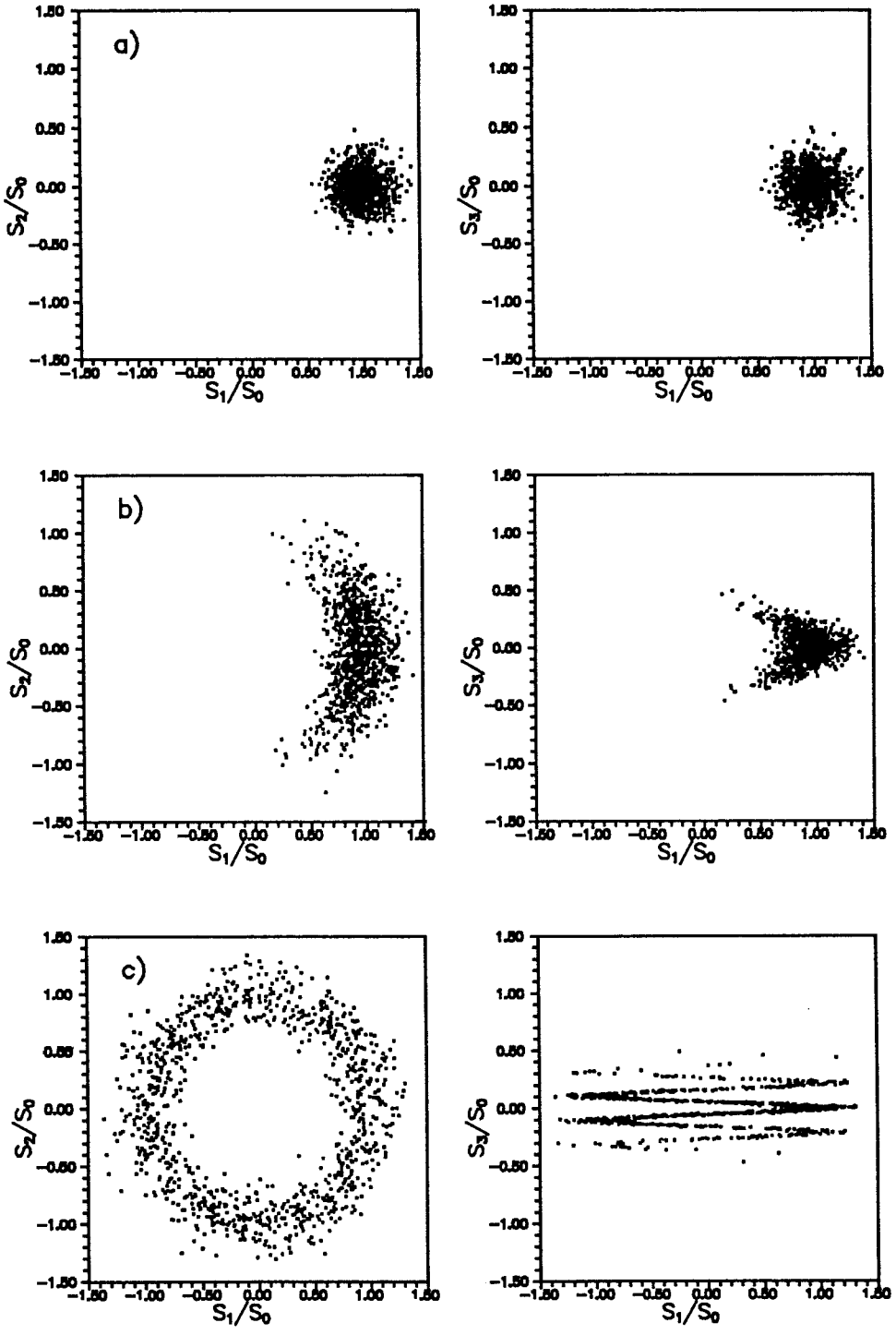

Figure 5.4 The distribution of instantaneous polarisation states of a linearly polarised beam, $r_{initial}=0.9$, in an isotropic nonlinear medium for a variety of propagation distances. Left-hand graphs: S_2 vs. S_1, right-hand graphs: S_3 vs. S_1. a) $d=0$, b) small d, c) large d.

but consisting of a linearly polarized component superimposed on a component with random polarization (i.e. of the same form as the originally input light), where there is no relationship between the values of the different stokes vector components the value of r would decrease during propagation through this medium exactly as it would if the light were input into the original medium.

It is also worth noting that the volume occupied by the distribution of polarization states in the space defined by s_1, s_2, s_3 remains unchanged during propagation in the isotropic nonlinear medium. This can be simply demonstrated if we consider that all states with a particular value of s_3 will be rotated around the s_3 axis by the same amount. The area of all cross-sections through the distribution perpendicular to the s_3 axis will be unchanged, and hence the total volume occupied by the distribution of instantaneous polarisation states will not change.

5.5 Comparison with Analytical Results

In [Svirko, 94a], a number of conclusions were drawn about the evolution of a light wave in a nonlinear medium. It was stated that totally polarised light will remain totally polarised in any linear or nonlinear medium. Changes in the degree of polarisation of partially polarised light may occur in an absorbing medium, and intensity-dependent change in degree of polarisation may occur in a medium which displays nonlinear absorption. It was also concluded, however, that in an absorptionless medium with isotropic nonlinear response (and linear response of arbitrary symmetry), intensity-dependent change in degree of polarisation will not occur. This last conclusion is not supported by the results of the computer simulation described above.

We believe that the approach developed in [Svirko, 94a] is essentially sound, and that the above discrepancy originates from limitations placed on the scope of applicability of this approach by the assumption made that the statistical properties of the light do not change significantly during propagation. In [Svirko, 94a] it was found that

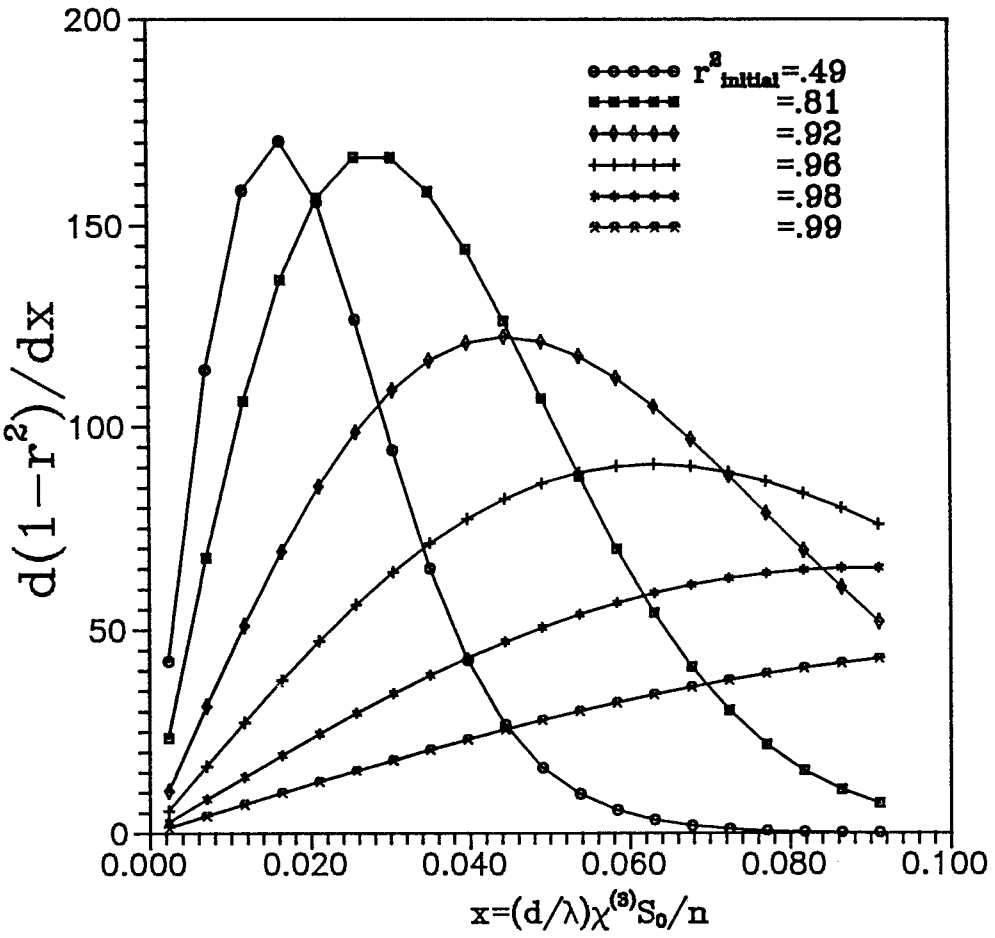

Figure 5.5 First derivative of the degree of polarisation of initially linearly polarised light propagating in an isotropic nonlinear medium as a function of $(d/\lambda)\chi^{(3)}S_0$

changes to the statistical properties of the light give rise to terms in the evolution equations of the Stokes' vector of order $(\chi^{(3)}S_0)^2$ and higher which may alter the degree of polarisation of the light. The main terms resulting from the nonlinearity of the medium, of order $\chi^{(3)}S_0$, do not change the degree of polarisation of the light. In [Svirko, 94a] the higher order terms in $\chi^{(3)}$ are neglected on the basis that for most nonlinear optical problems $\chi^{(3)}S_0 \ll 1$. Correspondingly, the alteration of degree of polarization mainly results from the linear anisotropy while nonlinear effects lead only to small corrections. While this assumption may be considered reasonable in most situations, in cases where the third order nonlinearity is the sole or main cause of polarisation alteration, it is not safe to neglect the higher order terms in $\chi^{(3)}$.

Hence, the case where the degree of polarization alters due only to the nonlinearity

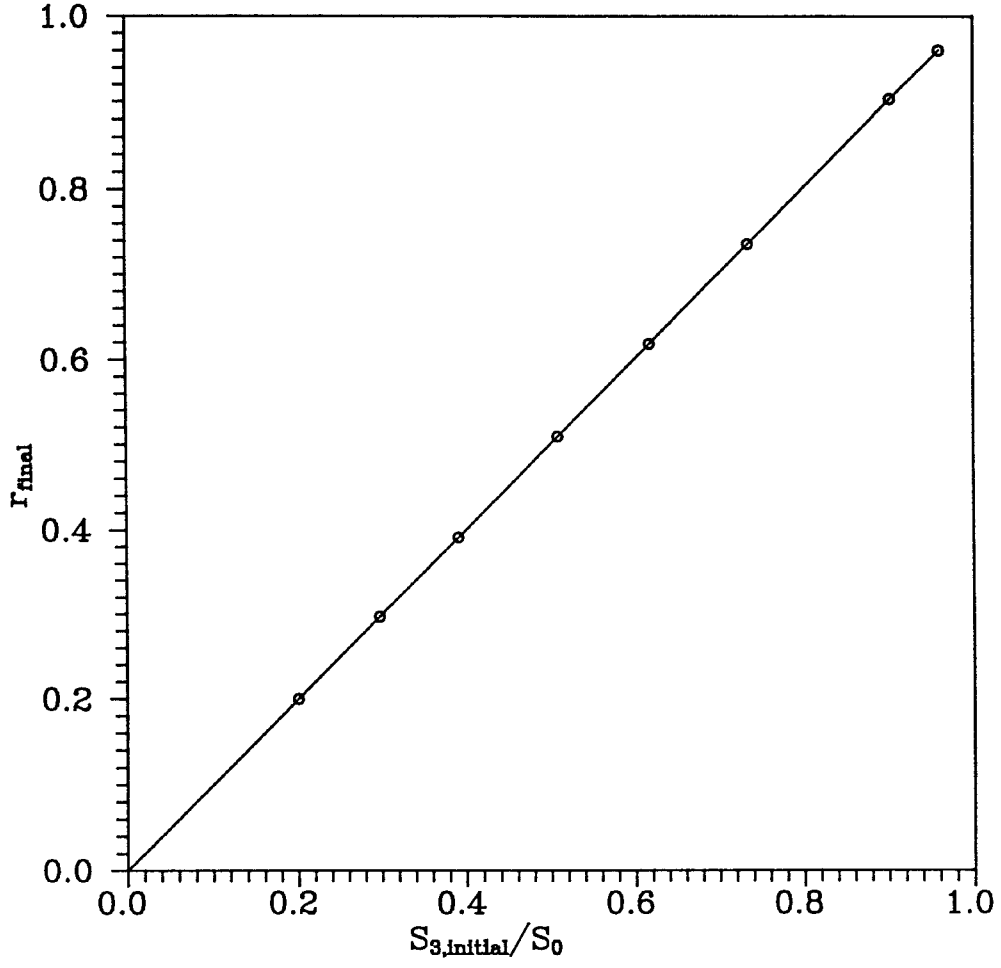

Figure 5.6 Asymptotic values of degree of polarisation *r* for light propagating in an isotropic nonlinear medium as a function of initial value of S_3

of the medium requires consideration of the higher order terms in $\chi^{(3)}$. In an isotropic dissipationless medium the linear anisotropy vanishes and the spatial evolution of the polarization of the wave is determined by the third-order nonlinearity only. To calculate the spatial evolution of the degree of polarization one must take account of terms of higher order, i.e. take into consideration the transformation of the probability distribution function of the totally depolarized component of the light wave. This gives corrections to the equations for the Stokes parameters proportional to $(\chi^{(3)}S_0)^2$. This may be seen from figure 5.5 which presents the dependence of the derivative of the degree of polarization against $(d/\lambda)\chi^{(3)}S_0$. Specifically, this derivative is equal to zero at zero intensity of the light wave, *i.e. the degree of polarization is a function of* $(\chi^{(3)}S_0)^p$ *where* $p>1$.

Comparison of results obtained by the computer program was also made with the asymptotic values of degree of polarisation calculated by Crosignani et.al. [Crosignani, 86]. Figure 5.6 shows a plot of the final degree of polarisation of initially partially polarised light with various initial values of S_3, after propagation through a very long isotropic nonlinear medium. The results obtained match the prediction of Crosignani that the asymptotic degree of polarisation of elliptically polarised light with an arbitrary intensity distribution will tend asymptotically to the initial value of S_3.

5.6 Conclusions

A computer program based on the quaternion description of the light polarisation, constitutive equation and the wave equation and suitable for calculation of evolution of partially polarised light has been developed. The program was used to simulate the behaviour of partially polarised light in an isotropic nonlinear medium. It was found that the partially polarised light undergoes a decrease of its degree of polarisation. This is explained by the fact that the nonlinear interaction significantly changes the statistics of the distribution of the instantaneous polarisation state of the light from the initial gaussian condition. In order to develop an analytical approach to this phenomenon the scope of the theory developed in [Svirko, 94a] would have to be expanded to include consideration of terms of order $(\chi^{(3)})^2$ and higher.

5.7 References

[Born, 80]	Born M, Wolf E, "Principles of Optics", 6th edn., Pergamon, Oxford, 1980.
[Box, 58]	Box G.E.P, Muller M.E, Annals of Mathematical Statistics, **29**, (1958), 610.
[Bratley, 87]	Bratley P, Fox B.L, Schrage L.E, "A Guide to Simulation", 2nd edn., Springer-Verlag, NY, 1987.
[Chernov, 93]	Chernov V.E, Zon B.A, J. Opt. Soc. Am. B, **10**, (1993), 210.
[Crosignani, 85]	Crosignani B, Daino B, Optica Acta, **32**, (1985), 1251.
[Crosignani, 86]	Crosignani B, Daino B, Porto P.D, J. Opt. Soc. Am. B, **3**, (1986), 1120.
[David, 90]	David D, Holm D.D, Tratnik M.V, Physics Reports, **187**, (1990), 281.

[Goodman, 85] Goodman J.W, "Statistical Optics", John Wiley & Sons Inc., 1985.

[Kubo, 80] Kubo H, Nagata R, Opt. Comm., **34**, (1980), 306.

[Kubo, 81] Kubo H, Nagata R, J. Opt. Soc. Am., **71**, (1981), 327.

[Maker, 64] Maker P.D, Terhume R.W, Savage C.M, Phys. Rev. Lett., **12**, (1964), 507.

[Mandel, 63] Mandel L, Proc. Phys. Soc., **81**, (1963), 1104.

[Press, 86] Press W.H, Flannery B.P, Tenkolsky S.A, Vetterung W.T, "Numerical Recipes", C.U.P., 1986

[Sala, 84] Sala K.L, Phys. Rev. A, **29**, (1984), 1944.

[Svirko, 94] Svirko Yu.P, Zheludev N.I, Jnl. of Luminescence, **58**, (1994), 399.

[Svirko, 94a] Svirko Yu.P, Zheludev N.I, Phys. Rev. A, **50**, (1994), 709.

[Tratnik, 87] Tratnik M.V, Sipe J, Phys. Rev. A, **35**, (1987), 2965.

[Walser, 94] Walser R, Zoller P, Phys. Rev. A, **49**, (1994), 5067.

[Zheludev, 89] Zheludev N.I, Sov. Phys. Usp., **32**, (1989), 357.

[Zheludev, 90] Zheludev N.I, Svirko Yu.P., in "New Semiconductor Diagnostic Methods" ed. S.A.Akhmanov and N.I.Zheludev, VINITI, Moscow, 1990 (in Russian).

Chapter 6
Summary and Further Work

6.1 Summary of Results

A novel reflective configuration polarimeter for pump-probe measurements was developed. The polarimeter was used in conjunction with two lasers; a Nd:YAG laser producing 80 picosecond pulses, and a specially constructed femtosecond modelocked Ti:Sapphire laser. Determination was made of the sensitivity and time resolution of the polarimeter in its various configurations. Sensitivity to pump-induced reflected probe polarisation rotation of $< 10^{-6}$ radians combined with time resolution up to 70 femtoseconds was achieved. The limit on sensitivity is set by laser noise. Time resolution of 30 femtoseconds was achieved by reducing the amount of dispersion arising from the components of the polarimeter, with loss of sensitivity of approximately an order of magnitude. The polarimeter has been tested in a variety of spectroscopic configurations and with different types of materials (metals, semiconductors and superconductors) and was found to be a useful tool for the investigation of the transient nonlinear optical properties of opaque materials. A new type of optical autocorrelator based on ultrafast nonlinearity in metallic nickel and use of the Specular Inverse Faraday effect was designed, and used to measure the pulse lengths of femtosecond lasers with wavelengths 810 nm and 1260 nm. This autocorrelation technique has the potential to be used over a wide wavelength range in the visible and infrared.

The recently developed spectroscopic polarimetric technique of the Specular Inverse Faraday effect was used to study a variety of materials. The semimagnetic

semiconductor $Cd_{0.6}Mn_{0.4}Te$ and the high T_c superconductor $YBaCuO_{7-\delta}$ were studied with 80 picosecond time resolution at a wavelength of 532 nm. Values of degenerate $\chi^{(3)}$ of 2.5 10^{-6} esu in $Cd_{0.6}Mn_{0.4}Te$ and 8.4 10^{-9} esu in $YBaCuO_{7-\delta}$ were found. No dynamics were resolved in either material with this time resolution. The thermalisation and spin-relaxation dynamics of the Specular Inverse Faraday effect were investigated with an unprecedented 70 femtosecond time resolution in the semiconductor GaAs. A complex response involving an initial positive rotation which decayed over a few hundred femtoseconds and a negative rotation with a decay time of 10 picoseconds was observed. A model of free carrier population dynamics was outlined to interpret these results. The ferromagnetic metal Ni was studied with 32 femtosecond time resolution at a wavelength of 810 nm. A strong ($\chi^{(3)} \sim 2\ 10^{-9}$) and exceptionally fast ($\tau < 30$ fs) nonlinearity was found. This raises the possibility of using this material in optical switching, or for optical autocorrelation measurements, as described above.

Investigations were undertaken into natural and light induced reflective anisotropy in zincblende structure crystals. The natural effect, which had previously been observed in GaAs, was observed in InSb and $Cd_{0.6}Mn_{0.4}$. Transient measurements of induced anisotropy, its orientation dependence and intensity dependence were made in GaAs, InSb and $Cd_{0.6}Mn_{0.4}Te$. At λ=532nm the natural rotation was observed to have a value of 6.4 10^{-4}rad corresponding to γ^s_{xyz} (natural) $=4.5\times10^{-8}$ cm in GaAs, 3.2 10^{-4}rad corresponding to γ^s_{xyz} (natural) $= 2.0\times10^{-8}$ cm in InSb and 5 10^{-4}rad corresponding to γ^s_{xyz} (natural) = 2 10^{-8}cm in $Cd_{0.6}Mn_{0.4}Te$. The pump induced effect was observed to have values of 1.1×10^{-11} rad cm^2W^{-1} in GaAs, 4.3×10^{-11}rad cm^2W^{-1} in InSb and 6 10^{-11} rad cm^2W^{-1} in $Cd_{0.6}Mn_{0.4}Te$. A phenomenological picture of light propagation and a microscopic picture of optical transitions in zincblende structure materials have been developed to explain the linear and nonlinear effects. This allowed attribution of the observed anisotropic effects to the time-nonreversible phenomenon of gyrotropic linear dichroism. The induced effect decays on the timescale of carrier recombination and is interpreted as being an enhancement to the linear effect produced by renormalisation of the band gap in these materials due to

the creation of a dense electron hole plasma. Theoretical backing for the time-nonreversible nature of this effect comes from studies of the light-matter interaction Hamiltonian for non-centrosymmetric materials and consideration of the nonreciprocal nature of the predicted optical consequences of these time-nonreversible terms.

A computer program based on the quaternion description of the light polarisation, constitutive equation and the wave equation and suitable for calculation of evolution of partially polarised light was developed. The evolution of the polarisation state of partially polarised light during propagation in an isotropic medium with cubic nonlinearity has been investigated in detail and compared with published analytical and semi-analytical data. It was found that the partially polarised light undergoes a decrease of its degree of polarisation. This is explained by the fact that the nonlinear interaction significantly changes the statistics of the distribution of the instantaneous polarisation state of the light from the initial gaussian condition.

6.2 Further Work

There exists the possibility of further improvement of the time resolution of the polarimeter by means of the use of negative dispersion to compensate for the remaining dispersion of the elements of the polarimeter and of the laser output coupler. This might be achieved by the use of a prism pair, as in the Ti:Sapphire laser cavity. Whether this complication of the design of the polarimeter is considered worthwhile depends on the decay times of the phenomena being investigated. It might well prove useful for investigations of nonlinearities in metals, which have been found to be effectively instantaneous with the time resolution currently available. Improvement to the resolution of the polarimeter might be achieved by using a much higher modulation frequency, since noise levels might be expected to be lower at higher frequencies.

The Specular Inverse Faraday effect has proved to be an effective means of investigating the optical properties of opaque materials. In the light of the strong and

very fast nonlinear response in nickel, in the range required for all-optical switching applications, a major project investigating nonlinearities in a wide variety of metals is in prospect. Measurements of nonlinearity by this technique have already been made in several metals using a femtosecond Cr:Forsterite laser [Zheludev, 95; Bennett, 95].

Understanding of the effect of specular gyrotropic linear dichroism may be enhanced by extending the investigation to a wider variety of materials. Linear experiments are currently in progress in the 23 point group materials BGO ($Bi_{12}GeO_{20}$) and BSO ($Bi_{12}SiO_{20}$), where gyrotropic linear dichroism may be observed on a background of natural optical activity.

The program simulating the evolution of partially polarised light clearly has the potential to be applied to more complicated cases than that of simple isotropic nonlinearity. A case that may be worth studying, for example, is that of partially polarised light propagating in a nonlinear medium with weak birefringence, where polarisation instability may be observed [Sala, 84]. It might also be interesting to extend the program to deal with light with different statistical properties (e.g. partially polarised thermal light).

6.3 References

[Bennett, 95] Bennett P.J, Loh H, Popov S.V, Shatwell I.R, Svirko Yu.P, Zheludev N.I, Kamalov V.F. and Slobodchikov E.V, Paper QWA8, QELS 95, Baltimore, Maryland, May 1995.

[Sala, 84] Sala K.L, Phys. Rev. A, **29**, (1984), 1944.

[Zheludev, 95] N.I.Zheludev, Bennett P.J, Loh H, Popov S.V, et.al., Optics Letters, **20**, (1995), 1368.

Appendix A: Journal Papers

Published or accepted for publication:

(1) **Giant Specular Inverse Faraday-Effect in $Cd_{0.6}Mn_{0.4}Te$**
N.I.Zheludev, M.A.Brummell, R.T.Harley, A.Malinowski, S.V.Popov, D.E.Ashenford, B.Lunn
Solid State Communications, 1994, vol.89, pp.823-825

(2) **Transient Optical-Excitation Breaks Time-Reversibility In GaAs and InSb Crystals**
A.Malinowski, D.Paraschuk, S.V.Popov, N.I.Zheludev
Journal of Luminescence, 1994, vol.58, pp.244-247

(3) **Coherent and Incoherent Specular Inverse Faraday-Effect in $YBa_2Cu_3O_{7-\delta}$**
N.I.Zheludev, S.V.Popov, A.Malinowski, Yu.P.Svirko, W.Y.Liang, C.T.Lin
Solid State Communications, 1994, vol.90, pp.287-289

(4) **Observation of Time-Nonreversible Optical Interaction with Zincblende semiconductors**
N.I.Zheludev, S.V.Popov, Yu.P.Svirko, A.Malinowski, D.Y.Paraschuk
Physical Review B, 1994, vol.50, pp.11508-11513

(5) **Observation of Time-Nonreversible Optical Interaction With Zincblende Semiconductors - Comment**
N.I.Zheludev, S.V.Popov, Yu.P.Svirko, A.Malinowski, A.R.Bungay
Physical Review B, 1995, vol.52, pp.2203-2205

(6) **Reciprocity in Nonlocal Optics**
A.Malinowski, Yu.P.Svirko, N.I.Zheludev

accepted by Journal of the Optical Society of America B

Prepared for submission:

(7) **Pump-probe Reflective Polarisation Sensitive Measurements with Microradian Angular Sensitivity and Femtosecond Time Resolution: A New Technique for the Spectroscopy of Opaque Solids**
A.R.Bungay, A.Malinowski, S.V.Popov, B.D.Rainford, N.I.Zheludev

(8) **Femtosecond Pulse Duration Measurements Utilizing Ultrafast Nonlinearity in Nickel**
A.Malinowski, P.J.Bennett, S.V.Popov, B.D.Rainford, I.R.Shatwell and N.I.Zheludev

In preparation:

(9) **Propagation of Partially Polarised Light in Nonlinear Media**
A.Malinowski, Yu.P.Svirko, N.I.Zheludev

Appendix B: Papers Presented at Conferences

(1) **Transient Optical Excitation Breaks Time-Reversality in GaAs Crystal**
A.Malinowski, S.V.Popov, N.I.Zheludev, D.Paraschuk
9-th International Conference on the Dynamical Processes in Excited States of Solids, MIT, Cambridge, Massachusetts, 2-6 August 1993.

(2) **Optically-Induced Violation of Time-Reversality in GaAs: Probing by Time-Resolved Micropolarimetry**
A.R.Bungay, A.Malinowski, S.V.Popov, N.I.Zheludev
11-th UK National Quantum Electronics Conference, Belfast, 30 August-2 September 1993, paper 35.

(3) **Time-Nonreversible Linear and Nonlinear Optical Phenomena in a Dilute Magnetic Semiconductor**
A.Malinowski, S.V.Popov, Yu.P.Svirko, N.I.Zheludev
International Quantum Electronics Conference, Anaheim, California, 8-13 May 1994, paper QTU01.

(4) **Transient Coherent and Incoherent Specular Inverse Faraday Effect: Measurements of Surface Cubic Optical Nonlinearities**
A.R.Bungay, A.Malinowski, S.V.Popov, Yu.P.Svirko, R.E.Worsley, N.I.Zheludev
International Quantum Electronics Conference, Anaheim, California, 8-13 May 1994, paper QWC47.

(5) **Transient Time-Irreversible Optical Interaction in Zinc-Blende Semiconductors**
A.R.Bungay, H.Loh, A.Malinowski, S.V.Popov, N.I.Zheludev, V.F.Kamalov, E.V.Slobodchikov
Quantum Electronics and Laser Science Conference, Baltimore, Maryland, May 22-26 1995, paper QFD4.

(6) **Nonreciprocal Interaction of Light with Zinc-Blende Semiconductors**

A.Malinowski, S.V.Popov, Yu.P.Svirko, N.I.Zheludev

Progress in Electromagnetics Research Symposium , Seattle, Washington, 24-28 July 1995, proceedings p.166 (session on Nonreciprocity and Highly Anisotropic Media).

(7) **Pump-Probe Reflective Polarisation Sensitive Measurements with Microradian Sensitivity and Femtosecond Time Resolution: A New Technique in the Spectroscopy of Opaque Solids**

A.R.Bungay, A.Malinowski, S.V.Popov, B.D.Rainford, N.I.Zheludev

12-th UK National Quantum Electronics Conference, Southampton, 4-8 September 1995, paper 10-5.

(8) **Application of Nonlinearities of Metals in Ultrashort Pulse Measurements**

P.J.Bennett, A.R.Bungay, A.Malinowski, S.V.Popov, I.R.Shatwell and N.I.Zheludev

Conference on Lasers and Electro-Optics, Anaheim, California, 2-6 June, 1996, paper CTuX2.

The following published papers were included in the bound thesis. These have not been digitised due to copyright restrictions, but their doi are provided.

N.I. Zheludev, M.A. Brummell. R.T. Harley, A. Malinowski, S.V. Popov, D.E. Ashenford, B. Lunn (1994) **Giant specular inverse Faraday effect in Cd0.6Mn0.4Te** Solid State Communications: 89 (10), 823-825 https://doi.org/10.1016/0038-1098(94)90064-7

A. Malinowski, D. Paraschuk, S.V. Popov, N.I. Zheludev (1994) **Transient optical excitation breaks time-reversibility in GaAs and InSb crystals** Journal of Luminescence: 58 (1-6), 244-247 https://doi.org/10.1016/0022-2313(94)90406-5

N.I. Zheludev, S.V. Popov, A. Malinowski, Yu.P. Svirko, W.Y. Liang, C.T. Lin (1994) **Coherent and incoherent specular inverse Faraday effect in YBa2Cu3O7–δ** Solid State Communications: 90 (5), 287-289 https://doi.org/10.1016/0038-1098(94)90152-X

N. I. Zheludev, S. V. Popov, Yu. P. Svirko, A. Malinowski, and D. Yu. Paraschuk (1994) **Observation of time-nonreversible optical interaction with zinc-blende semiconductors** Physical Review B: 50 (16), 11508-11513 https://doi.org/10.1103/PhysRevB.50.11508

N. I. Zheludev, S. V. Popov, Yu. P. Svirko, A. Malinowski, and A. R. Bungay (1995) **Reply to ''Comment on 'Observation of time-nonreversible optical interaction with zinc-blende semiconductors' ''** Physical Review B: 52 (3), 2203-2205 https://doi.org/10.1103/PhysRevB.52.2203

A. Malinowski, Yu P. Svirko, and N. I. Zheludev (1996) **Reciprocity in nonlocal optics** Journal of the Optical Society of America B: 13 (8), 1641-1644 https://doi.org/10.1364/JOSAB.13.001641

P.J. Bennett, A. Malinowski, B.D. Rainford, I.R. Shatwell, Yu.P. Svirko, N.I. Zheludev (1998) **Femtosecond pulse duration measurements utilizing an ultrafast nonlinearity of nickel** Optics Communications: 147 (1-3), 148-152 http://dx.doi.org/10.1016/S0030-4018(97)00563-4

PUMP-PROBE REFLECTIVE POLARISATION SENSITIVE MEASUREMENTS WITH MICRORADIAN ANGULAR SENSITIVITY AND FEMTOSECOND TIME RESOLUTION: A NEW TECHNIQUE FOR THE SPECTROSCOPY OF OPAQUE SOLIDS

A.R.Bungay, A.Malinowski, S.V.Popov, B.D.Rainford and N.I.Zheludev
Department of Physics, University of Southampton
Southampton SO17 1BJ, UK

Abstract

A new pump-probe polarisation sensitive spectroscopic technique for the transient reflective nonlinear spectroscopy of opaque solids is reported. We present the first measurements of the transient specular inverse Faraday effect in bulk GaAs and the instantaneous effect in metallic Nickel.

Polarisation sensitive techniques in the nonlinear spectroscopy of solids are well known both in transmission [1-8] and on reflection [9-17]. In this paper we report on progress in a relatively new spectroscopic method which is based on the specular inverse Faraday effect (SIFE). The SIFE is the nonlinear optical phenomenon of rotation of the polarization azimuth of a weak probe wave reflected from a medium's surface resulting from stimulation of the medium by a circularly polarized pump wave [10,18,19]. This technique is promising for the study of opaque materials. The time-integrated effect has recently been demonstrated with ~80 ps optical pulses in various solids including CuCl and HgI_2 [10], InSb and GaAs [13], $YBa_2Cu_3O_{7-\delta}$ [14] and $Cd_{1-x}Mn_xTe$ [15]. Here we report, for the first time, transient SIFE measurements. A time resolution of 60 fs was achieved.

The SIFE technique involves accurate detection of the probe polarisation azimuth rotation. Our polarimetric approach relies upon the simultaneous modulation of two parameters: the probe beam polarisation azimuth and the pump beam intensity. The signal is recovered by phase sensitive detection at the sum frequency of the modulations. The polarimeter is based on a single birefringent calcite prism (Cotton prism) acting as both polariser and analyzer (see figure 1). The light source was a Kerr-lens mode-locked Ti:Sapphire laser, pumped by an argon-ion laser, producing 40 fs pulses at wavelengths centred at λ=810nm. In the polarimeter, the laser beam was split into pump and probe. Both the pump and probe passed through the birefringent prism initially acquiring a linear polarisation with purity better than 10^6. The probe beam was directed normally to the crystal surface and reflected back through the polarisation prism. The polarisation of the pump beam was set as circular using a first order waveplate. It was focused on the sample to a spot diameter of 20μm by the same lens as the probe beam. The pump intensity and the incident probe polarization azimuth were simultaneously modulated at Ω_1=1.8kHz by a chopper and Ω_2=6.2kHz by a Faraday modulator (FM) respectively. The orthogonal polarisation component of the reflected probe was directed to the photodetector, the output of which allowed measurement of the reflected probe beam polarisation azimuth rotation by phase-sensitive detection at the sum frequency, $\Omega_1+\Omega_2$=8kHz, which may be understood as follows. Directly after the polariser, the probe light is linearly polarised along the x axis and may be represented by the Stokes vector I{1;1;0;0}. The probe polarisation azimuth is modulated by a Faraday cell (FM) which cosinusoidally alters the polarisation azimuth of the light by an angle $\phi=2A\cos\Omega_1 t$, where A is the amplitude of the modulation and this is doubled because the beam is reflected back through the Faraday cell. The Stokes vector of the light emerging from the Faraday cell after reflection from the sample and the second pass through the modulator is given by

$$S=I_r\begin{bmatrix} 1 \\ \cos2\phi\cos2\alpha_r\cos2\eta_r+\sin2\phi\sin2\alpha_r\cos2\eta_r \\ -\sin2\phi\cos2\alpha_r\cos2\eta_r+\cos2\phi\sin2\alpha_r\cos2\eta_r \\ \sin2\eta_r \end{bmatrix} \quad (1)$$

where I_r is the reflected light intensity, α_r is the probe polarisation azimuth rotation and η_r is the ellipticity angle which have changed as a result of reflection from the

sample and which are being measured. The reflected signal is analyzed using the same birefringent prism which is equivalent to a polariser oriented in the y direction if the orthogonal polarisation component is picked up. The overall light intensity emerging from the analyzer is

$$I_{out}=\frac{I_r}{2}(1-\cos 2\phi\cos 2\alpha_r\cos 2\eta_r-\sin 2\phi\sin 2\alpha_r\cos 2\eta_r). \quad (2)$$

Assuming that α_r, η_r and $A \ll \pi$,

$$I_{out}=I_r[8A^2-4\alpha_r A\cos\Omega_1 t+8A^2\cos 2\Omega_1 t] \quad (3)$$

which contains components on both the modulation frequency, Ω_1,

$$I_{out}(\Omega_1) = -4\alpha_r I_r A\cos\Omega_1 t \quad (4)$$

and on its second harmonic

$$I_{out}(2\Omega_1) = 8I_r A^2\cos 2\Omega_1 t. \quad (5)$$

In order to detect only pump induced rotation of the probe polarisation azimuth, we now introduce the pump intensity, $I_p(t)=\frac{1}{2}I_p(1+\cos\Omega_2 t)$, which is modulated at frequency Ω_2. The pump induced rotation depends on the intensity of the pump and may be represented by $\alpha_{ind} = \mu I_p(t)$ where μ is a constant. Substituting $I_p(t)$ into equation (4) shows that the output of the photodiode has a component oscillating at the sum frequency, $\Omega_1+\Omega_2$, the amplitude of which is proportional to the stimulated component of the probe polarisation azimuth rotation, α_{ind}, and is given by

$$I_{PD}(\Omega_1+\Omega_2) = A I_r \alpha_{ind}\cos(\Omega_1+\Omega_2)t. \quad (6)$$

The induced probe polarisation rotation may be directly measured by phase sensitive detection of the photodiode output at the sum frequency $\Omega_1+\Omega_2$. This signal is only sensitive to polarisation azimuth rotation and is not affected by any induced ellipticity.

The time domain evolution of the probe beam polarisation azimuth rotation due to the incoherent SIFE was studied by delaying the probe pulse with respect to the pump pulse using a variable corner cube delay line. The coherent component of the SIFE rotation was suppressed using the technique explained in [14]. Test experiments measuring the SIFE in a sample of Nickel, a material with effectively instantaneous nonlinear response (see figure 2), gave the temporal resolution of the polarimeter of 60 fs which is slightly longer than the laser pulse duration of 40 fs. This difference is attributed to the group velocity dispersion of the optical elements of the polarimeter. The practical limit on the angular sensitivity is set by the laser noise

$$\alpha_{min}^{LASER} = \frac{ENP \times (8A^2 + h)}{P_L \times \sqrt{T} \times 4A} \qquad (7)$$

where h is the extinction ratio of the prism, T is the lock-in integration time and ENP/P_L is the relative equivalent noise power of the laser at the frequency of the lock-in detection which was measured as $5.10^{-5} \div 1.10^{-4}$ $Hz^{-½}$. This gives a practical limit on the sensitivity of the polarimeter in the range $2.10^{-7} \div 4.10^{-7}$ radians which is ten times higher than the quantum limit .

The transient SIFE was observed in bulk GaAs. GaAs is opaque at 810 nm ($\hbar\omega$=1.53eV) with light penetration depth of about 1 μm. This photon energy is 0.12 eV above the band gap, allowing excitation of electrons from the light and heavy hole bands but not from the split-off valence band. Pump intensities in the range from 0.7 - 5 GW cm^{-2} were used corresponding to estimated optically induced free carrier concentrations of up to 6.10^{18} cm^{-3}. The corresponding reflected probe polarization azimuth rotation and its behaviour in the time domain is shown in figure 3 for I_p = 5 $GWcm^{-2}$. The induced rotation shows a bipolar time dependence which may be clearly decomposed into two parts. The first is a sharp positive peak which rises with the pump pulse and decays with a relatively fast tail of approximately 30-60 fs. The second component is negative and relaxes with an 11ps decay time. This relaxation time was independent of the pump intensity within our experimental range and accuracy. Figure 3 also shows "peak" values of the polarisation azimuth rotation as a function of intensity at zero and 1.5 ps pump-probe delays. Reversal of the pump chirality gave similar results but with the sign of probe polarization rotation reversed.

Interpretation of these observations is based on the fact that the rotation of reflected polarization is proportional to the difference between the absorption coefficients for the right and left circular components into which the initial linear polarization state of the probe may be decomposed [18,19]. A microscopic model, which is due to be published shortly [20] is based on a six band model of the GaAs band structure. It attributes the slow decay of the second peak to the electron spin relaxation, which was measured here to be 11±1 ps, and the fast decay of the first peak to at least two separate mechanisms: the hole spin relaxation and the intraband carrier thermalisation.

In conclusion, a new polarisation sensitive technique for the spectroscopy of opaque solids based on the transient specular inverse Faraday effect has been demonstrated. It allows extraction of information about the dynamics of the nonlinear optical properties of various opaque media. At present, 1 μradian sensitivity to polarisation azimuth rotation and 60fs time resolution is reported. We observed, for the first time, the transient specular inverse Faraday effect in GaAs revealing electron and possibly hole spin dynamics.

This work is funded by the Engineering and Physical Sciences Research Council grant numbers GR/J26854 and B63-R421 as well as the R.W.Paul instrument fund. The authors are grateful to R.T.Harley for fruitful discussion.

References

1. A.M. Danishevskii, S.F. Kochegarov and V.K. Subashiev, JETP Lett., **33**, (1981), 611.
2. M.M. Afanas'ev, B.P. Zakharchenia, M.E. Kompan, V.G. Fleisher and S.G. Shul'man, JETP Lett., **21**, (1975), 224.
3. M. Kuwata, J. Phys. Soc. Japan, **53**, (1984), 4456.
4. S.P. Apanasevich, D.N. Dovchenko and N.I. Zheludev, Opt. Spectrosc., **62**, (1987), 287.
5. A. Tackeuchi, S. Muto, T. Inata, and T. Fujii, App. Phys. Lett. **56**, (1990), 2213.
6. T. Kawazoe, Y. Masumoto and T. Mishina, Phys. Rev. **B47**, (1993), 10452.
7. J.J. Baumberg, S.A. Crooker, D.D. Awschalom, N. Samarth, H. Luo and J.K. Furdyna, Phys. Rev. B., **50**, (1994), 7689.
8. M.G. Dubenskaya, T.M. Ilyinova, A.V. Trukhov and A.A. Fortigin, Bull. Russ. Ac. Sci., **57**, (1992), 1192.
9. G.C. Cho, W. Kutt and H.Kurz, Phys. Rev. Lett., **65**, (1990), 764.
10. M. Kuwata, J. of. Luminescence **38**, (1987), 247.
11. T. Saiki, K. Takeuchi, M. Kuwata-Gonokami, T. Mitsuyu and K. Ohkawa, Appl. Phys. Lett., **60**, (1992), 192.
12. A.R. Bungay, S.V. Popov, Yu.P. Svirko and N.I. Zheludev, Opt. Lett., **20**, (1995), 356.
13. S. V. Popov, Yu. P. Svirko, N. I. Zheludev. Opt. Lett. **19**, (1994), 1.
14. N. I. Zheludev, S. V. Popov, A. Malinowski, Yu. P. Svirko, W. Y. Liang, and C. T. Lin, Sol. St. Comm. **90**, (1994), 287.
15. N. I. Zheludev, M. A. Brummell, R. T. Harley, A. Malinowski, S. V. Popov, D. E. Ashenford and B. Lunn. Sol. St. Comm. **89**, (1994), 823.
16. A.R. Bungay, A. Malinowski, S.V. Popov, Yu.P. Svirko, R.E. Worsley and N.I. Zheludev, QWC47, International Quantum Electronics Conference, Anaheim, California, May 8-13, (1994).
17. D.H. Austin and C.V. Shank, Phys. Rev. Lett., **32**, (1974), 1120.
18. Yu.P. Svirko and N.I. Zheludev, JOSA B, **11**, (1994), 1388.
19. A. R. Bungay, Yu. P. Svirko and N. I. Zheludev, Phys. Rev. **B47**, (1993), 16141.
20. A.R. Bungay, R.T. Harley, S.V. Popov, I.R.Shatwell and N.I. Zheludev, Paper 1.4.SS.26, Condensed Matter and Materials Physics Conference, Warwick, UK, (1994), Dec 19-21.

Figure Captions

1. Outline of the polarimeter.

2. SIFE in Nickel. Appears as an instantaneous cross-correlation of the pump and probe pulse and gives the temporal resolution of the polarimeter of 60 fs.

3. Transient SIFE in GaAs. On the right: a) shows the intensity dependence of the magnitude of the first peak (at the moment of stimulation); b) shows the intensity dependence of the SIFE at 1.5 ps delay.

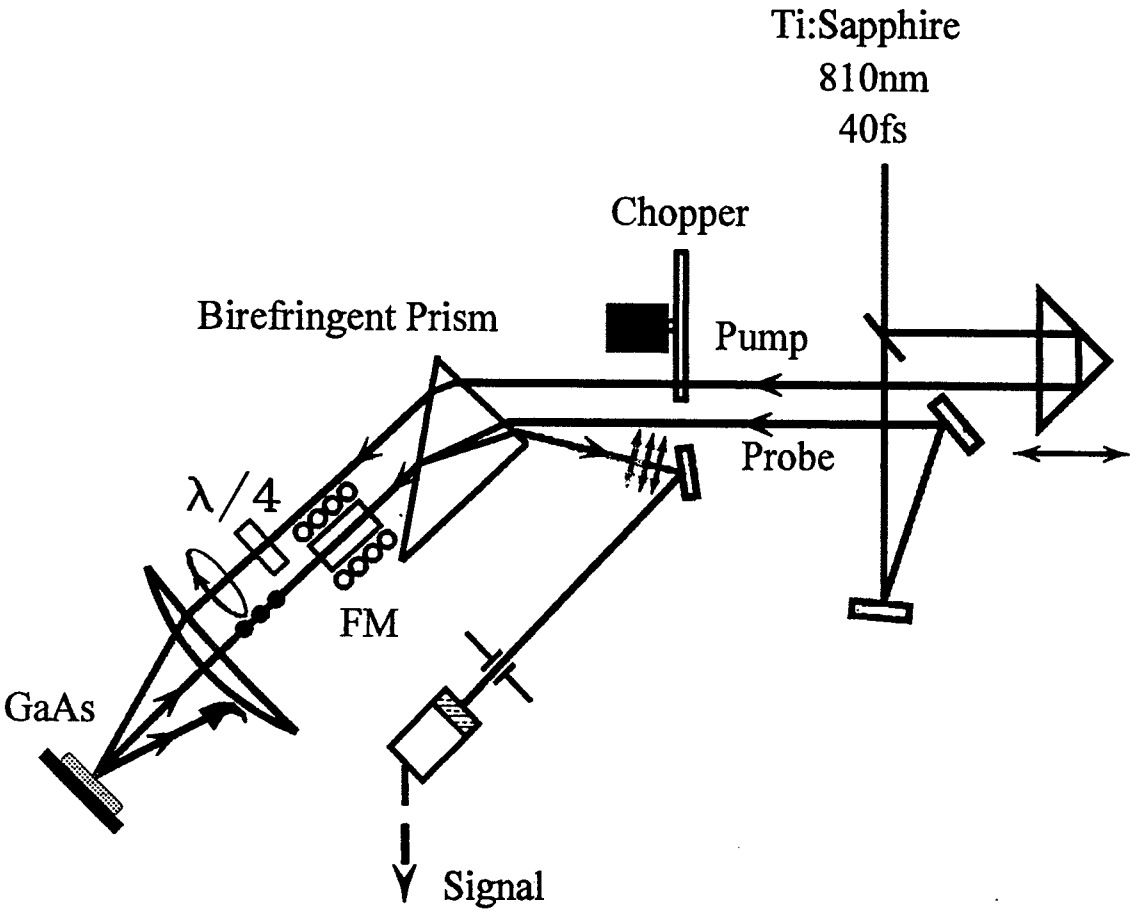
Ti:Sapphire
810nm
40fs
Chopper
Birefringent Prism
Pump
Probe
λ/4
FM
GaAs
Signal

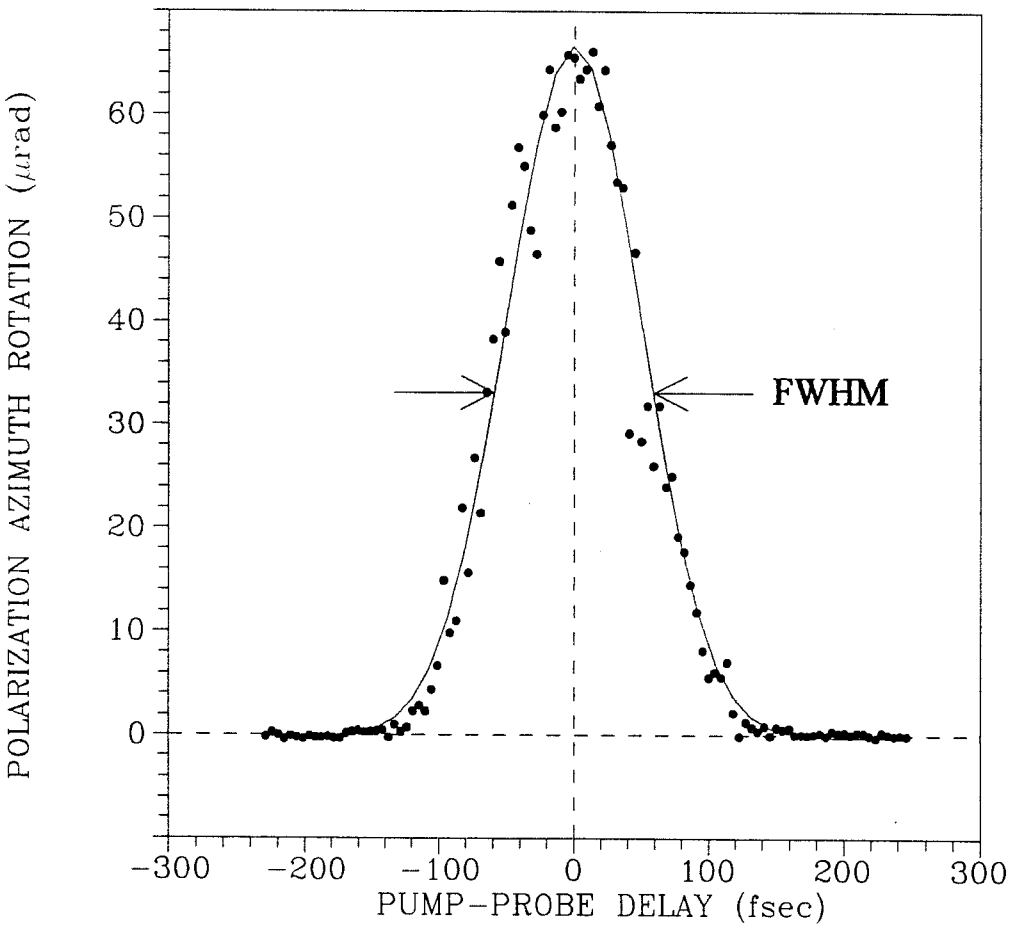
POLARIZATION AZIMUTH ROTATION (μrad)
60
50
40
30
20
10
0
FWHM
−300
−200
−100
0
100
200
300
PUMP−PROBE DELAY (fsec)

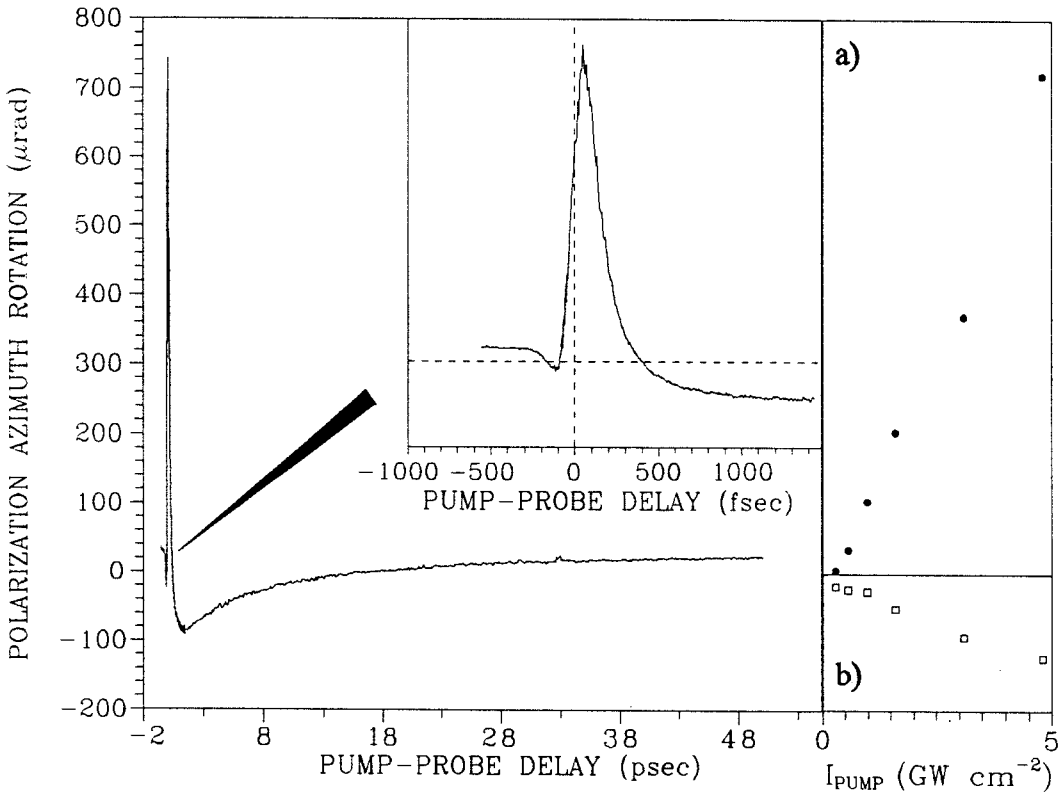
POLARIZATION AZIMUTH ROTATION (μrad)
800
700
600
500
400
300
200
100
0
−100
−200
−2
8
18
28
38
48
PUMP−PROBE DELAY (psec)
−1000 −500 0 500 1000
PUMP−PROBE DELAY (fsec)
a)
b)
0
5
I_{PUMP} (GW cm^{-2})